Generation of a Human Disease Model for KCNA2-related Developmental and Epileptic Encephalopathy using iPSC-derived Neurons

Dissertation

zur Erlangung des Grades eines

Doktors der Naturwissenschaften

der Mathematisch-Naturwissenschaftlichen Fakultät

und

der Medizinischen Fakultät

der Eberhard-Karls-Universität Tübingen

vorgelegt

von

Betül Uysal

aus Sakarya, Turkey

2023

Tag der mündlichen Prüfung:	11.05.2023
Dekan der Math.-Nat. Fakultät:	Prof. Dr. Thilo Stehle
Dekan der Medizinischen Fakultät:	Prof. Dr. Bernd Pichler
1. Berichterstatter:	Prof. Dr. Holger Lerche
2. Berichterstatter:	Prof. Dr. Ingrid Ehrlich
Prüfungskommission:	Prof. Dr. Holger Lerche
	Prof. Dr. Ingrid Ehrlich
	Prof. Dr. Peter Heutink
	Prof. Dr. Stefan Liebau

Erklärung / Declaration:

Ich erkläre, dass ich die zur Promotion eingereichte Arbeit mit dem Titel:

„Generation of a Human Disease Model for *KCNA2*-related Developmental and Epileptic Encephalopathy using iPSC-derived Neurons"

selbständig verfasst, nur die angegebenen Quellen und Hilfsmittel benutzt und wörtlich oder inhaltlich übernommene Stellen als solche gekennzeichnet habe. Ich versichere an Eides statt, dass diese Angaben wahr sind und dass ich nichts verschwiegen habe. Mir ist bekannt, dass die falsche Abgabe einer Versicherung an Eides statt mit Freiheitsstrafe bis zu drei Jahren oder mit Geldstrafe bestraft wird.

I hereby declare that I have produced the work entitled

"Generation of a Human Disease Model for KCNA2-related Developmental and Epileptic Encephalopathy using iPSC-derived Neurons"

submitted for the award of a doctorate, on my own (without external help), have used only the sources and aids indicated and have marked passages included from other works, whether verbatim or in content, as such. I swear upon oath that these statements are true and that I have not concealed anything. I am aware that making a false declaration under oath is punishable by a term of imprisonment of up to three years or by a fine.

Tübingen, den 08.08.2023 .....

Datum / Date Unterschrift /Signature

Table of Contents

List of Abbreviations

4-AP	4-Aminopyridine
AAVS1	adeno-associated virus integration site 1
AI	apoptosis inhibitor
BIC	bicuculine
BR	burst rate
Ca_V	voltage-gated calcium channels
CV	coefficient variation
DAPI	4',6-diamidino-2-phenylindole
DEE	developmental and Epileptic Encephalopathy
DMEM	dulbecco's modified eagle medium
DMSO	dimethyl sulfoxide
DNA	deoxyribonucleic acid
dox	doxycycline
DPBS	dulbecco's phosphate-buffered saline
EEG	electroencephalogram
EPSC	excitatory postcynaptic current
ESC	embryonic stem cell
FCS	fetal calf serum
FGF2	fibroblast Growth Factor 2
GFAP	glial fibrillary acidic protein
GOF	gain-of-function
GTCS	generalized tonic-clonic seizures
HCN	hyperpolarization-activated cyclic nucleotide–gated channels
IBI	inter burst interval
iPSCs	induced pluripotent stem cells
ISI	inter spike interval
K_V	voltage-gated potassium channels
$K_V1.1$	voltage-gated potassium channel 1.1 α-subunit
$K_V1.2$	voltage-gated potassium channel 1.2 α-subunit
$K_V1.4$	voltage-gated potassium channel 1.4 α-subunit
LB	lysogeny broth

LOF	loss-of-function
MAP2	microtubule-associated protein 2
MEA	multielectrode array
MEF	mouse embryonic fibroblast
MFR	mean firing rate
miRNA	microRNA
MNTB	medial nucleus of the trapezoid body
MW	multi-well
Na_V	voltage-gated sodium channels
NBR	network burst rate
NGN	Neurogenin
NGS	normal goat serum
PCR	polymerase chain reaction
PDL	Poly-D-Lysine
qRT-PCR	quantitative real-time polymerase chain reaction
RNA	ribonucleic acid
rpm	rotations per minute
SAP97	synapse-associated proten-97
sem	standard error of the mean
VGAT	vesicular GABA transporter

1 SUMMARY

In this thesis, I have investigated the functional outcomes of the recently identified *de novo KCNA2* mutations on neuronal firing behavior. To do so, induced pluripotent stem cells were derived from the fibroblasts of the patients carrying four different *KCNA2* mutations as well as of healthy individuals. Patient and healthy control iPSCs were then differentiated into cortical excitatory neurons, and their electrophysiological features were assessed and compared on both single cell and network levels, using patch-clamp and microelectrode array techniques, respectively.

In the first part, the aim was to reveal the pathophysiological outcome of the *KCNA2*-T374A mutation that causes the most severe phenotype among *KCNA2*-mediated DEEs and was found to have both gain- and loss-of-function effect on the $K_V1.2$ channels. The functional outcomes of the *KCNA2*-T374A mutation on single neuron physiology have been investigated longitudinally, from week one to four after the neuronal differentiation start. To do so, the patient iPSCs carrying the *KCNA2*-T374A mutation and the healthy control iPSCs were differentiated into neurons, and active and passive electrical properties of these neurons were assessed and compared over four consecutive weeks. Although the *KCNA2*-T374A patient-derived neurons' input resistances decreased over the weeks, confirming changing ion channel composition of maturing neuronal membranes, the patient-derived neurons had higher input resistances during early development, indicating slower maturation of the neurons compared to the controls. At early timepoints (week two and three), the patient-derived neurons were found to have longer action potential time-to-peak durations and half-widths while their evoked firing response to depolarizing current stimulations were altered only at week four compared to the controls. In the second part of this thesis, the patient-derived neuronal populations carrying the *KCNA2*-T374A mutation was also examined on a network level, and they were found to be more active, with a significantly higher mean firing rate compared to the controls, from early time points (week two) on. They had higher bursting rates and lower burst spike frequencies at different time points during the development, that were observed to be comparable at later time points to the controls. Nevertheless, burst durations were observed to be prolonged from week three on, remaining to be the robust indication of hyperexcitable networks.

The *KCNA2*-R297Q mutation, that was identified in the patients with severe DEE phenotypes with generalized epilepsy and was found to have prominent gain-of-function effect on the channel function, also caused a strong phenotype in iPSC-derived neuronal cultures. Compared to the controls, the patient iPSC-derived neuronal populations had significantly increased mean firing rates on the network level already after one week of development *in vitro*. Increased burst rates (with a narrowing gap over weeks) and burst durations (with robustly strong difference over weeks) were observed consistently whereas the burst spike frequency was higher compared to the controls only at later stages of development. On a single cell level, these patient-derived neurons responded to depolarizing current stimulations differently than the controls. The change in the pattern of evoked action potentials from week four to six was also different than the observed pattern in control case, that was opposite to what is expected from developing neurons, revealing a pathophysiological difference in patient-derived networks. Moreover, the patient-derived neurons were found to have increased action potential time-to-peak and half-width durations, especially at later time points.

The *KCNA2*-L328V mutation, that was identified in a severely affected DEE patient and was found to cause both loss- and gain-of-function of the $K_V1.2$ channels, gave rise to increased firing activities in patient iPSC-derived neuronal cultures compared to the controls. While the burst spike frequency was lower compared to the controls at earlier weeks, burst rates were higher in these patient populations, nevertheless by week six, which is the last examination time point in this study, both burst rates and burst spike frequencies were stabilized at the levels comparable to the controls. Interestingly, burst durations were observed to remain longer than those of the controls even at week six. Evoked firing response of the single neurons was different than that of the controls at both time points, week four and six, when these populations were examined on a single cell level. The change in the evoked firing response of the patient-derived neurons from week four to six, similarly to the neurons carrying the *KCNA2*-R297Q mutation, was in the opposite manner to what was observed in control cultures, indicating a crucial pathophysiological difference in firing behavior of developing patient-derived neurons.

The *KCNA2*-P405L mutation, that was identified in patients with milder DEE phenotypes with focal epilepsy and was found to have a pure loss-of-function effect on the channel function, also caused the mildest phenotype among the iPSC-derived neuronal

populations carrying *KCNA2* mutations. This mutation caused a developmental delay in neurons. Although the patient cultures always had comparable mean firing rates to the controls, appearance of bursting activity and localization of spikes within bursts, which are important steps in neuronal development, were observed with a delay. The mean input resistance of the patient-derived neurons was also found to be higher than that of the controls at an earlier time point, confirming the developmental delay of these patient-derived neurons, whereas at a later time point there was no difference anymore, suggesting a comparable ion channel composition on membranes of both patient and control-derived neurons by week six. Evoked firing patterns of patient-derived neurons was different from controls at week four, when the patient-derived neurons could fire only a smaller number of action potentials, whereas at week six there was no difference anymore. On a network level, although the bursting rate was not different in the patient cultures, burst spike frequencies were lower and the burst durations were consistently longer compared to the control-derived networks.

Overall, the *KCNA2* mutations examined in this study have been found to cause prolonged burst durations in neuronal networks. Although the underlying mechanism leading to longer bursts must be different between GOF- and LOF-causing mutations, it has been revealed that the mutations with a gain-of-function effect on the channel function prolonged the action potential durations mainly slowing down the rising phase of action potentials. The patient-derived neurons carrying these mutations were found to have prolonged action potential time-to-peak and/or half-width durations at different time points they were examined. Although these differences were time-specific, all these patient lines had hyperexcitable phases because of widened action potentials. Even though the differences in single action potential parameters were not observed at later time points, the cultures remained to be more active, exhibiting prolonged bursts. These findings raised a question whether structural changes may have happened during hyperexcitable periods in early development, resulting in sustained hyperexcitability of networks at later time points, potentially due to increased synaptic connectivity. To follow up the findings of this thesis, further experiments not only on single cell and network levels but also on a transcriptomic level should performed to shed light on the cause of robustly prolonged burst durations.

2 INTRODUCTION

2.1 Epilepsy

Epilepsy is one of the most common neurological disorders worldwide. The point prevalence of active epilepsy is 6.38 per 1,000 persons while the lifetime prevalence is 7.60 per 1,000 persons (1). Epileptic seizures are caused by spontaneous, abnormal electrical activity of neuronal networks which can result in impaired consciousness, muscle tension as well as more complex manifestations. A patient is diagnosed with epilepsy when epileptic seizures occur repeatedly and without an obvious reason. According to the latest classification proposed by ILAE, this neuronal network excitability disorder is diagnosed on three levels, seizure type, epilepsy type and epilepsy syndrome (2).

A patient can be diagnosed by epilepsy that is classified into more than one of the following etiologic categories, structural, genetic, infectious, metabolic, and immune, as well as an unknown group (2). Non-genetic forms of epilepsies usually have a focal origin from where the seizures start and spread. Clinical representation of such epilepsies depends on the focal region and vary from mild symptoms to severe convulsions. Idiopathic epilepsies are characterized by the lack of structural causes and are genetically determined. Genetic defects can cause both focal and generalized forms of epilepsy. Clinical representations have a wide range from mild seizures to severe epileptic encephalopathies with pharmaco-resistant epilepsy and other neurological symptoms (3).

Idiopathic epilepsies account for 50% of all cases. In most of the cases, complex inheritance comprising of many different genetic factors play a role in idiopathic epilepsies. Childhood and juvenile absence epilepsies are examples for the most common forms of idiopathic epilepsies with a complex inheritance. In relatively rare cases, monogenic inheritance, with a mutation in a single gene, results in epileptic phenotypes (4). Epileptic encephalopathies caused by single mutations in the genes like *CDKL5*, *CHD2, KCNQ2* or *KCNA2* are examples for this group (2).

In recent years, thanks to the advancing technologies of genome and exome sequencing, identification of disease-causing genetic modifications in patient cohorts has

accelerated. In case of epilepsies, genetic defects are found quite often in ion channels which are crucial players of electrical excitability of the brain. For example, several mutations have been identified in the *SCN2A* gene encoding the voltage-gated sodium channel $Na_V1.2$ (5), in the *KCNQ2* gene encoding the voltage-gated $K_V7.2$ potassium channel (6) as well as in the *KCNA2* gene encoding the voltage-gated $K_V1.2$ potassium channel (7,8). Functional studies following genetic identification of disease-causing mutations are required for a better understanding of genotype-phenotype relationships and to enable healthcare providers to find the right therapy for the patients more quickly. In case of *KCNA2*-mediated epileptic encephalopathies, such efforts have already been beneficial for some patients (9).

2.1.1 Developmental and Epileptic Encephalopathy

Developmental and epileptic encephalopathy (DEE) is recently defined by the International League Against Epilepsy (ILAE) to cover either or both of following descriptions: (I) developmental encephalopathy without frequent epileptic activity related to regression or further slowing of development and (II) epileptic encephalopathy without pre-existing developmental delay and where the genetic defect is not a cause for regression (2).

In some cases where a single genetic mutation is identified as a cause for the phenotype, the term DEE can be subsumed by using the gene-associated nomenclature. For example, as the genes *STXBP1*, *KCNQ2* and *KCNA2* are well known to cause DEEs, corresponding disorders are called as *STXBP1*, *KCNQ2* or *KCNA2* encephalopathies (2).

2.1.1.1 *KCNA2* Encephalopathy

The *KCNA2* gene, encoding the voltage-gated potassium channel $K_V1.2$ alpha-subunit, has been identified as a causative gene for DEE in 2015 (8,10). After the two initial studies conducted in parallel, where several *de novo KCNA2* mutations were identified in patients with DEE with mild to moderate intellectual disability, involvement of *KCNA2* in further exome analysis of DEE patients resulted in identification of more novel *KCNA2* mutations as well as more patients carrying already identified mutations (Table 1).

Upon the identification of *de novo KCNA2* mutations, the need to understand functional outcomes of these newly identified mutations arose and the first insights have been

obtained from the functional studies performed with *Xenopus laevis* oocytes two-microelectrode voltage clamp system. In the study led by Masnada&Hedrich et. al., twelve mutations identified in 23 patients were investigated to understand the resulting effects on the channel gating properties. Out of twelve missense mutations investigated, three mutations were found to have gain-of-function (GOF) effect, four to have loss-of-function (LOF) effect whereas other four missense mutations were found to have both gain- and loss-of-function effects (GOF+LOF). Interestingly, electrophysiological differences correlated with distinct phenotypes; patients with LOF mutations had predominantly focal seizures whereas patients with GOF mutations had more severe epilepsies with generalized seizures, developmental problems and ataxia as well as atrophy of the cerebellum. The most severe phenotypes were caused by GOF+LOF mutations identified in the patients with early-onset phenotypes, occasionally with neonatal onset epilepsy and developmental impairment, as well as EEG abnormalities (7).

As the severe phenotypes were caused by either GOF or combined GOF+LOF KCNA2 mutations and the patients carrying these mutations were largely pharmaco-resistant, 4-Aminopyridine was used in a recently reported clinical study, as a new therapeutic option for such patients, to antagonize the gain-of-function effect of these mutations (19). 4-AP is a K_V1 channel blocker and is a licensed drug that is used to treat gait disturbance in adults with multiple sclerosis (20). It has also been shown to help patients with downbeat nystagmus and episodic ataxia type 2 (21,22). In the recent study, eleven patients carrying either a GOF or a combined GOF+LOF *KCNA2* mutation were treated with 4-AP over a period of four years. Nine out of eleven patients experienced a clinical improvement in seizure frequency, ataxia and cognition upon the 4-AP treatment. Upon the worsening effects on one patient the treatment was discontinued and the patient carrying *KCNA2*-T374A mutation did not respond to the treatment even when treated with the maximum dose (1.5mg/kg per day).

Table 1| List of recently identified de novo *KCNA2* mutations causing DEEs.

Mutation	**Functional effect**	**# of reported cases**	**Age of onset**	**Published in**

Glu157Lys	GOF	1	9 months	(11)
Gln213*	LOF	1	2 months	(11)
Ile263Thr	LOF	1	11 months	(12)
Leu290Arg	GOF+LOF	1	7 weeks	(13)
Leu293His	GOF+LOF	1	1 month	(11)
Arg297Gln	GOF	7	15 months	(10)
			5 months	(12)
			10 mo, 15 mo, infantile, 6 mo, 1 yr	(11)
Arg297Trp	Not known	1	4 years	(15)
Leu298Phe	GOF	1	6 months	(12)
Gln357Arg	No effect	1	5 months	(11)
Leu328Val	GOF+LOF	1	6 months	(11)
Thr374Ala	GOF+LOF	4	since birth	(16)
			since birth, 4 mo, since birth	(11)
Gly398Cys	LOF	1	2 months	(11)
Val399Met	Not known	1	3 years	(15)
Pro405Leu	LOF	6	17 mo, 10 mo, and 9.5 months	(12)
			2 and 14 months.	(11)
			1 year	(15)
Pro407Ala	Not known	1	0.25 months	(17)
Val408Ala	Not known	1	4 months	(18)

2.2 Voltage-gated ion channels

Ion channels are pore-forming transmembrane proteins located on cellular membranes and are responsible for influx and outflux of ions across the membranes. Ions are passively transported across the membrane based on their electrochemical potential. In neurons, electrical excitability is controlled by ion channels. Hence, selectivity of ion channels as well as gating characteristics are crucially important for establishment of the resting membrane potential, action potential shape and transmission (3,19)

Based on their gating mechanism, ion channels are divided into different subgroups. They can be light-activated, mechanosensitive, cyclic nucleotide- or calcium-gated while the most common types are ligand- and voltage-gated ion channels (20).

Voltage-gated ion channels are one of the first ion channels identified, thanks to the voltage-clamp experiments performed more than half a century ago. Pioneering work of Hodgkin & Huxley demonstrated the crucial roles of voltage-gated sodium and potassium channels in action potential generation and propagation in the squid giant axon (21). Following their work, further electrophysiological studies revealed a rich consortium of voltage-gated ion channels located in different compartments of neurons and possessing different roles in neuronal excitability (22).

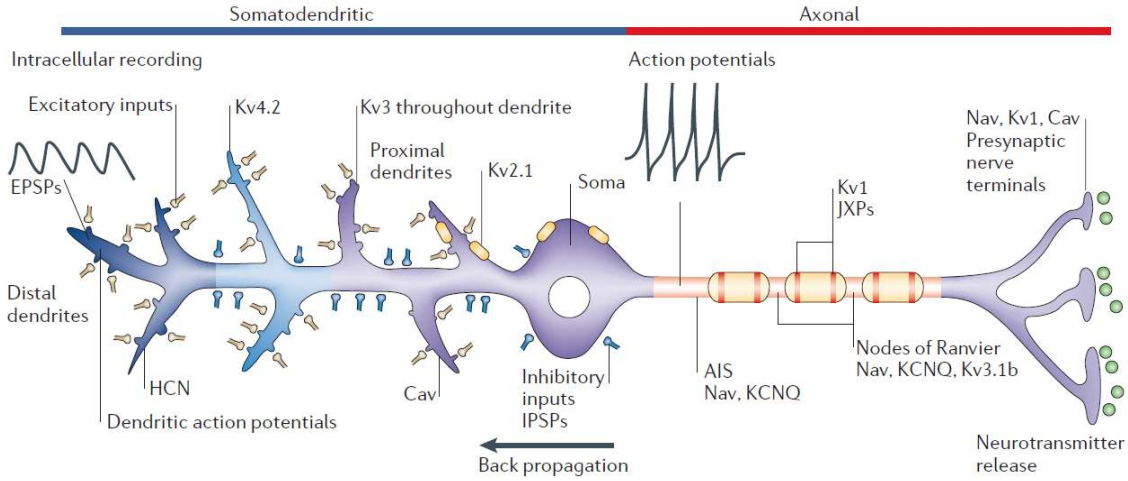

Figure 1| General distribution of voltage-gated ion channels across a neuronal membrane. Commonly, Na_V channels are found in axon initial segments, nodes of Ranvier and presynaptic terminals whereas different subtypes of K_V1 channels are localized at distinct regions of neuronal membranes from dendrites to presynaptic terminals, playing roles in distinct neuronal events. (Reprinted from Lai, H., Jan, L. The distribution and targeting of neuronal voltage-gated ion channels. Nat Rev Neurosci 7, 548–562 (2006), https://doi.org/10.1038/nrn1938. Copyright: COPYRIGHT 2006 Nature Publishing Group) (22).

Although ion channel conformations and distributions differ among different neuronal types, a general overview of ion channel distribution along a neuronal membrane can be demonstrated as in Figure 1. Received excitatory and inhibitory inputs in the somatodendritic region are summated and cause membrane potential changes at the axon initial segment where voltage-gated sodium and potassium channels are located and determine the threshold for action potential generation. When the threshold is reached, upon the corresponding activity of these channels, an action potential is generated and propagated further along the axon. Once it reaches the axon terminals, activation of voltage-gated calcium channels causes calcium influx, resulting in

neurotransmitter release from the terminals. In addition, voltage-gated potassium channels and hyperpolarization-activated cyclic nucleotide-gated cation channels on dendrites control action potential back propagation affecting synaptic plasticity (22).

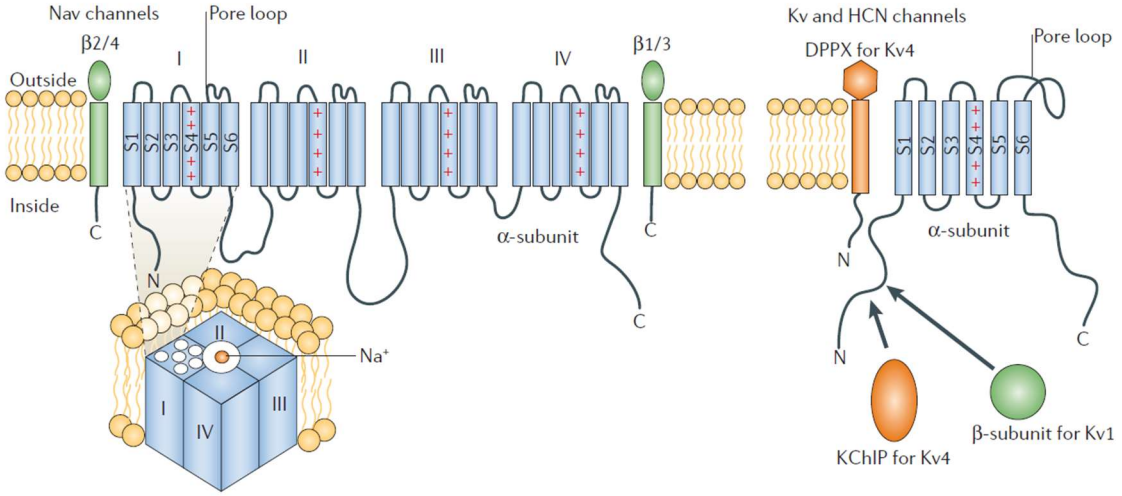

Figure 2| General structural topology of voltage-gated sodium and potassium channels. Voltage-gated sodium channels are formed from a single polypeptide consisted of for domain each possessing six transmembrane segments. Voltage-gated potassium channels as well as hyperpolarization-activated cyclic-nucleotide-gated cation channels have four alpha subunits. Kv1 channels possess cytoplasmic ß-subunits in interaction with the N-terminal T1 domains. (Reprinted from Lai, H., Jan, L. The distribution and targeting of neuronal voltage-gated ion channels. Nat Rev Neurosci 7, 548–562 (2006), https://doi.org/10.1038/nrn1938. Copyright: COPYRIGHT 2006 Nature Publishing Group) (22).

Voltage-gated ion channels possess specific sequence motifs not only for ion selectivity but also for their targeting. They have either one alpha subunit which is a long polypeptide that contains four repeats of domains, as in the cases of Na_V and Ca_V, or four alpha subunits as in the cases of K_V and HCN channels (see Figure 2). In either case, a single alpha subunit domain contains six helical transmembrane segments. The fourth segment has multiple positively charged arginines which cause conformational changes in response to changes in membrane potential, hence this segment functions as a voltage sensor. The fifth and the sixth transmembrane segment of alpha-subunits, together with the re-entrant loop in between – which is the narrowest part of the pore, forms the pore region of the channel. Interaction between the alpha subunits and auxiliary subunits (α2, β, γ or δ), depending on the channel type, modify the channel function and enables targeting of the channels to specific neuronal compartments (22).

There are ten genes that encode alpha subunits of Na_V channels, namely $Na_V1.1$ to $Na_V1.9$ and Na_X, and four genes that encode Na_V protein ß-subunits while there are

approximately 40 genes for K_V channel alpha subunits that are grouped into 12 families, namely K_V1 to K_V12 (22). Channel diversity is further enhanced by homo- and hetero-tetrameric composition of K_V channels formed within these families.

2.2.1 Voltage-gated potassium channel $K_V1.2$

The voltage-gated potassium channel $K_V1.2$, encoded by the *KCNA2* gene, is the mammalian orthologue of the *Shaker* channel which has been extensively studied in *Drosophila Melanogaster*. Since the first time the channel was cloned in 1987 (23), studies on *Shaker* channels have provided valuable insights on K_V1 channels' gating, permeability and structure. As the homology between the $K_V1.2$ and *Shaker* channels is very high, having 66% match in their voltage sensor domain for example, most of the information we have on $K_V1.2$ channels have been derived from the findings on *Shaker* channels (24).

In mammalian brain, K_V1 channels are found in the axons and synaptic terminals of neurons as well as at juxtaparanodal regions of myelinated neurons (25,26). K_V1 channels have also been shown to be present in the somatodendritic regions of some neurons, for example in mitral cells in the mouse olfactory bulb (27).

Although a precise mechanism of K_V1 channels' targeting has yet to be elucidated, there is a fair amount of information regarding K_V1 subunits' interaction and colocalization with other proteins as well as motifs, which play a role in axonal targeting, channel trafficking and the clustering (see Figure 3). For example, N-terminal T1 domain initiates tetramerization of α-subunits and it is also essential for axonal targeting which is specific to a neuronal type (28). The T1 domain also regulates the interaction between $K_V\beta1$ and $K_V\beta2$ subunits and $K_V1.1$, $K_V1.2$ and $K_V1.4$ α-subunits (25,29,30). $K_V\beta$ subunits have been shown to promote axonal targeting and surface expression of Kv1 channels (31,32). K_V1 channels also have endoplasmic reticulum export or retention motifs, which in combination regulate surface expression. For example; $K_V1.2$, due to its VXXSN motif, is distributed along both ER and surface membranes (33,34). $K_V1.2$ has also an endocytic motif YXXϕ that regulates surface expression without guiding targeting of the channel (35). Other known binding proteins that regulate K_V1 channel trafficking are calnexin and synapse-associated proten-97 (SAP97). Calnexin, being an ER chaperone involved in folding and assembly of membrane proteins, regulates surface expression of $K_V1.2$

while SAP97, a membrane-associated guanylate kinase, inhibit trafficking of K_V1 channels by retaining the α-subunits in ER-derived vesicular structures (36).

Figure 3| Scheme of voltage-gated K_V1 channels and their interaction with auxiliary proteins. Tetrameric channels are shown as four ovals representing four subunits. N- and C- termini are shown only for one subunit. The protein and motifs involved in targeting, trafficking and retention of the channels are shown. For axonal targeting, interaction between T1 tetramerization domain in the N terminus and Kvß is crucial. For clustering and anchoring, binding of an extreme C-terminal PDZ binding motif to postsynaptic density protein-95 is important. Surface expression is regulated via several motifs; an endoplasmic reticulum (ER) retention motif, ER export motif, endocytic motif. For clustering, association of K_V1 channels with contactin-associated protein-2 (CASPR2), transient axonal glycoprotein (TAG1) and 4.1B might play a role. Interaction proteins are indicated in green while the motifs are in red, in this figure. (Reprinted from Lai, H., Jan, L. The distribution and targeting of neuronal voltage-gated ion channels. Nat Rev Neurosci 7, 548–562 (2006), https://doi.org/10.1038/nrn1938. Copyright: COPYRIGHT 2006 Nature Publishing Group) (22).

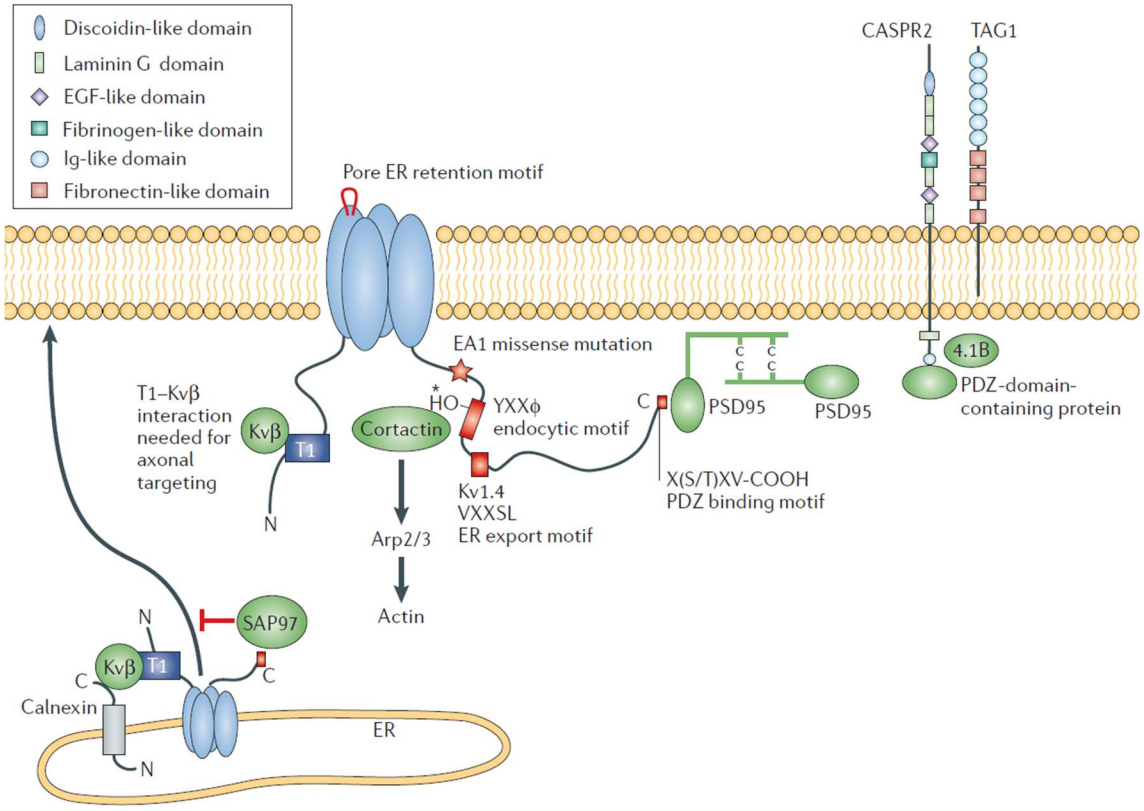

2.2.1.1 $K_V1.2$ structure

The pore domain of the $K_V1.2$ has a signature sequence "TVGYG" which is highly conserved among K_V channels, even among those from other species. In addition to that, K_V1 channels have a highly conserved region of ~120 amino acids within the N-terminal cytoplasmic domain T1. This domain has been known to play a role in subunit tetramerization as well as subfamily-specific channel assembly (37–39). Further experiments performed on T1 domain revealed that it also plays a role in channel gating

as changes in membrane potential causes conformational changes not only in the transmembrane segment but also in T1 domain (40).

Initial information regarding the structure of K_V channels were obtained from prokaryotic K+ channels as it was easier to express them in *Escherichia coli* to study (41). However, despite the conserved pore region and certain other domains, eukaryotic K_V channels possess unique features that do not exist in prokaryotic cells. To shed light on K_V1.2 structure, Long et. al. co-expressed the rat K_V1.2 channel together with the ß2 K+ channel ß subunit in the yeast *Pichia pastoris* to reveal the crystal structure of the channel. The resulting K_V1.2 complex with four-fold symmetry is shown in Figure 4, indicating four subunits of the channel with distinct colors. According to their model, the T1-S1 linker region has a spacer role between the transmembrane pore and intracellular regions. It's been also found that the alpha helices of the pore region (S5-S6) have an unexpected orientation in relation to the alpha helices of the voltage sensor (Figure 4B). Moreover, the voltage sensor has been found to position around the pore region of the adjacent subunit (Figure 4C). The S4-S5 linker that connects the pore and the voltage sensor of a given subunit is aligned parallel to the membrane surface at the level of inner-helix bundle crossing. The inner helix bundle was earlier defined as the right-handed bundle of four inner helices (42). This structure is crucial as it forms expandable constriction for opening and closing of the pore.

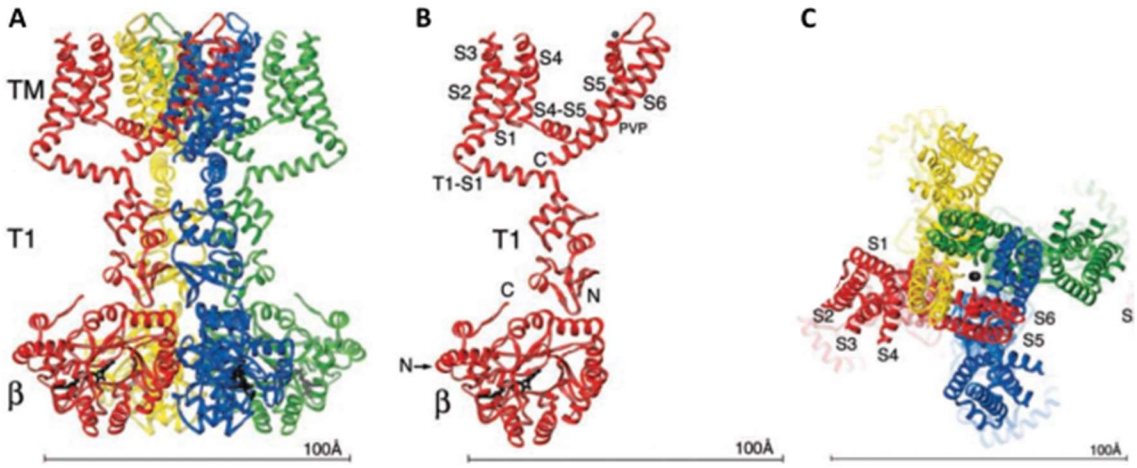

Figure 4| The Kv1.2–ß2 subunit complex. (A) Stereoview of ribbon representation of the four subunits of the K_V1.2 complex including T1 domain, pore and voltage sensor, from the side with intracellular solution below and extracellular solution above. All subunits are colored differently. (B) A single subunit of the channel together with the corresponding ß subunit from the side. Transmembrane segments (S1-S6), the Pro-Val-Pro sequence in S6 (PVP), N and T terminals are indicated. (C) Ribbon representation of the channel complex from above, with unique colors

representing different subunits. (Reprinted from Long SB, Campbell EB, Mackinnon R. Crystal structure of a mammalian voltage-dependent Shaker family K+ channel. Science. 2005 Aug 5;309(5736):897-903. doi: 10.1126/science.1116269. Epub 2005 Jul 7. PMID: 16002581. Reprinted with permission from AAAS) (43).

2.2.1.2 K_V1.2 function and expression

In general, voltage-gated potassium channels, by means of their K^+ selective pores, allows the movement of K^+ ions to repolarize the membrane toward the equilibrium potential for K^+. Hence, they substantially contribute to electrical properties of neurons; they influence subthreshold properties like resting membrane potential as well as membrane resistance, amplitude and frequency of sub-threshold oscillations, probability of spike generation as well as responsiveness of neurons to synaptic inputs. They help shaping postsynaptic potentials and determine repolarization of the action potential, spike shape and frequency (44).

Voltage-gated potassium channels differ greatly in their voltage-dependence and kinetic properties as well as their differential expression in neurons. This diversity contributes to the variable electrical properties of neuronal populations.

Although most studies reported that the K_V1.2 channels have fast activation kinetics, with half activation voltages ranging from -43 mV to -15 mV (45–47), Grissmer et. al. showed slower activation of K_V1.2 channels with a half activation level at +27 mV and even slower kinetics with a half activation at +40 mV during repetitive firing (48). Later Rezazadeh et. al. supported these observations showing that the activation kinetics of K_V1.2 channels are variable when expressed in mammalian cell systems. The K_V1.2 channels possessed two distinct gating modes, with half-activation values ranging from -40 mV to +30 mV. The channels' slow gating was associated with a half activation at +16.6 mV, whereas fast gating at -18.8 mV. Heterogeneity of the activation kinetics of the heterologously expressed K_V1.2 channels was not observed only in cell-to-cell comparisons but also pulse-to-pulse. The switch between the slow and fast gating modes was reported to be enabled by a single threonine residue in the S2-S3 linker, which is unique in K_V1.2 among the K_V channels (49).

K_V1.2 can form both homo-tetramers as well as hetero-tetramers with other K_V1 family subunits. Although our knowledge regarding K_V1.2-containing channel composition and expression as well as differential distribution and localization of these channels in

human neurons is still very limited, there have been several studies that investigated especially K_V1.1-K_V1.2 and K_V1.1-K_V1.4 tetramers so far.

In different studies, expression of K_V1.1-K_V1.2 tetramers in juxtaparanodal regions of the node or Ranvier have been reported, suggesting that these channels play a role in saltatory conduction (50–52). This finding has been supported by Rhodes et.al., showing the expression of K_V1.1-K_V1.2 tetramers in juxtaparanodal regions of the node or Ranvier as well as in the axon terminals in cerebellar basket cells of rats (30).

Gu et al. have shown that K_V1.2 channels are targeted to the tau-positive axons of cultured hippocampal neurons while being only weakly expressed in the distal dendrites. Interestingly, they have also proven that the T1 domain was responsible for axonal targeting as well as surface expression of the channels (35). Another important contribution came from Inda et. al., who studied the expression of K_V1.2 channels in human brain tissue and identified their expression in the axon initial segment of human cortical pyramidal cells (53).

Upon the detection of K_V1.1-K_V1.2 tetramers in axon terminals of basket cells in mouse cerebellum (52), in the electron micrographs of hippocampus and cerebellum K_V1.1-K_V1.2 tetramers were confirmed to be expressed at or near synaptic zones. This finding suggested a role for repolarization of the membrane at synaptic terminals and regulation of neurotransmitter release (27). In more recent studies, K_V1-mediated currents have been recorded in electrophysiological experiments in synaptic terminals of hippocampal and cerebellar neurons of rodents (54,55). Robbins and Tempel also showed that K_V1.2 subunits form complexes with K_V1.1 subunits in cerebellar basket terminals, at juxtaparanodal regions and axon initial segments of myelinated axons (56).

Moreover, very early studies showed that in some neurons, for example neurons of cerebellar nuclei in guinea pigs (57), cortical pyramidal cells of cats (58), mitral and tufted cells of the olfactory bulb of salamander (59), K_V1.1-K_V1.2 tetramers were found in cell somata, suggesting a role in excitability of cell soma. These channels are, hence, thought to determine the shape of action potentials, regulate discharge patterns like inter spike intervals and burst frequencies.

The K_V1.2 subunits has also been identified to form hetero-tetramers with the K_V1.4 subunits, Especially in the neuropil of the cerebral cortex, the terminal fields of the

hippocampus and axon tracts of the *corpus callosum.* Additionally, co-localization of these subunits has been detected in the mossy fiber tract of the hippocampus, particularly at the terminals (60).

2.3 Induced Pluripotent Stem Cells

Induced pluripotent stem cells are a type of pluripotent stem cells that are genetically reprogrammed from adult somatic cells. For the first time in history, mouse embryonic and adult fibroblast cells were reprogrammed into pluripotent stem cells by Takahashi and Yamanaka in 2006. They succeeded this conversion via forced expression of four factors, now so-called Yamanaka factors, Oct3/4, Sox2, c-Myc and Klf4. Oct3/4 and Sox2 are core transcription factors that have roles in maintaining pluripotency in embryonic stem cells while c-Myc and Klf4 are tumor-related factors which could not have been replaced by any other oncogenes for reprogramming purpose (61). This exciting breakthrough was followed immediately by Lowry et. al., confirming the applicability of the reprogramming method in human cells as well. They achieved reprogramming human fibroblasts into induced pluripotent stem cells using the same method (62).

To understand how brain functions in disease and in health, billions of its cells and trillions of its synapses have been studied in brain regions of interest in animal models. Nevertheless, to what extend the information obtained from animal models translate to human brain is a challenging question. Several studies have already proven species-specific differences of the functional and structural properties of pyramidal neurons (63). Human neocortex is known to be thicker, contain more white matter and larger neurons, as well as more synaptic connections (63–65). Such differences put emphasis on the challenges of translating the knowledge acquired from other animal models to humans and the need to model brain diseases using human models. However, due to ethical concerns, research on primary human brain tissue from healthy and living subjects is very limited while the access to post-mortem brain tissue is very restricted. The human samples are available only at the end stage of a disease or post-mortem. They are not only extremely limited, but also not useful for observation of pathological development. In contrast, the use of induced pluripotent stem cells has key advantages. The iPSCs possess the same genomic materials as the patients and are an unlimited

source for investigation of pathological mechanisms as well as development of new therapies.

Following the first discovery of iPSC technology, many methods have been developed to generate various cell types from induced pluripotent stem cells, including different types of neurons (66,67). Patient iPSCs have been used to model multiple epilepsy-related neurodevelopmental diseases so far, such as Dravet Syndrome, Angelman Syndrome and *STXBP1*-associated EEs. These models provided opportunities for identification of some new mechanistic pathways as well as compensatory mechanisms (68–70).

2.3.1 Neurogenin-2 based neuronal differentiation

Induced pluripotent stem cells have been successfully differentiated into neurons of mammalian brain, using various differentiation methods in the last years (66,67,71). Most of these methods were developed based on what's known about the development of human brain and the use of transcription factors and small molecules in a temporally systemic way to mimic developmental stages of brain, pushing the cells from one state to the next. Nevertheless, these protocols that require months to generate functional neurons have been suboptimal and prone to result in high variability and low yields of desired neurons (72). Therefore, there has been a need for a fast and efficient method for generation of functional mature neuronal networks. Simplifying existing neuronal differentiation protocols, a rapid and robust protocol that yields highly homogenous cortical neurons has been suggested by two different groups. Zhang et. al., 2013 showed that overexpression of a single transcription factor Neurogenin-2 can generate a neuronal network with robust synapse formation capabilities (72). Just a year later, Busskamp et. al. suggested that the combination of Neurogenin-1 and Neurogenin-2 homogenously generate functional bipolar neurons within 4 days (73). RNA sequencing and miRNA profiling of differentiating cells over time indicated that Neurogenin-mediated neuronal differentiation occurs indirectly via unstable progenitor states. Through activation and inhibition of various pathways and other transcription factors, overexpression of NGN2 regulate differentiation of glutamatergic neurons and the resulting neurons express cortical markers DCX, NEUN, OLIG2, SOX1, TUJ1, MAP2 and VGlut1/2 and lack the expression of the GABAergic marker GAD1 (72). They were classified as glutamatergic excitatory neurons since they express the layer II and III

cortical markers BRN2, CUX1, and FOXG1. Nevertheless, they lack the expression of cortical layer VI markers TBR1 and FOG2. Upon the protocol establishment and first characterization of the NGN2-induced neurons, co-culture of these cultures with rodent astrocytes has proven the necessity of glial cells for long term maintenance of the neuronal cultures as well as synaptic formation and network maturity (74).

2.4 Aim

Within this thesis, the main objective was to understand the disease mechanism of DEE caused by the recently identified *KCNA2* mutations, using human iPSC-derived neuronal cultures. As the functional outcomes of the *KCNA2* mutations on the K_V1.2 channel function were assessed earlier and the mutations were classified into three groups, causing gain-, loss- or combined gain- and loss-of-function effects, in this thesis mutations from all three groups were examined. Effects of these mutations on the physiological features of the iPSC-derived neurons were examined on both single cell and network level.

Specific aims were as follows:

(I) The functional outcomes of the *KCNA2*-T374A mutation, that was identified in the patients with the most severe DEE phenotypes and found to cause both gain- and a very strong dominant-negative loss-of-function effect on K_V1.2 channel function, were investigated on a single cell level during the first four consecutive weeks of iPSC-derived neuronal development. To do so, both patient- and healthy individual-derived iPSCs were differentiated into neurons, using the Neurogenin-2 overexpression method, and electrophysiological investigation of the resulting neurons was performed using the patch-clamp technique. Active and passive electrical properties of the patient-derived neurons were compared to those of the healthy individual-derived neurons, to reveal pathological features of the patients during neuronal development, that would help us to understand the disease mechanism.

(II) To understand how the mutations with different functional effects on the channel function cause DEE, four different patient iPSC-derived neuronal cultures carrying mutations from all three functional groups, *KCNA2*-R297Q (GOF), *KCNA2*-L328V (GOF plus less strong LOF), *KCNA2*-T374 (GOF plus very strong LOF) and *KCNA2*-P405L (LOF), were investigated on a network level. Electrophysiological features of the neuronal networks were assessed using multielectrode arrays for six consecutive weeks after the start of the neuronal differentiations, to detect the pathologically different features of

the patient-derived neuronal networks compared to the networks derived from the healthy individuals.

(III) As 4-Aminopyridine has been used in the clinical study where the patients carrying GOF mutations clinically improved, to understand how this drug improved the clinical phenotypes the effects of 4-AP on the neuronal networks were examined, using multielectrode array recordings. How 4-AP altered the bursting features of the patient- vs. healthy individual-derived networks was assessed, to reveal pathological features of the patient-derived networks, reversed by the 4-AP treatment.

(IV) To be able to explain the network behavior of the patient-derived neurons, showing differences compared to the healthy neurons, electrophysiological features of the patient-derived neurons carrying mutations from all three different functional groups as well as healthy individual-derived neurons were investigated also on a single cell level, at two different time points as the networks showed distinct features at these different time points. The active and passive electrical parameters of the single neurons were assessed to explain the distinct features observed in the patient-derived networks on a network level.

3 METHODS AND MATERIALS

3.1 Cell culture

3.1.1 Reprogramming of fibroblasts via viral transduction

Skin biopsies were obtained from the patients with DEE, with identified *KCNA2* mutations p.Leu328Val (L328V), p.Thr374Ala (T374A), p.Arg297Gln (R297Q) or p.Pro405Leu (P405L). The consents for the cell donations were obtained from the parents of the donors and were approved by the Ethics Committee of the Medical Faculty of the University Hospital Tübingen.

The patient with the p.Leu328Val (c.982T>G) mutation presented with febrile SE at the age of 6 months, which was followed by absence seizures, atonic seizures and GTCS. He has manifested psychomotor developmental delay, ataxia, severe ID as well as mild cerebellar atrophy (Masnada, Hedrich et al. 2017b).

The patient with the p.Thr374Ala (c.1120A>G) mutation presented with focal myoclonic seizures since birth as well as almost no development. Since birth, he has hypotonia, cannot turn around, has no eye contact, no language acquisition and almost no reaction to interactions (11).

The patient with the p.Arg297Gln (c.890G>A) mutation presented with febrile SE at the age of 5 months and consequently with absences as well as GTCS. He has manifested moderate-severe ataxia, hyper-reflexia and moderate ID (8).

The patient with the p.Pro405Leu (c.1214C>T) mutation presented with febrile SE at the age of 8 months, which was followed by focal motor seizures and secondary GTCS. He has manifested moderate ID and delayed speech development (8).

Cultivation and reprogramming of fibroblasts into induced pluripotent stem cells were performed by the lab technician.

3.1.1.1 Preparation and cultivation of human fibroblasts

Biopsy procedure yielded a skin sample with a diameter of around 5 mm. After the removal of fat and epidermis tissues, the remaining tissue was washed in DMEM (Thermo Fisher Scientific, Darmstadt, Germany) supplemented with 20% FCS (Pan

BioTech, Aidenbach, Germany) and penicillin/streptomycin (1:10) (Biochrom, Berlin, Germany) and then cut into approximately 1-2 mm large pieces. These pieces were then laid and dried in a 35 mm^2 dish in sterile conditions for 20 minutes. Afterwards, they were flooded in DMEM with 20% FCS. Fibroblasts were observed to grow out of the skin patches 3-8 days later. Once the confluency of fibroblasts was reached, another round of fibroblast extraction was facilitated by transferring and culturing of the skin pieces in a new 35 mm^2 dish. The obtained fibroblasts were cultured and further expanded in T25 flasks in DMEM with 10% FCS. For storing backups, the cells were frozen in aliquots of 20-30x10^4 cells/ml in DMEM with 20% FCS and 5% DMSO (PanReac Applichem, Darmstadt, Germany).

3.1.1.2 Production of retroviruses

For the reprogramming of fibroblasts into induced pluripotent stem cells, the protocol suggested by Takahashi et. al., 2007 was followed. The retroviruses were produced in HEK293T cells which were transfected with the plasmids encoding viral components, envelope and matrix proteins (pCMV-VSV-G, Addgene, Cambridge, USA), a reverse transcriptase apparatus (pUMVC, Addgene, Cambridge, USA) and the genes to be expressed in fibroblasts (pMXs-h-OCT4 / -Sox2 / -Kfl4 / -c-MYC, Addgene, Cambridge, USA). For the transfection of HEK 293T cells, 32 µl of TransIT-2020 Transfection Reagent (Mirus, Wisconsin, USA) was incubated with 4.05 µg of pUMVC, 450 ng of pCMV-VSV-G, as well as 4.5 µg of each transfer gene construct in 1.2 ml of OptiMEM (Thermo Fisher Scientific, Darmstadt, Germany) for 20 minutes. Afterwards, transfection mix for each gene was added drop-wise onto HEK293T cells. After 24 hours, media change was performed, and the cells were given fresh culture medium consisted of DMEM with 10% FCS and 2mM L-Glutamine (PAN-Biotech, Aidenbach, Germany). On the second day after the transfection, the media in the flasks were harvested and centrifuged for 5 minutes at 1200 rpm to separate the supernatant for filtering into a VIVASPIN tube (Stemcell Technologies, Köln, Germany) using 0.45 µm PVDF filter. Centrifugation at 4000 rpm for further 40 minutes at 4 °C yielded a supernatant with the viruses produced.

3.1.1.3 Retroviral transduction of human fibroblasts

30-50x10^4 fibroblasts per well were seeded in one well of a six-well plate in DMEM with 10% FCS. The next day, the fibroblasts were transduced with the produced retroviruses

with vectors expressing OCT4, Sox2, Kfl4 and c-MYC genes in presence of 6 mg/mL protamine sulphate. The transduction was performed twice and then the fibroblasts were cultured on mouse embryonic fibroblast (MEF) feeder cells.

3.1.1.4 Generation of iPSCs from fibroblasts

Transduced fibroblasts were maintained on MEF feeder cells in hESC medium supplemented with 1 mM valproic acid (Sigma Aldrich, Darmstadt, Germany) and the medium was refreshed daily until stem cell colonies appeared. hESC medium was composed of Knockout DMEM (Thermo Fisher Scientific, Darmstadt, Germany), 20% Knockout Serum Replacement (Thermo Fisher Scientific, Darmstadt, Germany), 0.1 mM beta-mercaptoethanol (Sigma Aldrich, Darmstadt, Germany), 1% penicillin/streptomycin (Biochrom, Berlin, Germany), 1% glutamine (Biochrom, Berlin, Germany), 1% nonessential amino acids (Biochrom, Berlin, Germany) with 5 ng/mL human basic Fibroblast Growth Factor 2 (FGF2) (PeproTech, Hamburg, Germany). Valproic acid was discontinued as soon as the first iPSC colonies were observed. Emerging iPSC colonies were mechanically transferred onto MEF layer in a new plate.

3.1.2 Karyotyping

For karyotyping of the newly generated induced pluripotent stem cell lines, the cells were passaged onto slide flasks (Nunc™ Lab-Tek™ Flask on Slide, Thermo Fisher Scientific, Darmstadt, Germany), as a mixture of single cells and small colonies. The flasks were then submitted to the Institute of Medical Genetics and Applied Genomics of Tübingen University for karyotyping analysis.

3.1.3 Maintenance of iPSCs in culture

Early passages of iPSC colonies were maintained on MEF layer up to passage 10. Afterwards, iPSC colonies were passaged onto Matrigel-coated (BD Biosciences, Heidelberg, Germany) wells in 6-well plates at 37°C temperature and 5% CO^2 level. From then on, iPSCs were always maintained in mTeSR™1 medium (Stemcell Technologies, Köln, Germany). The medium was refreshed daily during weekdays and over weekends mTeSR™1 medium supplemented with StemBeads FGF2 (Stem Cultures, Offenbach, Germany). Once the confluency was reached the passaging of cells was performed

mechanically, transferring small pieces of colonies into new wells which were coated with Matrigel for 1 hour at 37°C.

3.1.4 Preparation and cultivation of mouse astrocytes

Cortices of E17.5 mouse pups were dissected to obtain mixed cortical glial cultures, following the protocol by Schildge et. al., 2013 (76). Glial cultures were maintained in PDL-coated (Sigma Aldrich, Darmstadt, Germany) T75 flasks at 37°C temperature and 5% CO^2 level. Glial culture medium consisted of DMEM with high glucose (Thermo Fisher Scientific, Darmstadt, Germany) containing 10% Fetal Calf Serum (Pan BioTech, Aidenbach, Germany) and 1% Penicillin/Streptomycin (Biochrom, Berlin, Germany), and was refreshed every three days. 12-15 days after the isolation of glial cells, confluent flasks were shaken on an orbital shaker for 1 hr at 200 rpm at 37°C to detach the microglia, followed by overnight shaking at 200 rpm at 37°C to detach oligodendrocyte precursor cells. Alternatively, the flasks were vortexed for 3-5 minutes to remove microglia and oligodendrocyte precursor cells at the same time. Remaining astrocyte monolayer was trypsinized with 0.02 % Trypsin (Biochrom, Berlin, Germany) for passaging onto new T75 flasks freshly coated with 100 µg/ml PDL. The enriched astrocyte cultures were maintained in the same glial medium as before. For each experiment, 3-5 days before the start of co-culturing with neurons, the astrocytes were trypsinized and re-plated on Matrigel-coated 13 mm coverslips in 24-well plates with the density of $4x10^4$ cells per coverslip, on Multi-well Multielectrode Array plates with the density of $4x10^4$ cells per well.

3.2 Differentiation of human induced pluripotent stem cells into neurons

3.2.1 Generation of stable S-NGN2-iPSC lines

To integrate the NGN2 transgene in the safe harbor region of the iPSC lines, the Crispr-Cas9 gene editing method was used. The plasmid pAXT2 (Addgene plasmid #80494) containing the sequences for Cas9 protein and sgRNA-T2 (5’ ggggccactagggacaggat 3’) targeting the AAVS1 region and the plasmid pUCM-AAVS1-TO-hNGN2 (Addgene plasmid #105840) containing the NGN2 and rTTA sequences flanked by the AAVS1 homology arms were obtained from Addgene. Upon the receival of the plasmids in bacterial stab culture format, to isolate an individual clonal population from the stock LB agar plates

were streaked. After incubating the plates overnight at 37 °C, single colonies were picked with pipette tips and dropped in 8 ml of LB medium containing Ampicillin. Bacterial cultures were grown overnight at 37 °C on a shaker. The next day, before extracting the plasmids, glycerol stocks were prepared for each clone, mixing 500 µl of bacterial culture with 500 µl of 87% Glycerol. Glycerol stocks were transferred to -80°C immediately for long term storage. For the plasmid extraction from the remaining culture ExtractMe MiniPrep Kit was used following the manufacturer's guideline. The culture was taken into Eppendorf tubes and spinned at 5500 rpm for 5min. The pellet was resuspended in 250 µl of Resuspension buffer and mixed by inversion of the tube for several times. After incubating the mixture at room temperature for 2 min, 350 µl of Neutralization buffer was added and mixed. The mixture was spinned at 12000 rpm for 10 min. Resulting supernatant was taken into minicolumn provided by the kit and spinned at 11000 for 1 min. After discarding the flow through the column was washed with 750 µl of Wash buffer and spinned at 11000 for 1 min. To remove all the remaining EtOH, the column was spinned for another 2 min at 13000 rpm. After placing a new Eppendorf tube underneath the column, 30 µl Elution buffer was directly added onto the membrane to elute the plasmid DNA. After incubating it for 2 min at room temperature, the column was spinned at 11000 rpm for 1 min. The obtained plasmid DNA was measured at Nanodrop and sequenced to confirm the lack of unexpected mutations for both plasmids.

iPSCs were grown to sub-confluency and harvested in a single cell suspension. The cells were treated with 10 uM Apoptosis Inhibitor 1 hour before getting detached by Accutase (Pan BioTech, Aidenbach, Germany) and collected in single cell suspension. Using hemocytometer, the cells were counted and the appropriate volume containing 400.000 cells was centrifuged in a separate sterile vial and the cell pellet was resuspended in 20 µl of P3 Primary Cell 4D-Nucleofector™ X solution (Lonza, Basel, Switzerland). I µg of each pUCM-AAVS1-TO-hNGN2 and pXAT2 plasmids were added to the suspension and the mixture was transferred into a well of 16-well Nucleocuvette® Strips. The cells were electroporated using the embedded program CM 130 of Lonza 4D Nucleofector (Lonza, Basel, Switzerland). After the electroporation the cell suspension was mixed with warm mTeSR with 10 µM Apoptosis Inhibitor and plated on a well of 6-well tissue culture plate. Apoptosis Inhibitor was discontinued the next day. Once the

culture reached confluency corresponding antibiotics were added in the culture medium for selection of electroporated cells for up to a week. Selected lines stably expressing NGN2 gene under the TeT-ON promoter were expanded to be used in further experiments.

3.2.2 Differentiation of stable S-NGN2-iPSC lines into neurons

For all electrophysiological experiments, neurons were co-cultured with mouse astrocytes either on 13-mm glass coverslips in 24-well tissue culture plates or on MW-MEA plates (Multi Channel Systems MCS GmbH, Reutlingen, Germany). For this purpose, mouse astrocytes were plated with the density of 40.000 cells/well for both tissue culture and MW-MEA plates 2-3 days earlier than neuronal differentiation start. On the day of differentiation, stable S-NGN2-iPSC cultures were treated with 2.5 µg/ml doxycycline (Sigma Aldrich, Darmstadt, Germany) to induce Neurogenin-2 expression 5 hours before plating. 1 hour prior to plating, the cells were treated with 10 µM apoptosis inhibitor (Tocris Bioscience, WiesbadenNordenstadt,Germany) to enhance viability. For detachment, the cells were treated with Accutase (Capricorn, Ebsdorfergrund, Germany) for 20 min and triturated to get single cells. After counting, the induced cells were plated with the density of 60.000 cells/well on glass coverslips and 40.000 cells/well in MW-MEA plates in neuronal culture media (NCM) containing 1 µg/ml doxycycline, 10 µM apoptosis inhibitor and 3 µM DAPT (Tocris Bioscience, Wiesbaden-Nordenstadt,Germany). The next day, the culture medium was changed to NCM containing 1 µg/ml doxycycline, 10 µM DAPT and 10 µM PD (Tocris Bioscience, Wiesbaden-Nordenstadt,Germany). After day 5 in culture, the media was refreshed with only NCM by every 2-3 days. NCM medium consisted of 47% Neurobasal medium, 47% DMEM/F12, 2% B27 supplement, 1% N2 supplement, 1% Glutamax, 1% Penicillin/streptomycin and 1% nonessential amino acids (all from Thermo Fisher Scientific, Darmstadt, Germany).

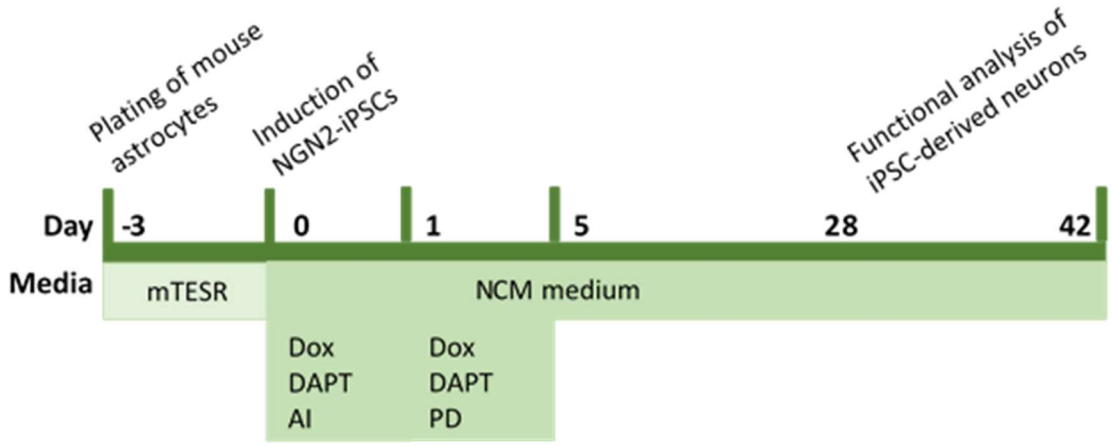

Figure 5| Experimental timeline of the neuronal differentiations. For both patch-clamp and multielectrode array experiments, mouse astrocytes were plated on coverslips or MEAs three days before the induction of Neurogenin-2. On the day of induction, iPSCs were incubated in neuronal culture medium (NCM) supplemented with doxycycline, DAPT and AI for one day, and dox, DAPT and PD during the next four days. Recordings were then performed at ever week time points until week six.

3.3 Immunohistochemistry

For immunostaining of the samples, cells to be stained were washed once with DPBS (+/+) (Thermo Fisher Scientific, Darmstadt, Germany) containing $CaCl_2$ and $MgCl_2$ before being fixed with 4% paraformaldehyde solution (Morphisto, Frankfurt Am Main, Germany) for 20 minutes at room temperature. After fixation they were washed three times with DPBS (-/-) and either stored in DPBS (-/-) in a cold room or continued with the staining protocol. The cells were permeabilized in DPBS (-/-) containing 10% normal goat serum (NGS) (Sigma Aldrich, Darmstadt, Germany) and 0.2% Triton X-100 (Sigma Aldrich, Darmstadt, Germany) for 1 hour at room temperature. Primary antibodies were diluted in DPBS (-/-) containing 1% NGS and 0.02% Triton X-100 and the cells were incubated in primary antibody solution overnight at 4°C. On next day, the cells were washed three times with DPBS (-/-) and then incubated in fluorescently labeled secondary antibodies diluted in DPBS (-/-) containing 1% NGS and 0.02% Triton X-100 for 1 hour at room temperature in dark. In the end, the cells were washed again with DPBS (-/-) three times and the coverslips were mounted on glass slides using DAPI-fluromounting medium (Southern Biotech, Birmingham, USA). All the primary and secondary antibodies used in this project are listed below in Table 2.

Table 2| The list of primary and secondary antibodies used in immunohistochemistry.

Antibody against	Species	Company	Dilution
Primary Antibodies			
Sox2	Rabbit	Abcam, Cambridge, UK	1:500
Oct4	Rabbit	Abcam, Cambridge, UK	1:1000
Tra1-60	Mouse	Abcam, Cambridge, UK	1:500
SSEA-4	Mouse	Abcam, Cambridge, UK	1:500
MAP2	Chicken	Abcam, Cambridge, UK	1:2000
Secondary Antibodies (Alexa Flour)			
Anti-mouse IgG 488	Goat	Thermo Fisher Scientific, Darmstadt, DE	1:500
Anti-rabbit IgG 555	Goat	Thermo Fisher Scientific, Darmstadt, DE	1:500
Anti-chicken IgG 647	Goat	Thermo Fisher Scientific, Darmstadt, DE	1:500

3.4 RNA isolation and quantitative Real-Time Polymerase Chain Reaction

To isolate bulk RNA from induced pluripotent stem cells the ISOLATE II RNA Mini Kit (Bioline, Luckenwalde, Germany) was used following the manufacturer's guideline. Using a lysis buffer containing 1% β-Mercaptoethanol the cells were lysed and the lysate was filtered and mixed with ethanol. The lysis mixture was then loaded into mini columns provided in the kit so that RNA binds to the column. After silica membrane was desalted and DNA was digested, the sample was washed three times with washing buffer. RNA was eluted in the end using RNAase-free water. RNA was converted to DNA using reverse transcriptase. To do so, RNA was incubated with reverse transcriptase for 30 min at 50°C. The enzyme's activity was stopped by 15 min incubation at 90°C.

For the characterization of the newly generated induced pluripotent stem cells, expression level of viral genes used for reprograming as well as endogenous Nanog expression of iPSCs were determined performing real time polymerase chain reaction (qRT-PCR). For each gene examined, expression levels were normalized to the housekeeping gene GAPDH. For qRT-PCR experiments QuantiTect SYBR Green Kit (Qiagen, Hilden, Germany) was used following the manufacturer's instructions. The ABI7000 Lightcycler device (Applied Biosystems, Thermo Fisher Scientific, Darmstadt,

Germany) was used to run a program consisting of 35 cycles of 15 seconds at 95°C, 30 seconds at 54°C and 30 seconds at 72°C. The sequences of primers used in silencing qRT-PCR experiments are listed below in the Table 3.

Table 3| Forward and reverse primer sequences used in silencing qRT-PCR.

The gene of interest	Forward primer seq. (5´-3')	Reverse primer seq. (5´-3')
viral OCT3/4	ccccagggccccattttggtacc	ttatcgtcgaccactgtgctgctg
viral Sox2	ggcacccctggcatggctcttggctc	ttatcgtcgaccactgtgctgctg
viral Klf4	acgatcgtggccccggaaaaggacc	ttatcgtcgaccactgtgctgctg
viral c-Myc	caacaaccgaaaatgcaccagccccag	ttatcgtcgaccactgtgctgctg
Nanog	cctgtatttgtgggcctg	gacagtctccgtgtgaggcat
GAPDH	ctggtaaagtggatattgttgccat	tggaatcatattggaacatgtaaacc

3.5 Genomic DNA extraction and Polymerase Chain Reaction

DNA was extracted from iPSCs using QuickExtract™ DNA Extraction Solution (Epicentre, Wisconsin, USA) according to manufacturer's instructions. Cells were incubated in the solution at 65°C for 6 min and then at 98°C for 2 minutes. Yielded solution containing PCR-ready DNA was directly used for PCR experiments.

To confirm the presence or absence of mutations in the patient or control iPSCs, the region of interest in the *KCNA2* gene was amplified using Phusion High Fidelity DNA Polymerase (Biozym, Oldendorf, Germany) according to the manufacturer's instructions, using the forward ('CCGAGGAGATGTGAGGGATT') and reverse ('GGTGTGACGTTGCTCTCCC') primers. The amplifying PCR program comprised of the initial step of 2 min at 95°C, followed by 60 cycles of 30 sec at 95°C, 30 sec at 60°C, 1 min at 72°C and last incubation step for 6 min at 72°C. Obtained PCR products were cleaned up with the SAP-exo mix (Jena Bioscience, Jena, Germany). The solution was added in PCR products in a 2:5 ratio and mixtures were incubated for 10 min at 37°C and for another 10 min at 80°C. Cleaned PCR products were sent to the GATC Biotech (Konstanz, Germany) for sequencing and the resulting sequences were analyzed using the CLC free Workbench 7 (Qiagen, CA, United States).

3.6 Electrophysiology

3.6.1 Patch clamp recordings

Whole cell voltage- and current-clamp recordings of IPSC-derived neurons were carried out at room temperature at consecutive weeks after the start of differentiations. Electrophysiological data were recorded using an Axopatch 200B amplifier (Molecular Devices, Sunnyvale, CA, USA) controlled by the Clampex 10.2 software. Recordings were filtered at 10 kHz and digitized at 10 kHz using a Digidata 1440A acquisition system (Molecular Devices, Sunnyvale, CA, USA). The analysis was performed offline using pClampfit 11.1 software (Molecular Devices, Sunnyvale, CA, USA). During the recordings, the bath solution, artificial cerebral spinal fluid (aCSF), consisted of 121 mM NaCl, 4.2 mM KCl, 29 mM NaHCO3, 0.5 mM Na2HPO4, 0.45 mM NaH2PO4 and 5 mM HEPES. Recordings pipettes were filled with intracellular solution consisting of 135 mM K-Gluconate, 4 mM NaCl, 0.5 mM CaCl2, 10 mM HEPES, 2 mM EGTA, 2 mM Mg-ATP and 0.4 mM GTP-Na. Osmolarity of the aCSF was adjusted to 300 mOsm and that of the intracellular solution to 310 mOsm, and pH was adjusted to 7.4 for both. Liquid junction potential was calculated as -15 mV and is not subtracted from the data. P/N leak subtraction was performed using the Clampex 10.2 software and the data are shown with leak subtraction.

To elicit inward and outward currents, after the whole-cell patch was formed on the soma of neurons, the voltage was clamped at -70 mV. Depolarization pulses from a holding potential of -70 mV to different potential levels, from -60 mV to +30 mV with 10 mV increments, for 24 seconds were applied as depicted in Figure 6A.

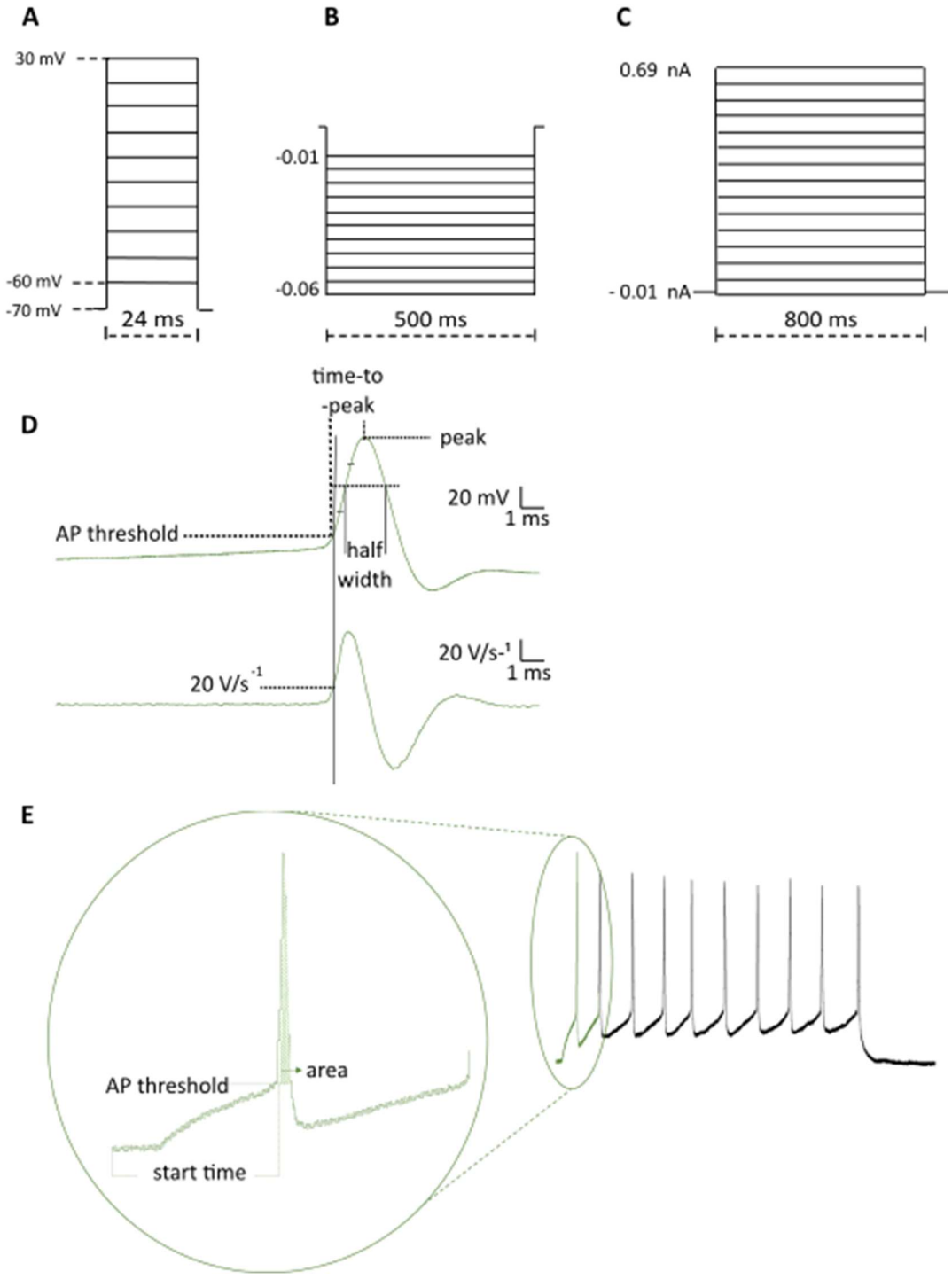

Figure 6| Waveform stimulations used for voltage- and current-clamp recordings and the analysis of single action potential parameters. (A) Stepwise depolarizing pulses from a holding potential of -70 mV in the voltage-clamp mode. (B) Stepwise current injections applied at resting membrane level of the neurons to measure input resistance. (C) Waveform stimulus displays for stepwise current injections in 0.005 nA steps, used to assess intrinsic firing activity of the neurons. (D) AP threshold voltage was calculated taking the first derivative of the first action potential generated in response to smallest current injections. Subsequently, AP amplitude, time-to-peak and half-width were calculated as shown. (E) The first action potentials fired in AP trains evoked in response to a range of depolarizing pulses were also used to assess single AP parameters, as well as start time and area.

The cells were recorded in a current-clamp gap free mode for 5 min to assess the spontaneous firing pattern as well as resting membrane potentials. To measure the input resistance, 500 ms long current stimulations from -0.01 nA to -0.06 nA were applied to each cell as shown in Figure 6B. The membrane potential was maintained around -70 mV under current-clamp conditions for the following recordings. To elicit single action potentials 1 or 2 ms long current pulses ranging from 0.1 to 0.775 nA in 0.075 nA increments were applied to the cells. The first elicited action potential was used to calculate rheobase, being the lowest injected current that was enough to generate at least one action potential, as well as the following single AP parameters. Action potential threshold was determined as the voltage at which dV/dt of the first action potential waveform generated reached 20 V/s^{-1}. Action potential time-to-peak duration was defined as the time needed to reach from the AP threshold to the AP peak. Action potential amplitude was defined as the change in membrane potential from the AP threshold to the peak while action potential half-width was defined as the width of an action potential at the half-amplitude level (Fig. 6D). To evoke action potential trains, stepwise current stimulations from -0.001 nA to 0.069 nA in 0.005 increments with a duration of 800 ms were applied (Figure 6C). Resulting action potential trains were used to create input-output curves of the neurons. Additionally, the first action potentials fired in these AP trains evoked in response to a range of depolarizing currents were also used to calculate single AP parameters, AP time-to-peak and half-width, as described earlier. In addition, single AP area was calculated as the area remaining under the AP waveform above the AP threshold level. AP start time was defined as the time duration from the start of a current stimulation to the threshold of the first evoked first action potential (Figure 6E).

3.6.2 Multi-well Multielectrode Array recordings

To record spontaneous network activity, 24-well Multi-well MEA plates (Multi Channel Systems MCS GmbH, Reutlingen, Germany) were used. Each well contained 12 gold electrodes (in 4x4 grid structure) on FR4 and 1 internal circular reference electrode. Recording electrodes had 100 µm diameter and 700 µm spacing between each other. Upon the induction of neuronal differentiation of S-NGN2 lines, the induced iPSCs were cultured in MW-MEA plates on top of previously plated mouse astrocytes. The neurons developing and forming networks in co-cultures with astrocytes were recorded at every

week up to six weeks, for 10 minutes following a 10 min of acclimatization period at 37°C. The raw signal, sampled at 10 kHz, was filtered with a low-pass fourth-order Butterworth filter with a 3500 Hz cutoff frequency and a high-pass second-order Butterworth filter with a 100 Hz cutoff frequency. Spike detection was performed via noise threshold method provided by the Multi-well Analyzer Software (Multi Channel Systems MCS GmbH, Reutlingen, Germany). For each recording, embedded algorithm was set to calculate the standard deviation from 50 different 100 ms long segments of raw data, and the threshold for spike detection was set at ±5 times standard deviation level.

Multi-well Analyzer Software was used for offline data analysis. Spike and bursting parameters were extracted using the software and further analysis to define the spontaneous network activity was performed using self-written scripts, in Python language using open-source software Jupyter Notebook. Neuronal networks with a mean firing rate (MFR) <0.1 Hz and a burst rate (BR) <0.4 bursts/min were excluded from analysis, based on the criteria that was set in earlier publications for the robust network activity of NGN2 neuronal populations (77). The wells that did not exhibit network burst activities after 4 weeks of development were also excluded.

The mean firing rate of the network was calculated as the average firing rate of the active channels in each well of the MEA. The random spike percentage was calculated as the percentage of spikes that belonged neither to a burst nor to a network burst to the overall spikes. Burst detection algorithm of the Multi-well Analyzer Software was used to detect bursts and network bursts. The algorithm was set to detect a burst when at least 4 spikes are detected with a maximum of 50 ms inter spike interval (ISI) to start and end a burst, and a minimum of 100 ms inter burst interval (IBI). If a burst is detected in more than 6 channels at the same time it was classified as a network burst. Burst rate was defined as the number of bursts recorded per minute, averaged for active electrodes in one well whereas network burst rate was defined as the number of network bursts recorded from one well per minute. Burst and network burst durations were defined as the time duration between the first and the last spike that belonged to the burst or network burst, respectively. Burst and network burst frequencies were defined as the frequency of the spikes within bursts or network bursts, respectively.

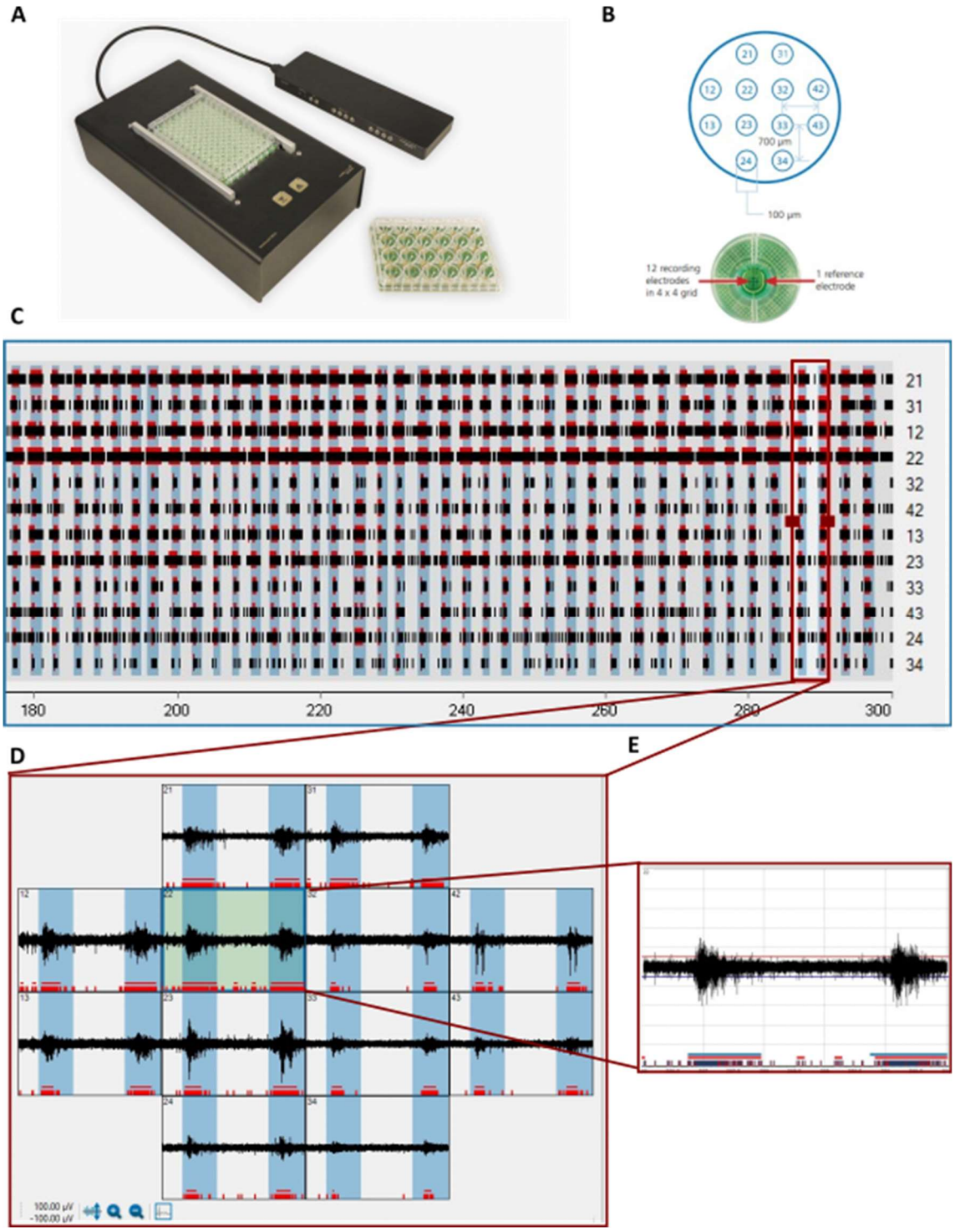

Figure 7| Multielectrode Array System. (A) The head stage together with the interface that enable network recordings from a 24-well MEA plates. (B) A close-up picture of inside one well, showing twelve recording electrodes and one reference electrode (lower), and organization of twelve electrodes with 100 µM diameters, spaced out with 100 µM between them in each well. (C) An example network activity detected from one well, showing the detected spikes (in black dashed) in each row separately for each electrode. Red markings indicate bursts while blue stripes mark the network bursts detected. (D) An exemplary raw data recorded from one well, recordings shown in an actual orientation of the electrodes located in a well. (E) An exemplary raw data recording from on single electrode, showing bursts detected as network bursts.

3.7 Data and Statistical Analysis

Single cell patch-clamp recording traces were displayed and initially analyzed off-line with the Clampfit 10.7 (Molecular Devices, Sunnyvale, CA, USA). Multiwell MEA recordings were displayed offline and the data were extracted using Multiwell Analyzer Software. Graphics were generated and the statistical tests were performed using GraphPad Prism 6 (GraphPad Software, San Diego, CA, USA). All data were tested for normal distribution via Shapiro-Wilk test. When appropriate, Student's t-test was used to test significance of normally distributed data and Mann–Whitney U test for not normally distributed data. When the parameters were compared between more than two lines at different time points, 2-way ANOVA and Sidak's or Tukey's multiple comparisons tests were applied. All data are shown as mean ± SEM. Throughout the thesis, statistically significant differences are shown only between the control vs. patient-derived cultures. Non-significant differences as well as the significant differences between different patient-derived cultures are not shown on the graph for simplicity. Data points plotted on the graphs represent individual neurons in case of single cell recordings and separate wells of Multiwell-MEA plates in case of network recordings. For all statistical tests, significance levels are indicated using the following symbols: *$p<0.05$, **$p<0.01$, ***$p<0.001$ and ***$p<0.0001$.

4 RESULTS

4.1 Differentiation of induced pluripotent stem cells into neurons

After the skin biopsies were obtained from the patients carrying the *KCNA2* mutations as well as from healthy individuals, fibroblasts were acquired from the biopsy samples and transduced with lentiviruses carrying Yamanaka factors following the reprogramming protocol as described in the Methods section (2.1.1). Reprogramming of the fibroblasts into induced pluripotent stem cells were confirmed by the expression of pluripotency markers for all the lines produced, as shown in Figure 8A for only one of the healthy individual-derived iPSC lines. Silencing of the expression of viral transgenes as well as chromosome integrity were confirmed by qPCR and karyotyping experiments for all lines, and the corresponding data have been already published (78–80).

A week later than the start of differentiations, the neurons were already MAP2-positive and the neuronal processes were observed to be projecting from the cell soma. At week four, the neurons were not only bigger in size, but also possessed many processes extending far from the cell somas (Fig 8B). Changing electrophysiological features of the neurons showed that they were developing and gaining maturity over weeks. Very immature neurons that were stimulated with depolarizing current pulses at week one had bigger changes in their membrane potential, indicating higher input resistances of immature neurons, whereas the amplitude of the change in their membrane potential in response to the same current stimulations got smaller over weeks. Exemplary responses of the neuronal membranes at weeks one and four are shown in Fig 8C.

One week after the differentiation start, the cells were not only positive for the neuronal marker MAP2 expression but were also able to fire action potentials when they were stimulated (Fig 10A). Nevertheless, spontaneously fired spikes were very rare, and the neurons were mostly silent in healthy control populations. In the following weeks, the neurons did not only start firing more action potentials, but they also showed bursting behavior that has become more robust as the neurons developed. In Figure 8D, exemplary gap-free current clamp recordings are shown from both weeks one and four.

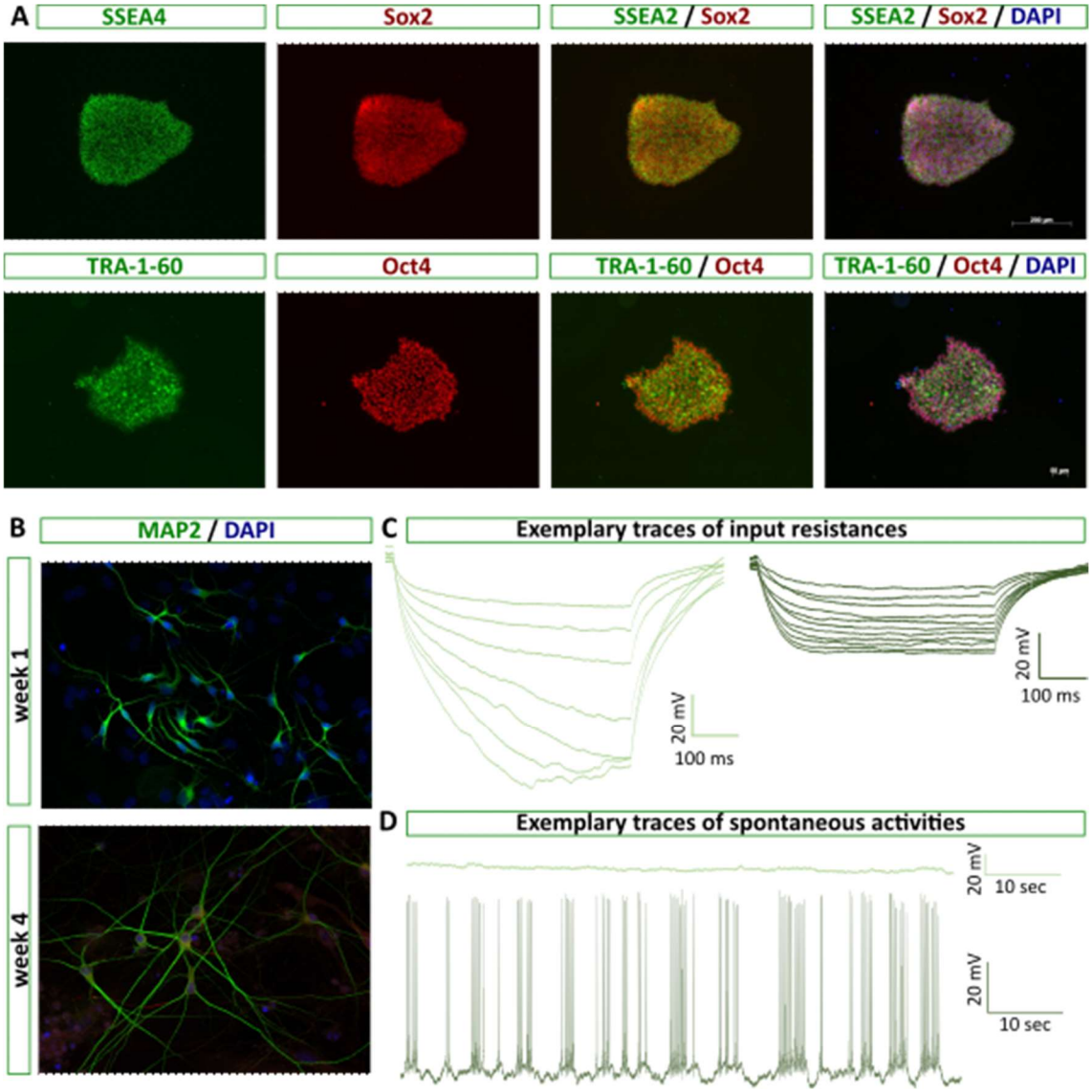

Figure 8| Differentiation of the iPSCs into neurons. (A) Exemplary immunostainings of the induced pluripotent stem cells that were positive for the pluripotency markers Sox2, Oct4, Tra1-60 and SSEA2 after reprogramming. (B) Immunostaining of the differentiating neurons against neuronal marker MAP2 after one (upper) and four (lower) weeks later than the differentiation start. (C) Exemplary traces of current clamp recordings of the neurons that were stimulated with increasing amplitudes of currents, showing the input resistances of the neurons at week one (left-light green) and four (right-dark green). (D) Exemplary traces of gap-free current clamp recordings of one (upper-light green) and four (lower-dark green) weeks-old neurons' the spontaneous activities.

4.2 Longitudinal electrophysiological investigation of the *KCNA2*-T374A mutation in IPSC-derived neuronal cultures using patch-clamp technique

Whole cell patch-clamp recordings were performed at four consecutive weeks for two control cell lines derived from two different healthy individuals and two patient cell lines derived from the same patient carrying the *KCNA2*-T374A mutation. The results from the control lines as well as the patient lines were pooled together after confirming that there were no significant differences between the two lines obtained from the same individuals. All results are shown as mean±sem.

4.2.1 Passive electrical properties of the control vs. patient IPSC-derived neurons carrying the *KCNA2*-T374A mutation

To assess the passive electrical properties of the neurons, cell capacitance, input resistance and resting membrane potentials were obtained and compared between the control- and patient-derived neurons. These results are shown in Table 4 and depicted in Figure 9.

Cell capacitances of the patient- vs. control derived neurons, that were recorded right after the whole-cell patch configuration was formed, without any compensation, are depicted in Figure 9A. Cell capacitances increased as the neurons matured over weeks in both patient- and control-derived neuronal cultures. There was no significant difference between the two lines' cell capacitances during the first three weeks of their development whereas at week four the patient-derived neurons were found to have significantly higher cell capacitances compared to control-derived neurons ($p=0.036$, Sidak's multiple comparison test).

In Figure 9B, resting membrane potentials (RMP) of the patient- vs. control- derived neurons, that were obtained from the current-clamp gap free recordings which were performed 7-12 minutes after a whole-cell patch configuration was successfully established, are depicted. The RMPs of both lines became more negative over weeks, indicating hyperpolarization of the neuronal membranes as the neurons matured. There was no significant difference between the RMPs of the control- and patient-derived neurons at any time points up to week four.

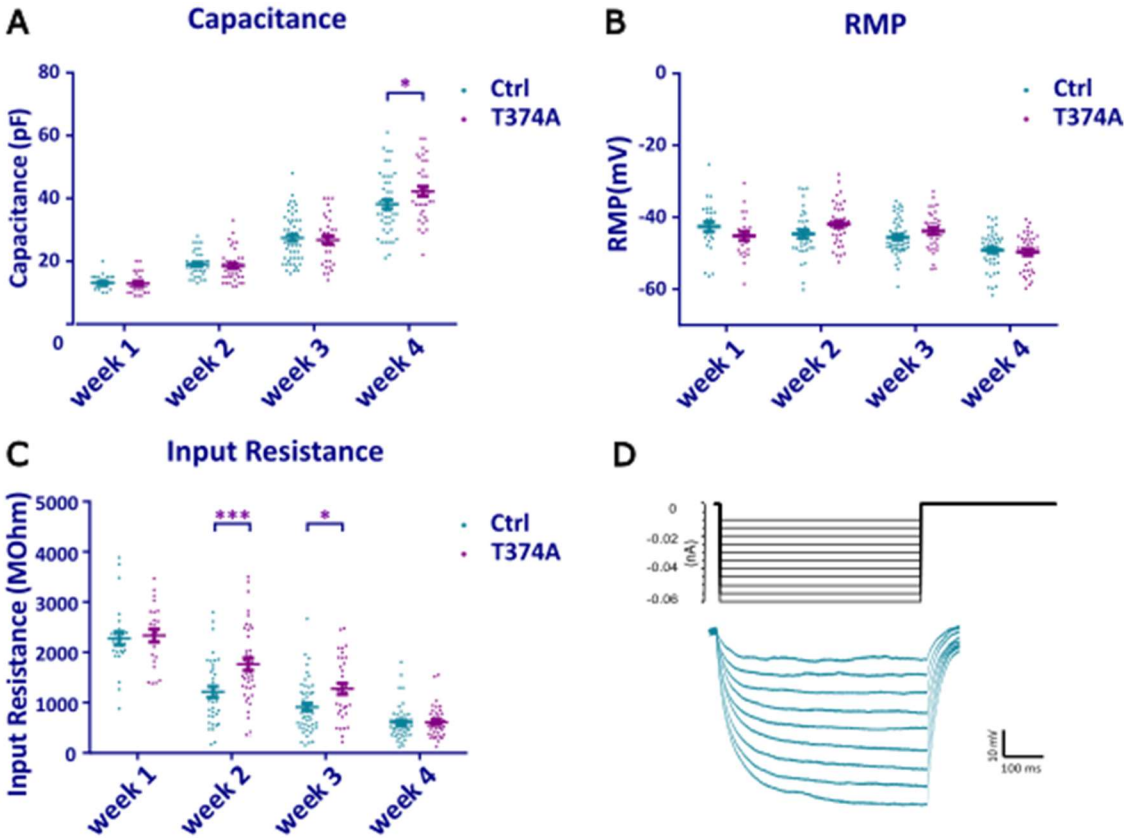

Figure 9| Passive properties of the iPSC derived control versus *KCNA2*-T374A neurons. Cell capacitances (A), resting membrane potentials (B) and input resistances (C) of the control (in blue) versus patient (in purple) neurons are shown from week one to four. (D) Exemplary raw traces of the current-clamp recordings of a control-derived neuron are shown together with the corresponding current injection steps used to calculate input resistances. From week one to four, n-numbers are 26, 36, 51, 49 for the controls and 23, 42, 34, 37 for the patients. (Two-way ANOVA, Sidak's multiple comparisons test *p < 0.05, **p < 0.01, ***p < 0.001 and ****p < 0.0001)

Input resistances were calculated from current-clamp recordings, during which neurons were stimulated with the hyperpolarizing current injections ranging from -0.01 pA to -0.06 pA, as depicted in Figure 9D (upper). Exemplary traces of the resulting changes in the membrane potential of a control iPSC-derived neuron in response to the given current injections are shown in Figure 9D (lower). Input resistances of the neurons were calculated from the relationship between the amount of injected current and the amplitude of the resulting change in their membrane potential. The input resistance became smaller as the neurons matured over weeks, in both patient- and control-derived neurons (see Fig. C). Nevertheless, the patient-derived neurons had significantly higher input resistances at week two and week three (p=0.0002 and p=0.0181 respectively, Sidak's multiple comparison test). Interestingly, when they were four

weeks old there was no significant difference between the patient and control-derived neurons' input resistances.

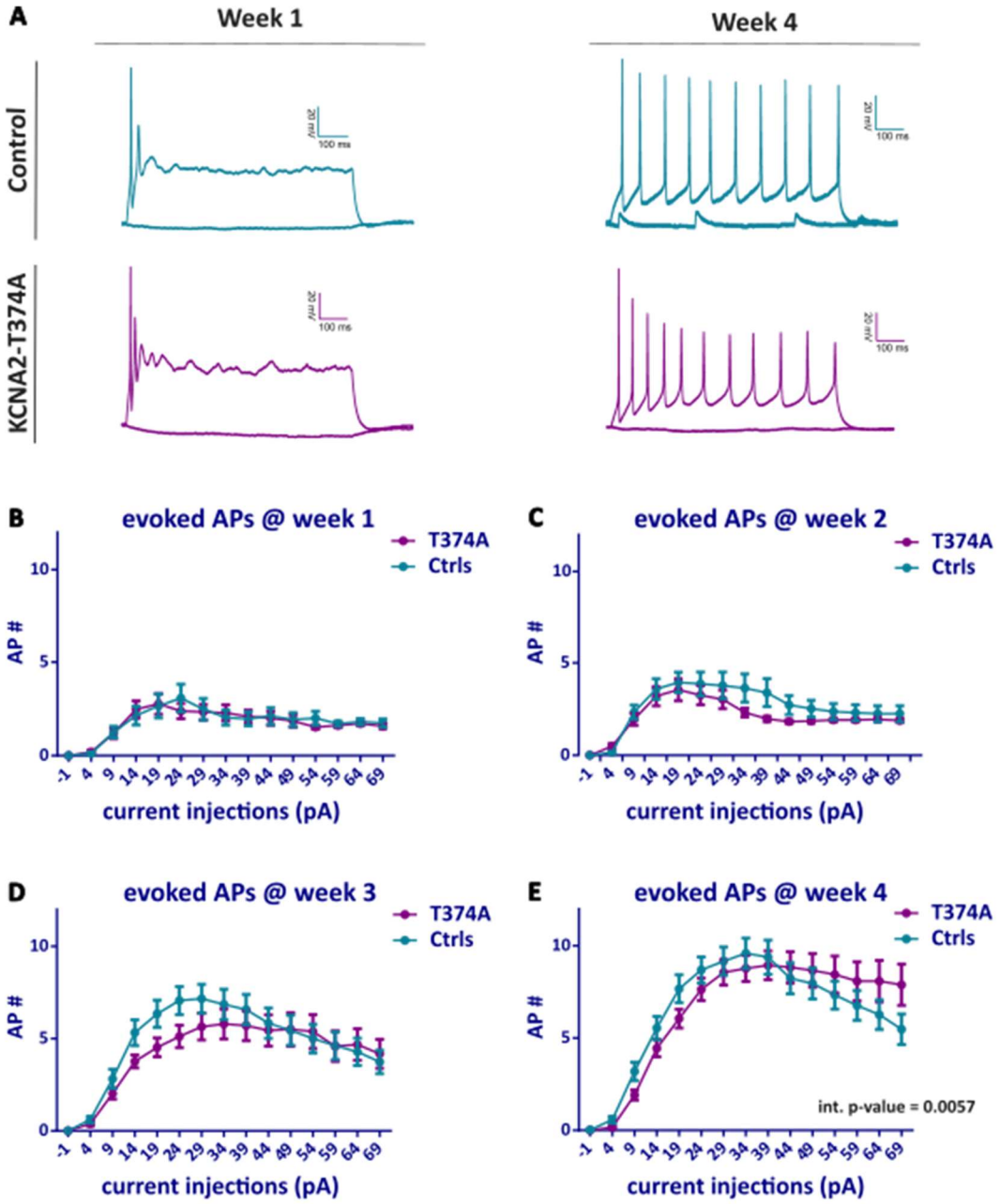

Figure 10| Input-output curves of the iPSC derived control versus *KCNA2*-T374A neurons. (A) Exemplary traces of evoked action potential trains recorded from a control- (blue) and a patient-derived (purple) neurons in response to -1 and 34 pA current injections, at weeks one (left) and four (right). The number of evoked action potentials evoked in response to a range of depolarizing currents at week one to week four (B-E) are compared between the control (blue) and patient (purple) neurons. From week one to four, n-numbers are 26, 36, 51, 49 for the controls and 23, 42, 34, 37 for the patients.

4.2.2 Evoked action potential trains of the control vs. patient IPSC-derived neurons carrying the *KCNA2*-T374A mutation

To investigate how the *KCNA2*-T374A mutation affects the intrinsic firing properties of the patient iPSC-derived neurons compared to the controls, the cell membranes were held at -70 mV level via constant current injections and then stimulated for 800 ms with different amplitudes of current injections ranging from -0.001 nA to 0.069 nA in 0.005 increments in the whole-cell current-clamp mode. Exemplary current-clamp traces of a control- and a patient-derived neurons, showing action potential trains evoked in response to different current injections, at weeks one and four, are shown below in Figure 10A.

In Figure 10 (B-E), the average number of action potentials evoked by different amplitudes of current injections were plotted for week one to four, separately. By the forced expression of Neurogenin-2 in iPSCs, fast differentiation of iPSCs into cortical neurons yielded functional neurons that can fire action potentials already at week one. Nevertheless, with increasing amplitudes of current injections, the cells were not able to fire higher number of action potentials as they had depolarization blocks. Over weeks, the average number of evoked action potentials increased for both control- and patient-derived neurons but with higher amplitudes of current injections the mean AP number dropped down in cases of both lines, as they faced depolarization blocks. Although the control- and patient- derived neurons behaved slightly differently in response to smaller or bigger amplitudes of current injections, overall, there was no significant difference between the evoked APs of the two lines over weeks. Nevertheless, the relationship between the injected current amplitudes and the evoked action potentials was found to significantly differ between these lines at week four (interaction $p=0.005$, two-way repeated measures ANOVA).

4.2.3 Single action potential properties

To assess single action potential parameters of the neurons, the first action potential evoked in response to the smallest 1-ms long depolarizing current amplitude was analyzed. Action potential thresholds, time-to-peak durations, amplitudes as well as half-widths were calculated and compared between the patient and control-derived neurons up to week four and depicted in Figure 11.

As expected from developing neurons, throughout weeks, the action potential thresholds became more and more hyperpolarized in both the control- and patient-neuronal populations and the AP amplitudes increased. There was no significant difference in single AP thresholds or amplitudes of the control- and patient-derived neurons.

The mean time-to-peak duration was slightly longer for the patient-derived neurons at week one and significantly longer at week two and three ($p<0.0001$ and $p=0.0032$ respectively, Sidak's multiple comparisons test) whereas at week four the difference was not significant anymore. Overall, time-to-peak durations of the control and patient-derived neurons significantly differed ($p<0.0001$, two-way repeated measures ANOVA). Also, the interaction between the age and the time-to-peak durations was found to be significantly different between the patient- and control-derived neurons (interaction $p=0.0005$, two-way repeated measures ANOVA).

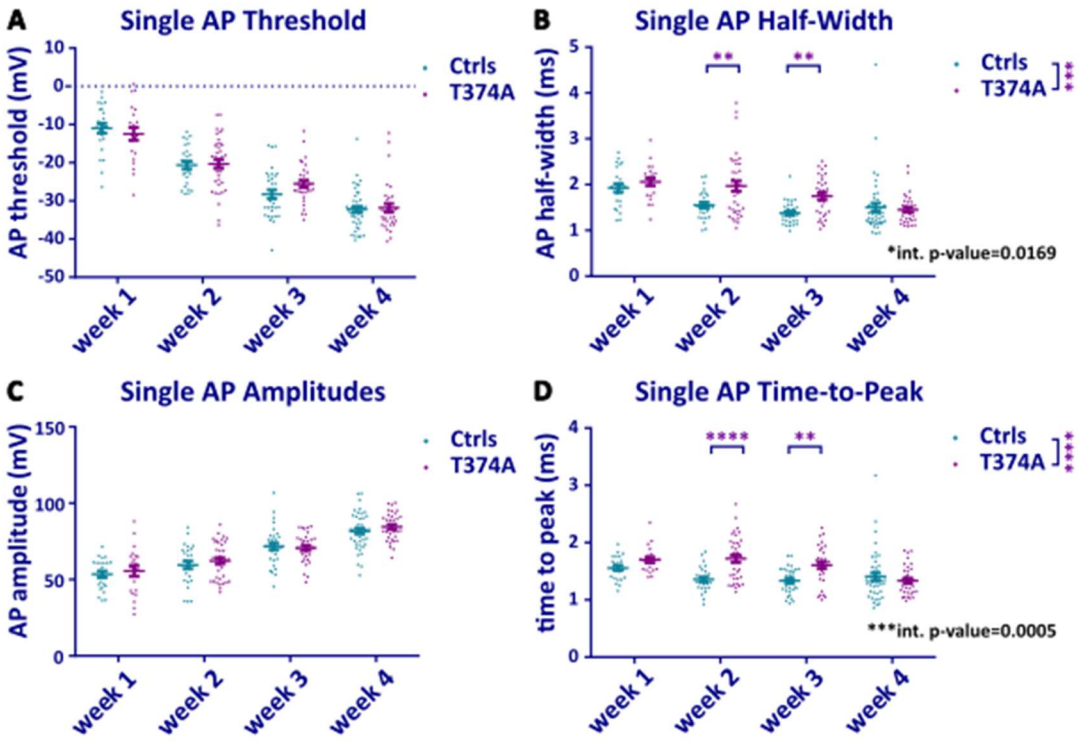

Figure 11| Single action potential parameters of the iPSC derived control versus *KCNA2*-T374A neurons. The single action potential parameters were calculated using the action potentials evoked by a 1 ms long smallest depolarizing pulse that was enough to elicit an action potential, at week one to week four (A-D) and are compared between the control (blue) and patient (purple) neurons. From week one to four, n-numbers are 26, 36, 51, 49 for the controls and 23, 42, 34, 37 for the patients.

Also expectedly, the AP half-widths became shorter over weeks during the neuronal development, in both control- and patient-derived neuronal cultures. The patient-derived neurons had significantly longer AP half-widths at weeks two and week three compared to the controls (p=0.0030 and p=0.0095, respectively, Sidak's multiple comparisons test). Overall, the difference in the mean AP half-widths of the control and patient-derived neurons was found to be significantly different over weeks (p=0.0005, two-way repeated measures ANOVA), as well as the relationship between the development stage and the AP-width of the control- vs. patient-derived neurons (interaction p=0.0169, two-way repeated measures ANOVA). Altogether, intrinsic and extrinsic features of the patient-derived neurons carrying the *KCNA2*-T374A mutation, that were found to differ from the controls at week two and three, were again comparable to the controls at week four, suggesting developmental delay of the patient neurons as well as compensatory mechanisms in action.

Table 4| Passive electrical properties and single action potential parameters of the control- and *KCNA2*-T374A mutation carrying patient-derived neurons at four consecutive weeks. Data are shown as mean±sem.

		week 1	**week 2**	**week 3**	**week 4**
Cell Capacitance (pA)	**Ctrl**	13.23±0.43	19.06±0.64	27.43±1.06	38.17±1.42
	T374A	12.96±0.75	18.48±0.78	26.77±1.29	42.25±1.55 *
RMP (mV)	**Ctrl**	-42.64±1.37	-44.66±1.13	-45.57±0.70	-49.18±0.77
	T374A	-45.21±1.27	-41.94±0.92	-43.84±0.96	-49.73±0.91
Input Resistance (mOhm)	**Ctrl**	2493.5±130.0	1429.8±110.2	1127.7±72.8	818.5±51.9
	T374A	2552.0±131.1	1980.9±120.6 ***	1491.8±108.7 *	827.6±52.2
Single AP		**week 1**	**week 2**	**week 3**	**week 4**
threshold (mV)	**Ctrl**	-11.0±1.3	-20.7±1.0	-28.3±1.7	-32.2±0.8
	T374A	-12.5±1.7	-20.3±1.6	-25.5±0.9	-1.8±1.1
time-to-peak (ms)	**Ctrl**	1.6±0.0	1.4±0.0	1.3±0.0	1.4±0.1
	T374A	1.7±0.1	1.7±0.1 ****	1.6±0.1 **	1.4±0.1
amplitude (mV)	**Ctrl**	55.3±2.1	61.4±2.6	73.5±2.3	83.5±1.8
	T374A	57.4±3.5	64.1±2.0	72.5±1.7	86.3±1.6
half-width (ms)	**Ctrl**	1.9±0.1	1.6±0.1	1.4±0.0	1.5±0.1
	T374A	2.1±0.1	2.0±0.1	1.8±0.1	1.5±0.1

Table 5| Average number of evoked action potentials in response to a range of depolarizing current injections, for the control- and *KCNA2*-T374A mutation carrying patient-derived neurons at four consecutive weeks.

Injected current	week1		week2		week3		week 4	
(pA)	Ctrl	T374A	Ctrl	T374A	Ctrl	T374A	Ctrl	T374A
-1	0.00	0.00	0.00	0.00	0.00	0.00	0.02	0.00
4	0.11	0.19	0.17	0.49	0.61	0.38	0.57	0.17
9	1.26	1.19	2.33	1.94	2.82	2.03	3.19	1.92
14	2.15	2.48	3.58	3.20	5.33	3.76	5.55	4.44
19	2.67	2.76	3.94	3.54	6.35	4.53	7.67	6.06
24	3.07	2.38	3.86	3.26	7.06	5.12	8.69	7.64
29	2.48	2.33	3.78	3.03	7.16	5.65	9.17	8.56
34	2.04	2.29	3.64	2.31	6.86	5.79	9.60	8.78
39	1.96	2.10	3.39	1.97	6.57	5.71	9.38	8.94
44	2.11	2.00	2.72	1.83	5.84	5.44	8.24	8.83
49	1.93	1.86	2.53	1.86	5.45	5.50	7.95	8.67
54	2.00	1.52	2.36	1.91	5.00	5.38	7.33	8.44
59	1.70	1.62	2.31	1.91	4.61	4.59	6.76	8.08
64	1.81	1.71	2.25	1.94	4.29	4.68	6.26	8.08
69	1.74	1.57	2.25	1.89	3.73	4.18	5.48	7.89

4.3 Investigation of the network activity in the control vs. patient IPSC-derived neuronal cultures carrying GOF, GOF+LOF and LOF *KCNA2* mutations, using Multi-well MEA System

Four different patient IPSC-derived neuronal cultures, carrying the *KCNA2*-R297Q (GOF), -L328V (GOF+LOF), -T374A (GOF+LOF) or -P405L (LOF) mutation, as well as two different healthy individual IPSC-derived neuronal cultures were grown on multi-well multielectrode arrays, in co-cultures with mouse astrocytes up to six weeks. The network activities of the cultures were recorded every week for ten minutes, after a ten minutes-long acclimatization period. The data obtained from two different lines derived from the same patient as well as from two different control lines were pooled together after confirming that there were no significant differences between the two lines derived from the same individuals and the data are shown as mean±sem here.

4.3.1 Spiking

Consistently with the single cell patch-clamp data, in all the patient- and control-derived neurons spontaneous action potentials were detected already one week after the differentiation start and expectedly, the mean firing rate increased over weeks (see Fig. 12 (A-F), Table 6).

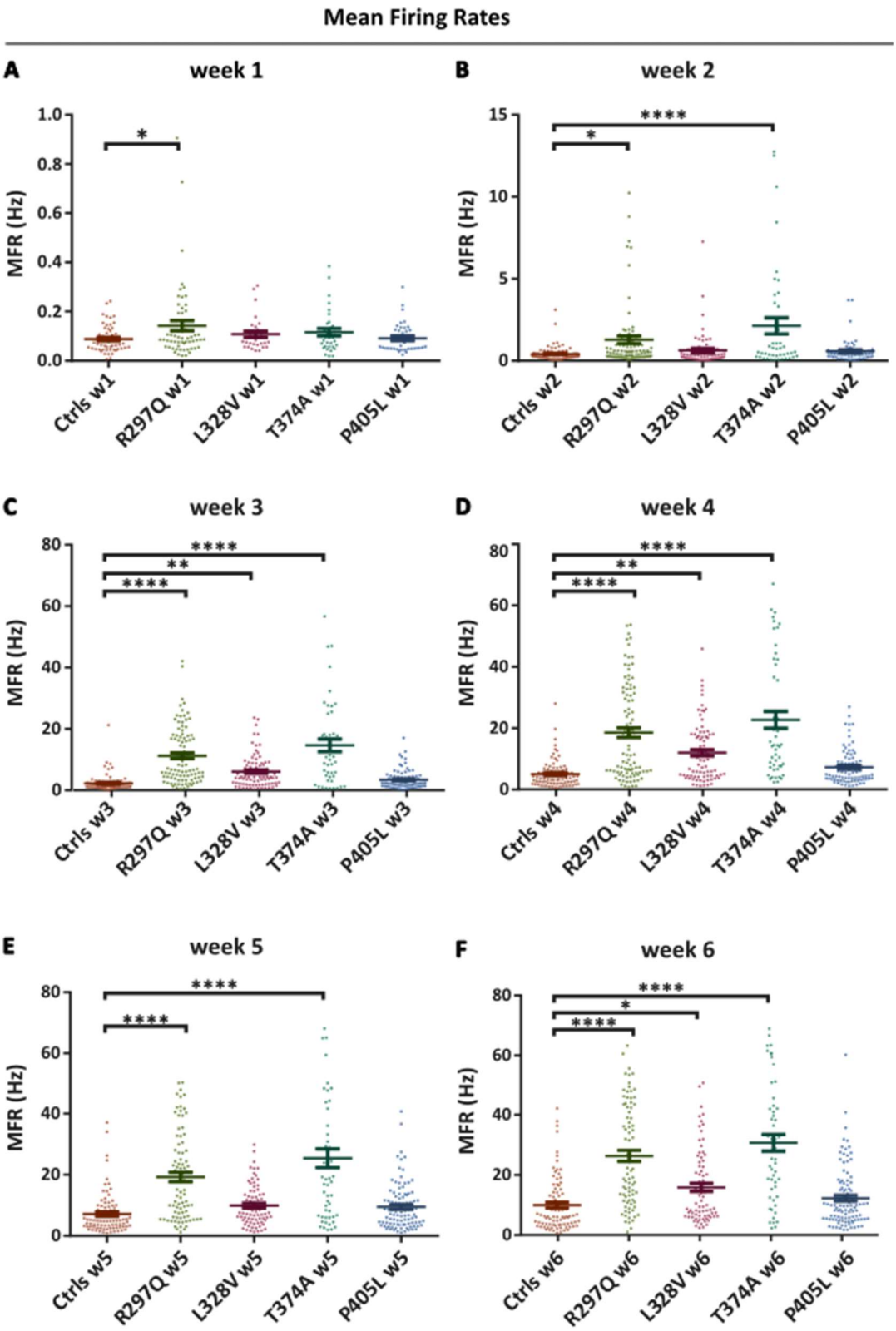

Figure 12| The mean firing rates of the iPSC-derived neuronal networks. The mean firing rates calculated from ten minutes long MEA recordings and compared between the control versus *KCNA2*-R297Q (light green), *KCNA2*-L328V (pink), -T374A (dark green) and P405L (blue) neurons from week one to six (A-F). From week one to six, n-numbers are 54, 82, 79, 82, 83, 87 for the control-, 58, 96, 96, 96, 87, 83 for the *KCNA2*-R297Q, 30, 66, 82, 82, 74, 70 for the *KCNA2*-L328V, 34, 46, 46, 50, 54, 52 for the *KCNA2*-T374A, 38, 61, 82, 82, 99, 103 for the *KCNA2*-P405L patient-

derived neurons. (Two-way ANOVA, Sidak's multiple comparisons test *p < 0.05, **p < 0.01, ***p < 0.001 and ****p < 0.0001)

The *KCNA2*-R297Q patient-derived neuronal networks' MFR was significantly higher than that of the controls already at week one (p=0.036, Tukey's multiple comparisons test). Despite increasing MFR of the control-derived networks, the MFR of the *KCNA2*-R297Q patient-derived neuronal networks was significantly higher than the controls at all time points, with increasing statistical significance, especially from week three on (p< 0.0001, Tukey's multiple comparisons test). The *KCNA2*-T374A patient-derived neuronal networks' MFR revealed a significant difference at week two for the first time and remained significantly higher than that of the controls throughout the following weeks (p< 0.0001 for week two to six, Tukey's multiple comparisons test).

The *KCNA2*-L328V patient-derived networks had significantly higher MFRs for the first time at week three (p=0.0096 and 0.0016, at week three and four, respectively, Tukey's multiple comparisons test). The gap between the MFRs of the control- and patient-derived neuronal cultures became narrower over the next weeks, not revealing a significant difference at week five and but again at week six (p=0.0442, Tukey's multiple comparisons test).

Surprisingly, the *KCNA2*-P405L patient-derived networks' MFR was not found to be significantly different than the control-derived networks' MFR at any time points.

The percentage of the spikes that did not belong to any bursts to the total spike count was calculated and depicted on Figure 13 as "% random spikes". As the bursting behavior was more prominent from week three on, the percentage of random spikes were calculated and compared between the lines from week three to six and are shown separately (Fig. 13A-D, Table 6).

Although the MFR was significantly elevated in the patient-derived networks carrying the *KCNA2*-R297Q mutation, the percentage of the random spikes for was significantly lower than that of the control-derived networks, from week three on at all time points (p< 0.0001, Tukey's multiple comparisons test). Similarly, the *KCNA2*-T374A patient-derived cultures had significantly lower random spike ratio from week four on (p=0.0002, =0.0036, <0.0001, from week four to six, respectively, Tukey's multiple comparisons test). Increased MFRs and lower random spike ratios indicated increased

bursting activity of these patient-derived cultures. On the contrary, the random spike percentage of the *KCNA2*-P405L patient-derived cultures was higher than that of the controls at week three ($p<0.0001$, Tukey's multiple comparisons test). The *KCNA2*-L328V patient-derived networks was not found to differ in their random spike percentage compared to the controls.

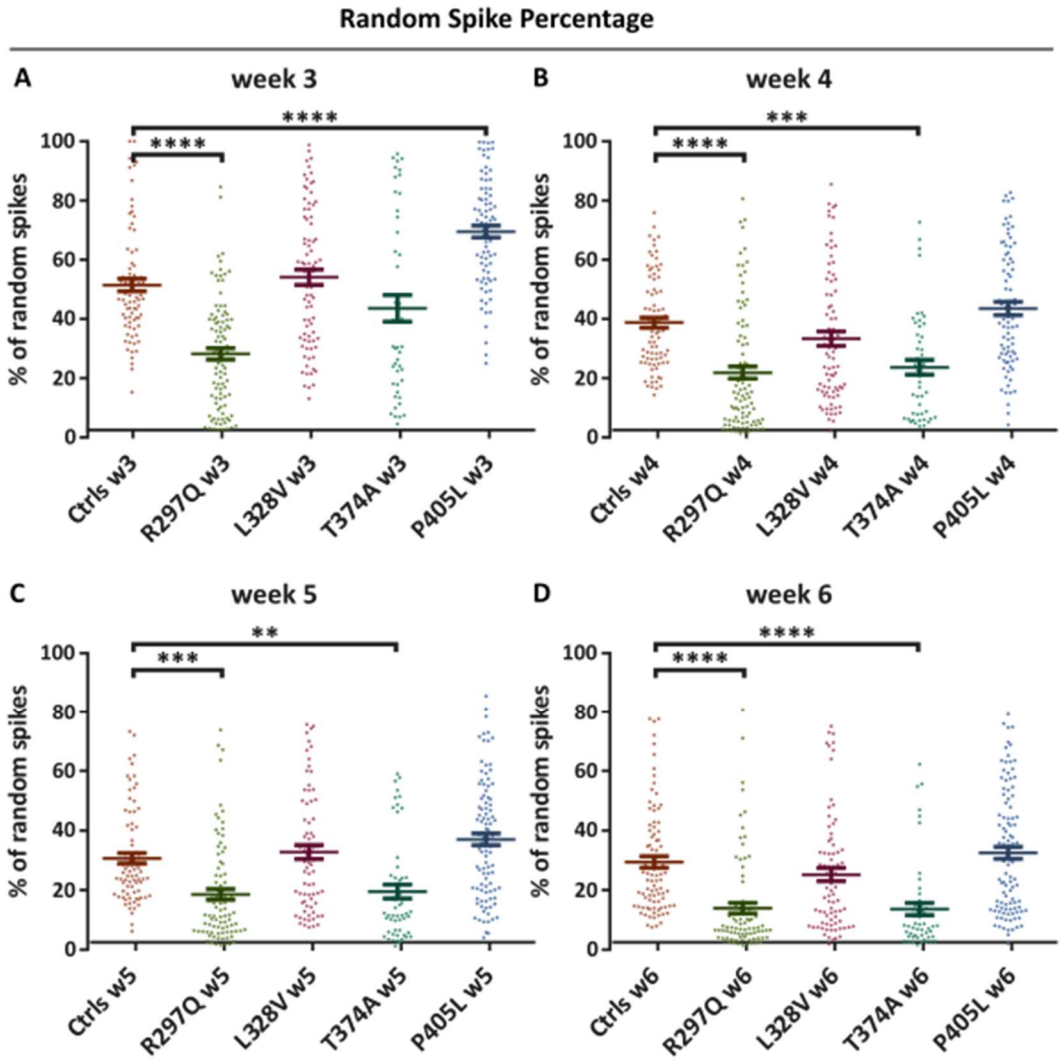

Figure 13| The random spike percentages of the iPSC-derived neuronal networks. The percentages of the random spikes, that did not belong to the bursts, to all spikes detected were calculated from ten minutes long MEA recordings and compared between the control versus *KCNA2*-R297Q (light green), *KCNA2*-L328V (pink), -T374A (dark green) and P405L (blue) neurons from week three to six (A-D). From week three to six, n-numbers are 79, 82, 83, 87 for the control-, 96, 96, 87, 83 for the *KCNA2*-R297Q, 82, 82, 74, 70 for the *KCNA2*-L328V, 46, 50, 54, 52 for the *KCNA2*-T374A, 82, 82, 99, 103 for the *KCNA2*-P405L patient-derived neurons. (Two-way ANOVA, Sidak's multiple comparisons test *$p < 0.05$, **$p < 0.01$, ***$p < 0.001$ and ****$p < 0.0001$)

Table 6 | Mean firing rates and random spike percentages of the control- and *KCNA2*-R297Q, -L328V, -T374A, and -P405L patient-derived neuronal networks, for six and four consecutive weeks, respectively. Data are shown as mean±sem.

MFR (Hz)	week 1	week 2	week 3	week 4	week 5	week 6
Ctrl	0.09±0.01	0.41±0.05	2.24±0.31	5.06±0.51	7.13±0.74	9.98±0.97
R297Q	0.14±0.01 *	1.28±0.23 *	11.20±0.93 ****	18.50±1.57 ****	19.20±1.51 ****	26.30±1.86 ****
L328V	0.11±0.01	0.63±0.13	6.01±0.59 **	12.00±1.05 **	9.90±0.78 *	15.90±1.36
T374A	0.12±0.01	2.13±0.49 ****	14.60±2.06 ****	22.70±2.78 ****	25.40±3.09 ****	30.70±2.83 ****
P405L	0.09±0.01	0.57±0.09	3.39±0.35	7.36±0.63	9.48±0.75	12.20±0.97
random spike %			**week 3**	**week 4**	**week 5**	**week 6**
ctrl			51.5±2.1	38.8±1.7	30.8±1.7	29.5±1.9
R297Q			28.2±1.9 ****	21.9±2.1 ****	18.6±1.8 ****	14.0±1.8 ****
L328V			54.1±2.6	33.4±2.5	32.8±2.1	25.2±2.2
T374A			43.6±4.5	23.7±2.5 ***	19.5±2.4 **	13.7±2.1 ****
P405L			69.6±2.0 ****	43.6±2.2	37.1±2.0	32.5±2.0

4.3.2 Bursting

As both the control- and patient-derived neuronal cultures exhibited robust bursting behavior from week three on, bursting parameters were assessed and compared between the lines from week three to six. Data are shown as mean±sem in Table 7.

In Figure 14(A-D), the number of bursts recorded per minute is shown. The *KCNA2*-R297Q, -L328V and -T374A patient-derived neuronal cultures exhibited significantly higher bursting rates compared to the control-derived cultures at week three. ($p<0.0001$ for all, Tukey's multiple comparisons test). All these three patient lines had a significantly higher bursting rate also at week four, nevertheless from five on only the *KCNA2*-R297Q patient-derived network was found to have a significantly higher mean bursting rate compared to the controls, with a descending significance level ($p=0.0002$ and $p= 0.0032$, week five and six respectively, Tukey's multiple comparisons test). The *KCNA2*-P405L patient-derived neurons bursting rate did not differ from the bursting rate of the control cultures at any time points from week three to six.

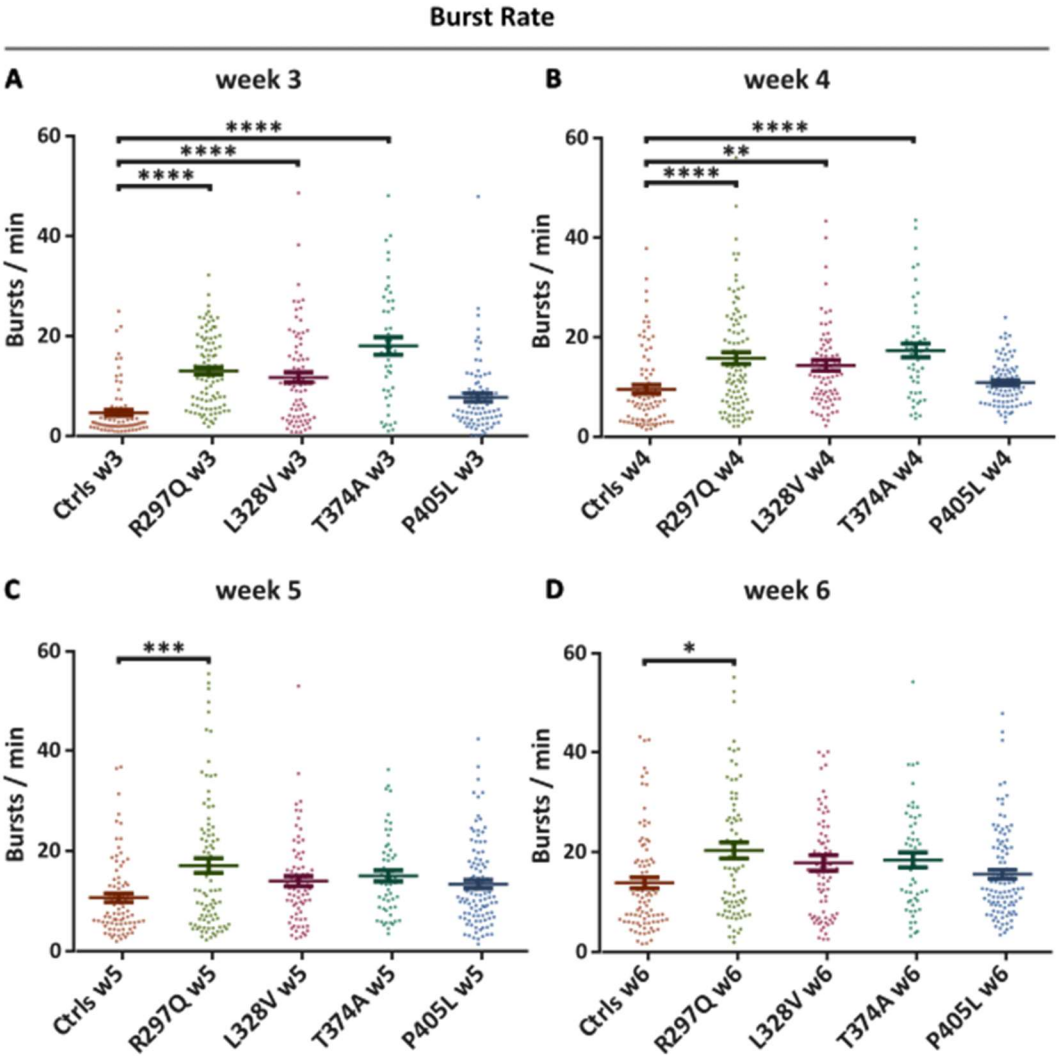

Figure 14| The burst rates of the iPSC-derived neuronal networks. The number of bursts per minute were calculated from ten minutes long MEA recordings and compared between the control versus *KCNA2*-R297Q (light green), *KCNA2*-L328V (pink), -T374A (dark green) and P405L (blue) neurons from week three to six (A-D). From week three to six, n-numbers are 79, 82, 83, 87 for the control-, 96, 96, 87, 83 for the *KCNA2*-R297Q, 82, 82, 74, 70 for the *KCNA2*-L328V, 46, 50, 54, 52 for the *KCNA2*-T374A, 82, 82, 99, 103 for the *KCNA2*-P405L patient-derived neurons. (Two-way ANOVA, Sidak's multiple comparisons test *p < 0.05, **p < 0.01, ***p < 0.001 and ****p < 0.0001)

The mean burst durations are depicted in Figure 15(A-D). The *KCNA2*-R297Q and -T374A patient-derived network had significantly longer burst durations compared to the control-derived networks starting from week three whereas *KCNA2*-L328V and -P405L patient-derived networks' mean burst duration was significantly longer than that of the controls at week four for the first time. All patient-derived neuronal networks had longer mean burst durations still at week six (p<0.0001 for *KCNA2*-R297Q and -T374A, p=0.0039 for -L328V and p=0.0009 for -P405L, Tukey's multiple comparisons test).

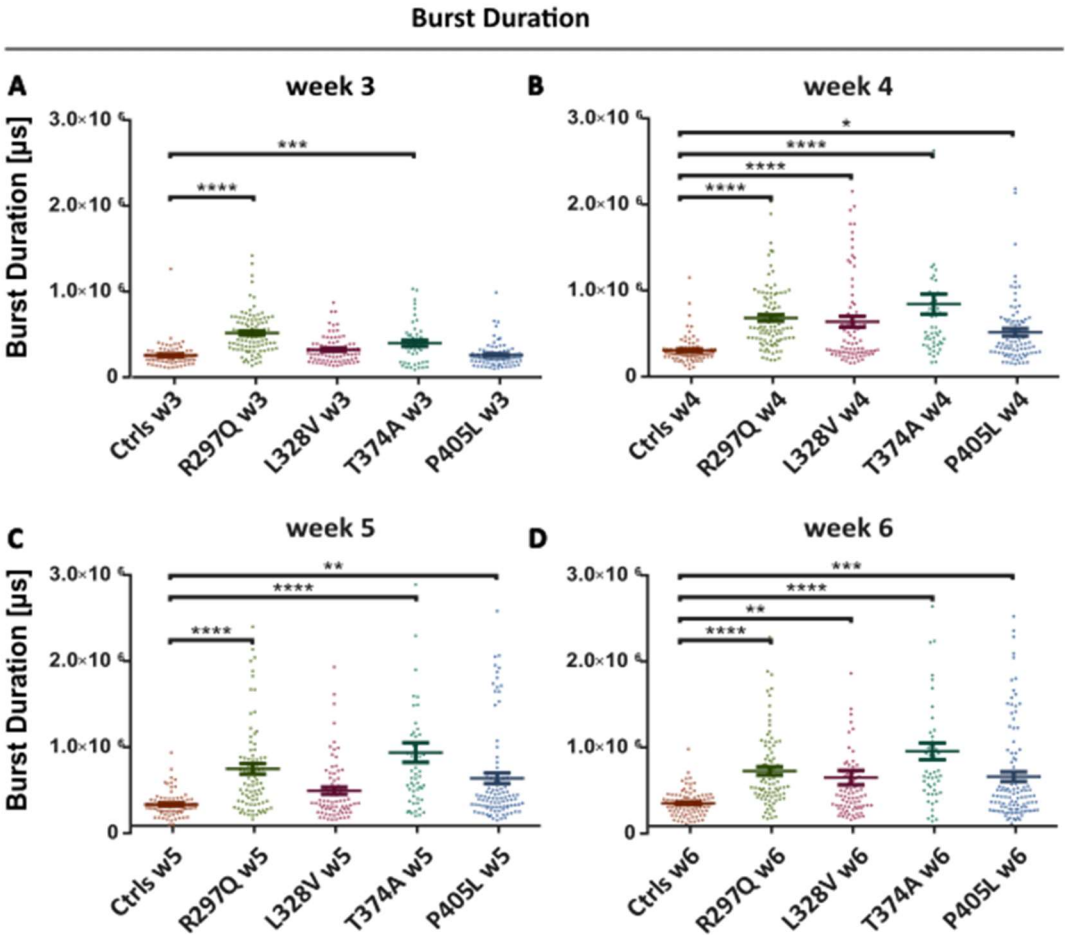

Figure 15| The mean burst durations of the iPSC-derived neuronal networks. The mean burst durations were calculated from ten minutes long MEA recordings and compared between the control versus *KCNA2*-R297Q (light green), *KCNA2*-L328V (pink), -T374A (dark green) and P405L (blue) neurons from week three to six (A-D). From week three to six, n-numbers are 79, 82, 83, 87 for the control-, 96, 96, 87, 83 for the *KCNA2*-R297Q, 82, 82, 74, 70 for the *KCNA2*-L328V, 46, 50, 54, 52 for the *KCNA2*-T374A, 82, 82, 99, 103 for the *KCNA2*-P405L patient-derived neurons. (Two-way ANOVA, Sidak's multiple comparisons test *p < 0.05, **p < 0.01, ***p < 0.001 and ****p < 0.0001)

The frequencies of the spikes fired within each burst were depicted in Figure 16 as "burst spike frequency". The *KCNA2*-L328V, -T374A and -P405L patient-derived neuronal networks had significantly lower spike frequency at week three ($p<0.0001$, $p=0.0063$, $p< 0.0001$, respectively, Tukey's multiple comparisons test). As the frequencies increased over time, the *KCNA2*-L328V and -T374A patient-derived networks did not reveal a significance difference by week six whereas *KCNA2*-P405L patient-derived neuronal networks remained to have lower burst spike frequency at week six ($p=0.0002$ at week six, Tukey's multiple comparisons test). On the contrary, the mean burst spike frequency of the *KCNA2*-R297Q patient-derived networks was significantly higher than that of the controls at week six ($p< 0.0001$, Tukey's multiple comparisons test).

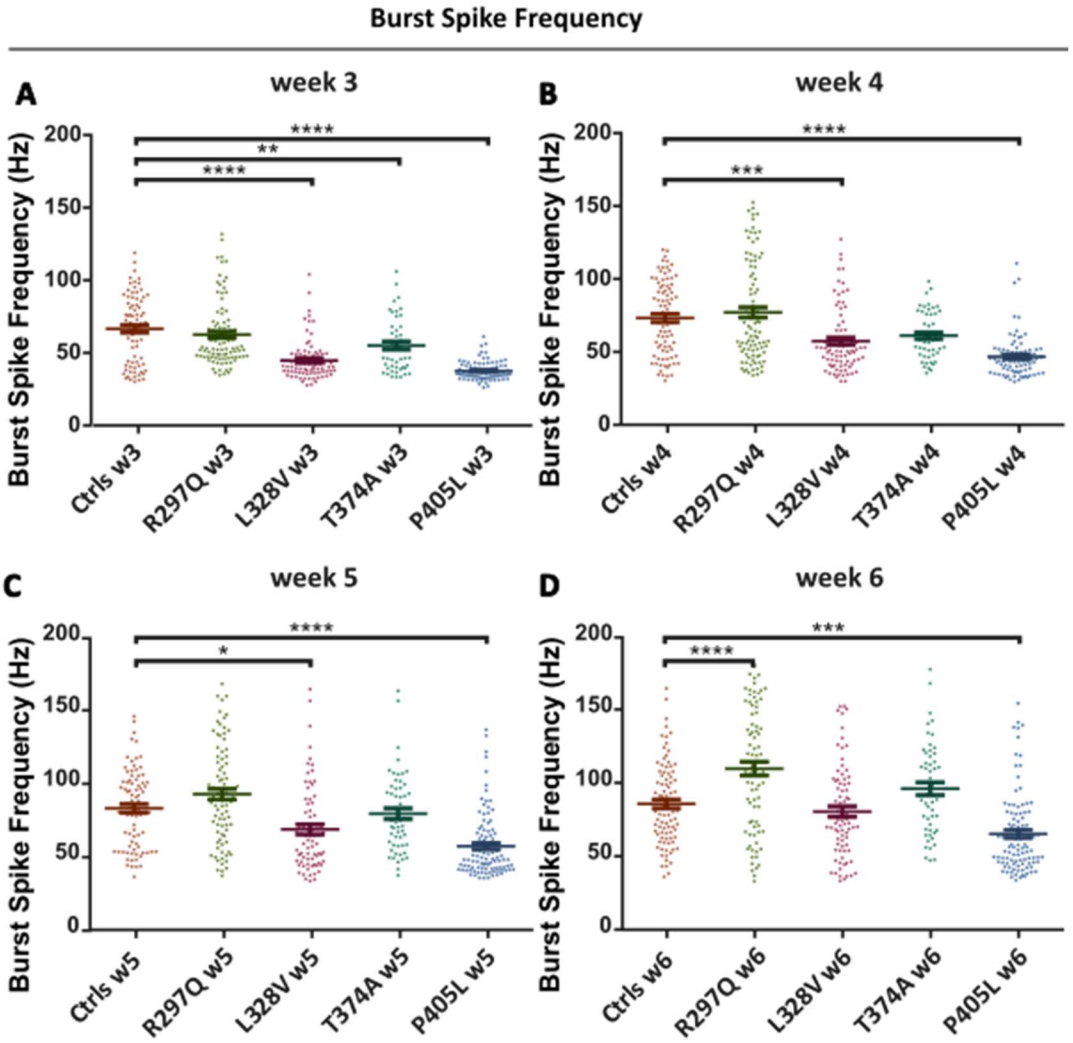

Figure 16| The mean burst spike frequencies of the iPSC-derived neuronal networks. The mean spike frequencies within bursts were calculated from ten minutes long MEA recordings and compared between the control versus *KCNA2*-R297Q (light green), *KCNA2*-L328V (pink), -T374A (dark green) and P405L (blue) neurons from week three to six (A-D). From week three to six, n-numbers are 79, 82, 83, 87 for the control-, 96, 96, 87, 83 for the *KCNA2*-R297Q, 82, 82, 74, 70 for the *KCNA2*-L328V, 46, 50, 54, 52 for the *KCNA2*-T374A, 82, 82, 99, 103 for the *KCNA2*-P405L patient-derived neurons. (Two-way ANOVA, Sidak's multiple comparisons test *p < 0.05, **p < 0.01, ***p < 0.001 and ****p < 0.0001)

4.3.3 Network bursting

The findings from the analysis of the network burst parameters aligned with the findings from single burst analysis, showing only slight differences in the statistical power and the temporal emergence of the observed differences between the different lines.

The number of network bursts recorded per minute are plotted on the Figure 17. Similar to the single bursting analysis, at week three, the *KCNA2*-R297Q, -L328V and -T374A patient-derived neuronal cultures were found to exhibit significantly higher network burst rates compared to the control-derived cultures (p<0.0001, p=0.0005, p<0.0001

respectively, Tukey's multiple comparisons test). Among them, only the mean network burst rate of the *KCNA2*-R297Q patient-derived cultures remained significantly higher than that of the controls up to week six (p=0.0209, p=0.0021, p=0.0376 respectively, Tukey's multiple comparisons test). The *KCNA2*-P405L patient-derived networks did not differ in their network burst rates compared to the controls at any time point between week three and six.

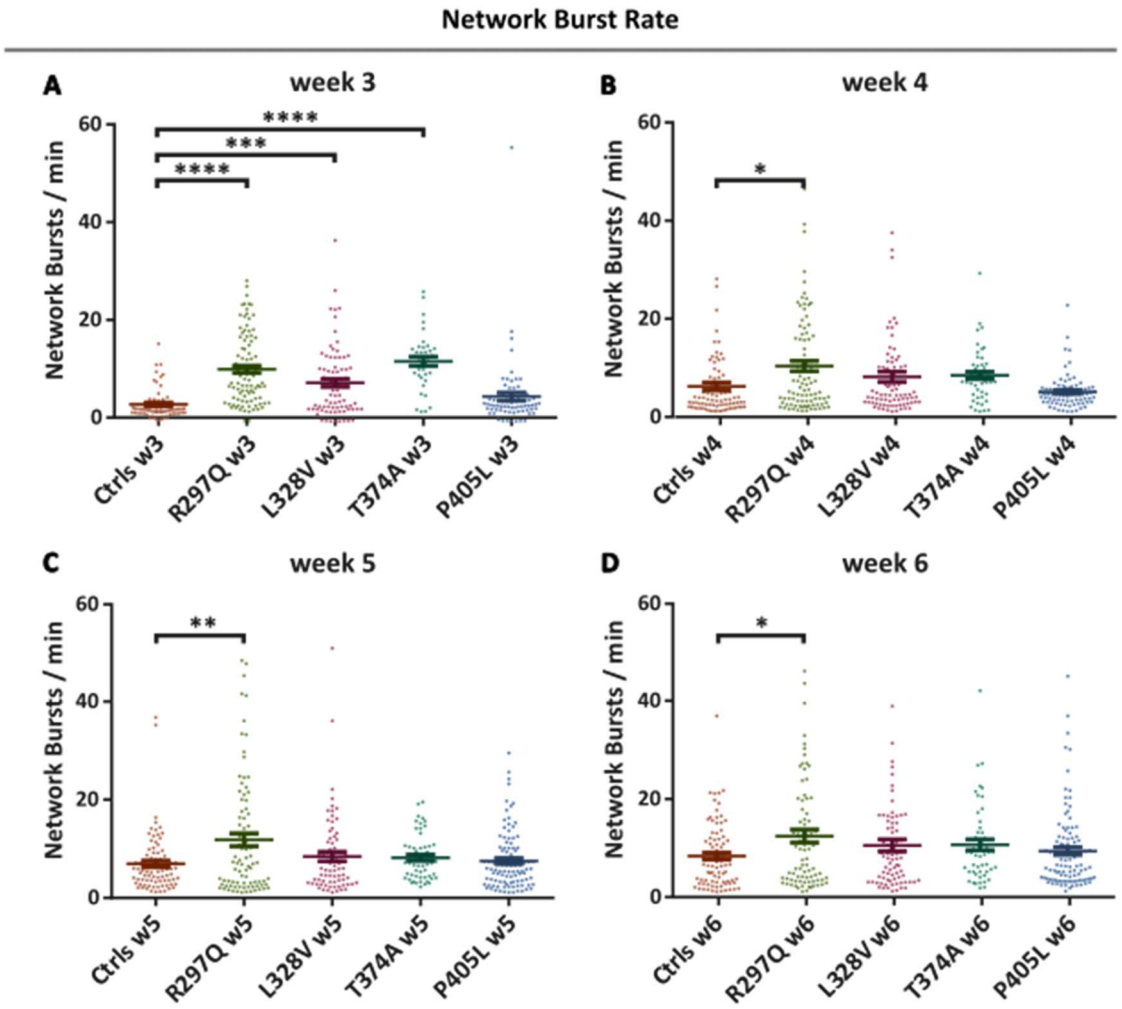

Figure 17| The mean network burst rates of the iPSC-derived neuronal networks. The numbers of networks bursts per minute were calculated from ten minutes long MEA recordings and compared between the control versus *KCNA2*-R297Q (light green), *KCNA2*-L328V (pink), -T374A (dark green) and P405L (blue) neurons from week three to six (A-D). From week three to six, n-numbers are 79, 82, 83, 87 for the control-, 96, 96, 87, 83 for the *KCNA2*-R297Q, 82, 82, 74, 70 for the *KCNA2*-L328V, 46, 50, 54, 52 for the *KCNA2*-T374A, 82, 82, 99, 103 for the *KCNA2*-P405L patient-derived neurons. (Two-way ANOVA, Sidak's multiple comparisons test *p < 0.05, **p < 0.01, ***p < 0.001 and ****p < 0.0001)

All patient-derived networks had prolonged network burst durations compared to the control-derived networks starting from week three (p= 0.0077 for the *KCNA2*-R297Q,

p=0.0208 for -L328V, p=0.0028 for -T374A and p<0.0001 for -P405L, Tukey's multiple comparisons test) (see Figure 18). Although the *KCNA2*-R297Q and the *KCNA2*-L328V patient-derived networks did not reveal significant difference at week four and five, respectively, at week six all the patient-derived networks were still found to have significantly prolonged network burst durations (p=0.0019 for the *KCNA2*-R297Q, p=0.0359 for -L328V, p<0.0001 for -T374A and -P405L, Tukey's multiple comparisons test).

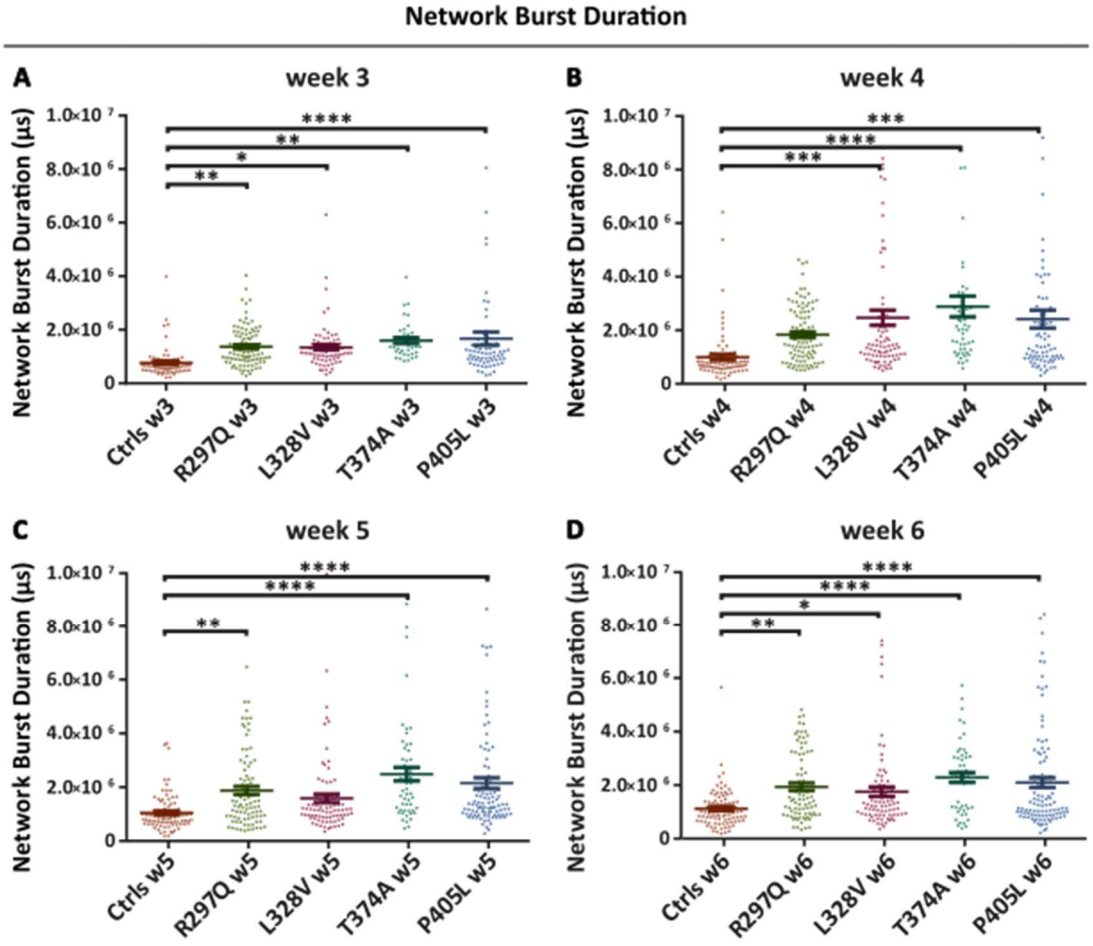

Figure 18| The mean network burst durations of the iPSC-derived neuronal networks. The mean network burst durations were calculated from ten minutes long MEA recordings and compared between the control versus *KCNA2*-R297Q (light green), *KCNA2*-L328V (pink), -T374A (dark green) and P405L (blue) neurons from week three to six (A-D). From week three to six, n-numbers are 79, 82, 83, 87 for the control-, 96, 96, 87, 83 for the *KCNA2*-R297Q, 82, 82, 74, 70 for the *KCNA2*-L328V, 46, 50, 54, 52 for the *KCNA2*-T374A, 82, 82, 99, 103 for the *KCNA2*-P405L patient-derived neurons. (Two-way ANOVA, Sidak's multiple comparisons test *p < 0.05, **p < 0.01, ***p < 0.001 and ****p < 0.0001)

The mean spike frequencies within network bursts are depicted in Figure 19. The mean network burst spike frequency of the *KCNA2*-R297Q and -T374A patient-derived neuronal networks was significantly higher than that of the controls from week four and

five on, respectively, increasing over time and revealing a strongly significant difference at week six ($p<0.0001$ for both at week six, Tukey's multiple comparisons test). The *KCNA2*-L328V and-P405L patient-derived networks had significantly lower mean network burst spike frequency than that of the controls at week three ($p<0.0001$ for both, Tukey's multiple comparisons test). Nevertheless, as the frequencies increased over time, only the *KCNA2*-P405L patient-derived network remained to have a significantly lower network burst spike frequency until week five ($p= 0.0151$, Tukey's multiple comparisons test).

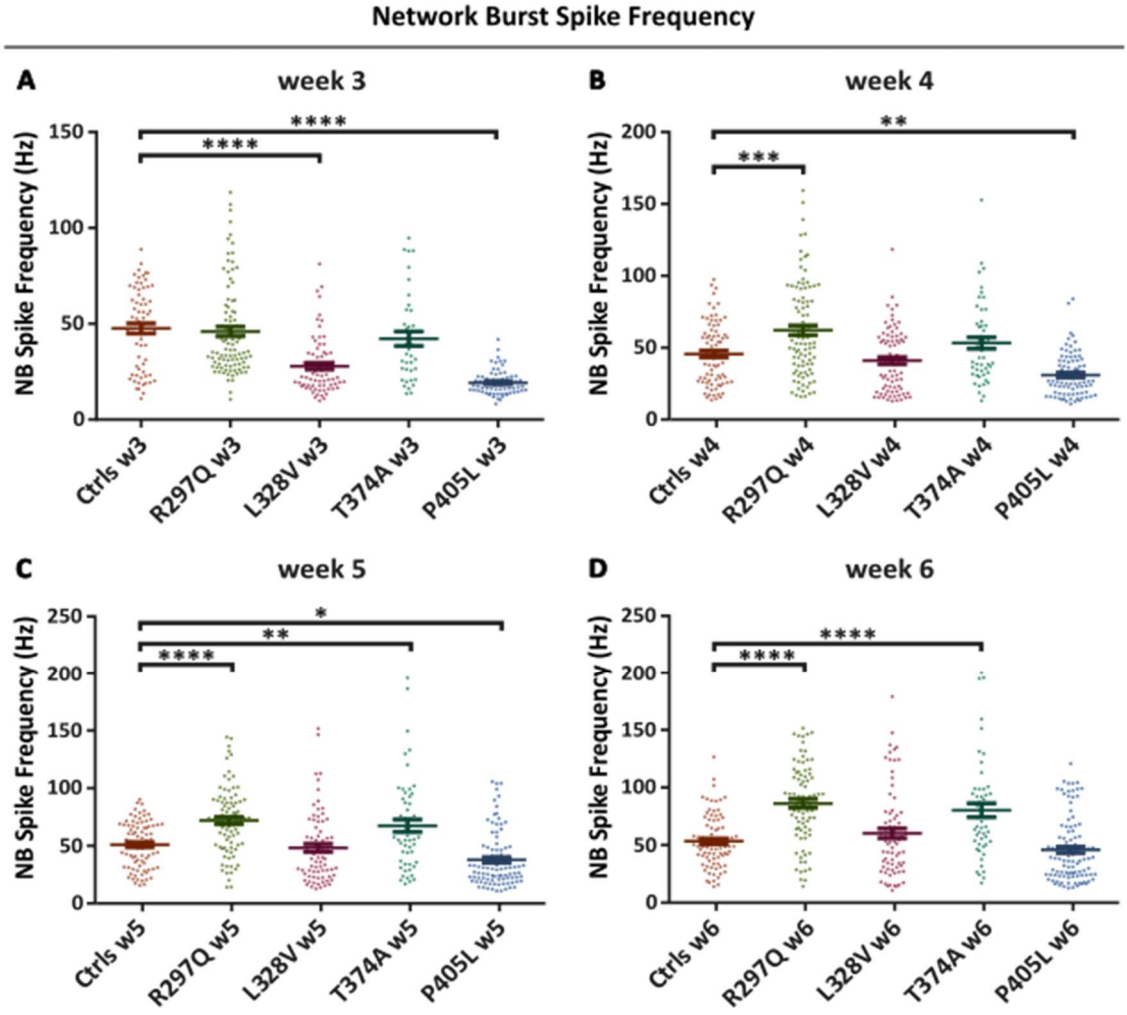

Figure 19| The mean network burst spike frequencies of the iPSC-derived neuronal networks. The spike frequencies within network bursts were calculated from ten minutes long MEA recordings and compared between the control versus *KCNA2*-R297Q (light green), *KCNA2*-L328V (pink), -T374A (dark green) and P405L (blue) neurons from week three to six (A-D). From week three to six, n-numbers are 79, 82, 83, 87 for the control-, 96, 96, 87, 83 for the *KCNA2*-R297Q, 82, 82, 74, 70 for the *KCNA2*-L328V, 46, 50, 54, 52 for the *KCNA2*-T374A, 82, 82, 99, 103 for the *KCNA2*-P405L patient-derived neurons. (Two-way ANOVA, Sidak's multiple comparisons test *p < 0.05, **p < 0.01, ***p < 0.001 and ****p < 0.0001)

Table 7| The statistical summary of burst parameters of the neuronal networks carrying *KCNA2*-R297Q, -L328V, -T374A and -P405L mutations versus control-derived neurons weeks three to six from the start of neuronal differentiation. (*p < 0.05, **p < 0.01, ***p < 0.001 and ****p < 0.001)

Burst rate (Hz)	**week 3**	**week 4**	**week 5**	**week 6**
ctrl	4.69±0.6	9.54±8.0	10.67±0.8	13.82±1.1
R297Q	13.04±0.7 ****	15.80±1.2 ****	17.06±1.5 ***	20.33±1.6**
L328V	11.75±1.0 ****	14.35±1.1 **	13.97±1.0	17.92±1.5
T374A	19.02±1.7 ****	17.35±1.4 ****	15.04±1.1	18.43±1.5
P405L	7.73±0.8	10.9±0.5	13.35±0.8	15.56±0.9
Burst duration (x10^6 us)				
ctrl	0.26±0.02	0.30±0.02	0.33±0.02	0.35±0.02
R297Q	0.52±0.02 ****	0.68±0.04 ****	0.75±0.06 ****	0.73±0.05 ****
L328V	0.32±0.02	0.64±0.06 ****	0.49±0.04	0.65±0.08 **
T374A	0.40±0.04 ***	0.84±0.12 ****	0.94±0.11 ****	0.96±0.10 ****
P405L	0.26±0.02	0.52±0.04 *	0.64±0.06 **	0.66±0.06 ***
Burst Spike Freq (Hz)				
ctrl	66.57±2.7	73.3±2.9	80.2±2.9	83.2±3.0
R297Q	62.51±2.3	77.1±3.5	89.8±3.5	107.3±4.6 ****
L328V	44.83±1.5 ****	57.43±2.5 ***	65.9±3.4 *	78.0±3.6
T374A	55.04±2.8 **	61.2±2.3	76.6±3.7	93.6±4.4
P405L	37.65±0.7 ****	46.7±1.6 ****	54.4±2.2 ****	62.7±2.6 ***

Table 8| The statistical summary of network burst parameters of the neuronal networks carrying *KCNA2*-R297Q, -L328V, -T374A and -P405L mutations versus control-derived neurons weeks three to six from the start of neuronal differentiation. (*p < 0.05, **p < 0.01, ***p < 0.001 and ****p < 0.001)

NB rate (Hz)	week 3	week 4	week 5	week 6
Ctrl	2.7±0.4	6.2±0.8	6.93±0.6	8.35±0.7
R297Q	9.9±0.7 ****	10.4±1.0 *	11.8±1.3 **	12.4±1.3 *
L328V	7.1±0.8 ***	8.2±1.0	8.4±0.9	10.5±1.2
T374A	11.5±0.9 ****	8.5±0.8	8.2±0.6	10.7±1.1
P405L	4.3±0.82	5.1±0.4	7.5±0.6	9.4±0.8
NB duration (x10^6 us)				
Ctrl	0.76±0.1	0.99±0.1	1.04±0.1	1.12±0.1
R297Q	1.37±0.1 **	1.83±0.1	1.88±0.1 **	1.94±0.1 **
L328V	1.34±0.1 *	2.5±0.3 ***	1.59±0.2	1.76±0.2 *
T374A	1.60±0.1 **	2.9±00.4 ****	2.49±0.3 ****	2.29±0.2 ****
P405L	1.67±0.2 ****	2.4±0.3 ***	2.15±0.2 ****	2.09±0.2 ****
NB Spike Freq (Hz)				
ctrl	47.55±2.6	45.58±2.4	51.00±2.2	53.42±2.4
R297Q	45.98±2.4	62.14±2.2	71.94±3.1 ****	86.23±3.8 ****
L328V	27.84±1.7 ****	41.02±2.4 ***	48.18±3.6	60.32±4.2
T374A	42.20±3.8	53.19±4.0	67.4±5.5 **	80.32±6.0 ****
P405L	19.3±0.77 ****	31.00±1.7 **	37.73±2.4 *	45.93±2.7

4.3.4 Effect of 4-AP on the network activity of the control and patient IPSC-derived neuronal cultures carrying GOF, GOF+LOF and LOF *KCNA2* mutations

The four different patient-derived neuronal cultures as well as the controls were treated with 50 and 100 µM 4-Aminopyridine (4-AP) at week six and recorded on multi-electrode arrays before and after the treatment. The effect of 4-AP on the neuronal network activity was assessed with a focus on the spiking and bursting behavior of the networks.

4.3.4.1 The effect of 4-AP on spiking behavior of the neuronal networks

On Figure 20, the effect of 4-AP on the mean firing rate of the control- and all four patient-derived lines is depicted. The application of 50 µM 4-AP significantly increased the mean firing rate of the control-derived neurons as well as of the *KCNA2*-R297Q, -L328V, -T374A, and -P405L patient-derived neurons ($p<0.0001$, $p<0.0001$, $p=0.0111$, $p=0.0047$ and $p=0.0014$ respectively, paired t-test) (Fig. 20B). Before the application of 4-AP, *KCNA2*-R297Q and -T374A patient-derived neurons had a significantly higher mean firing rate compared to that of the controls ($p<0.0001$ for both, Tukey's multiple comparisons test) (Fig. 20C). After the application of 50 µM 4-AP, the *KCNA2*-R297Q neurons' MFR was comparable to that of the controls while the *KCNA2*-T374A neurons still had significantly higher MFRs compared to the controls ($p=0.0232$ and $p=0.0160$ respectively, Tukey's multiple comparisons test) (Fig. 20C-D).

The *KCNA2*-R297Q and -T374A patient-derived neuronal cultures had significantly lower random spike percentages in comparison to the control before 4-AP application ($p<0.0001$ for both, Tukey's multiple comparisons test) (Fig. 21A). 4-AP increased the random spike percentage in the *KCNA2*-R297Q patient-derived neuronal cultures whereas the control-derived neurons' random spike percentage did not change in response to the 4-AP treatment. As a result, after the application of 50 µM 4-AP, the difference between the random spike percentages of the *KCNA2*-R297Q patient- and control-derived neurons was not significant anymore ($p= 0.5005$, Tukey's multiple comparisons test) (Fig. 21B). However, 4-AP application did not affect the random spike percentage in the *KCNA2*-T374A neuronal cultures which remained to have a significantly lower random spike percentage compared to the controls ($p=0.0649$ and $p=0.0004$ after 50 and 100 µM 4-AP, respectively, Tukey's multiple comparisons test) (Fig. 21B-C).

Figure 20| Effect of 4-AP on the mean firing rate of the iPSC-derived neuronal networks. (A) Exemplary raw traces of network activity recorded from one well in a Multiwell-MEA plates, each with 12 electrodes, before (left) and after (right) 100 µM 4-AP application are shown for control (top), *KCNA2*-R297Q (middle) and *KCNA2*-T374A (bottom) patient-derived networks. (B) The changes in the MFRs of (left to right) the control, *KCNA2*-R297Q, -L328V, T374A and -P405L patient-derived networks are depicted. The comparisons between the control and all patient-derived networks' MFRs are shown before 4-AP (C), after 50 µM 4-AP (D) and after 100 µM 4-AP (E). n-numbers before, after 50 µM and 100 µM 4-AP are 62, 51 and 55 for the control-, 48, 44 and 44 for the *KCNA2*-R297Q, 23, 16 and 18 for the *KCNA2*-L328V, 46, 42 and 45 for the *KCNA2*-T374A, 23, 16 and 16 for the *KCNA2*-P405L patient-derived neurons. (paired t-test and one-way ANOVA, *$p < 0.05$, **$p < 0.01$, ***$p < 0.001$ and ****$p < 0.0001$).

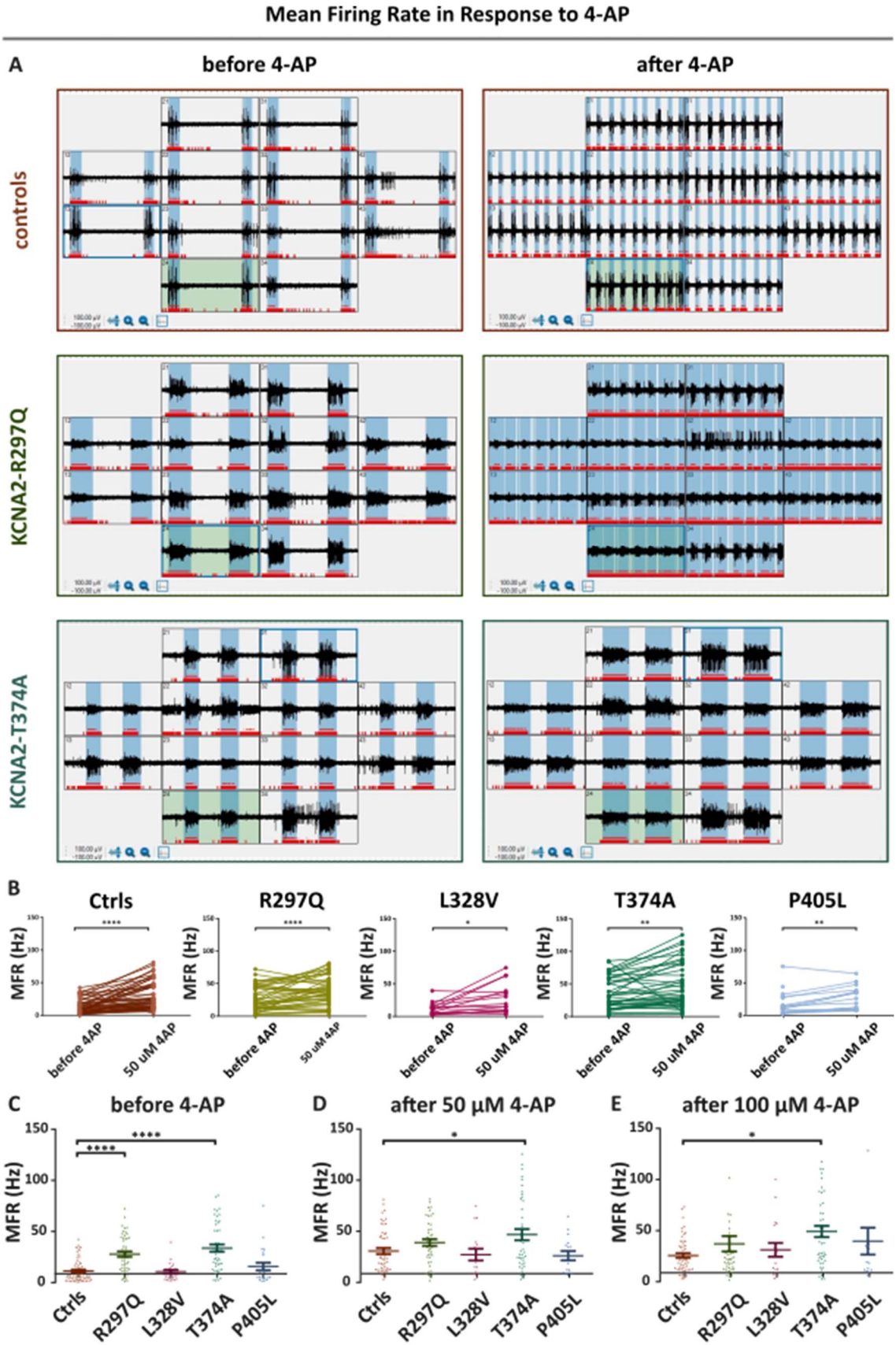
Mean Firing Rate in Response to 4-AP
A
before 4-AP
after 4-AP
controls
KCNA2-R297Q
KCNA2-T374A
B
Ctrls
R297Q
L328V
T374A
P405L
MFR (Hz)
before 4AP
50 uM 4AP
C
before 4-AP
D
after 50 µM 4-AP
E
after 100 µM 4-AP
Ctrls
R297Q
L328V
T374A
P405L

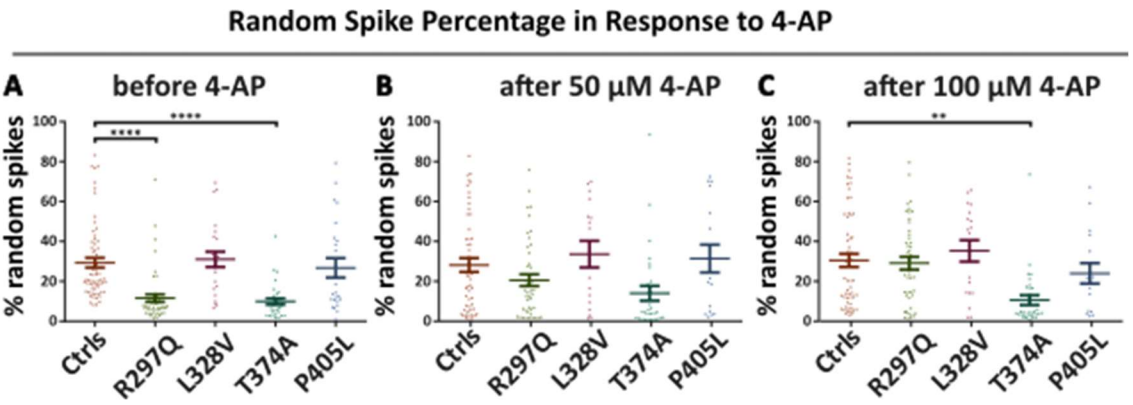

Figure 21| Effect of 4-AP on the percentage of random spikes. The percentages of the random spikes that did not belong to any bursts to all spikes were calculated and compared between the control and all patient-derived networks before 4-AP (A), after 50 µM 4-AP (B) and after 100 µM 4-AP (C). n-numbers before, after 50 µM and 100 µM 4-AP are 62, 51 and 55 for the control-, 48, 44 and 44 for the *KCNA2*-R297Q, 23, 16 and 18 for the *KCNA2*-L328V, 46, 42 and 45 for the *KCNA2*-T374A, 23, 16 and 16 for the *KCNA2*-P405L patient-derived neurons. (One-way ANOVA, *p < 0.05, **p < 0.01, ***p < 0.001 and ****p < 0.0001).

4.3.4.2 Effect of 4-AP on bursting behavior of neuronal networks

The application of 50 µM 4-AP caused a significant increase in the mean burst rates of the control-derived neuronal cultures as well as of *KCNA2*-R297Q, -L328V, -T374A, and -P405L patient-derived cultures (p<0.0001, p<0.0001, p=0.0008, p<0.0001, and p=0.0003 respectively, paired t-test) (Fig. 22A). Before the 4-AP treatment, the *KCNA2*-R297Q cultures had a significantly higher mean burst rate compared to the controls (p=0.0265, Tukey's multiple comparisons test) (Fig. 22B). After 4-AP increased the burst rates significantly in both cultures, *KCNA2*-R297Q cultures' burst rate was found to be comparable to the controls. (p=0.0948 after 100 µM 4-AP, Tukey's multiple comparisons test) (Fig. 22D). Although 4-AP also increased the burst rate of the *KCNA2*-T374A neuronal cultures, this increase was smaller than that of the controls and created a significant difference between the control- and the *KCNA2*-T374A patient-derived cultures' burst rates in response to both 50 and 100 µM 4-AP (p=0.0013 and p=0.0004 respectively, Tukey's multiple comparisons test) (Fig. 22C-D).

The application of 50 µM 4-AP shortened the mean duration of the bursts in the *KCNA2*-R297Q neuronal cultures whereas the mean burst duration was not affected in the control cultures or in the other patient cultures (Fig. 23A). Although the *KCNA2*-R297Q neuronal cultures had significantly longer burst durations before 4-AP application (p=0.0005), due to the shortening effect of the 4-AP on this line's burst duration, there was no significant difference between the control and *KCNA2*-R297Q cultures when

treated with 4-AP (p=0.9792 and p=0.9941 after 50 and 100 µM 4-AP, Tukey's multiple comparisons test) (Fig. 23B-D).

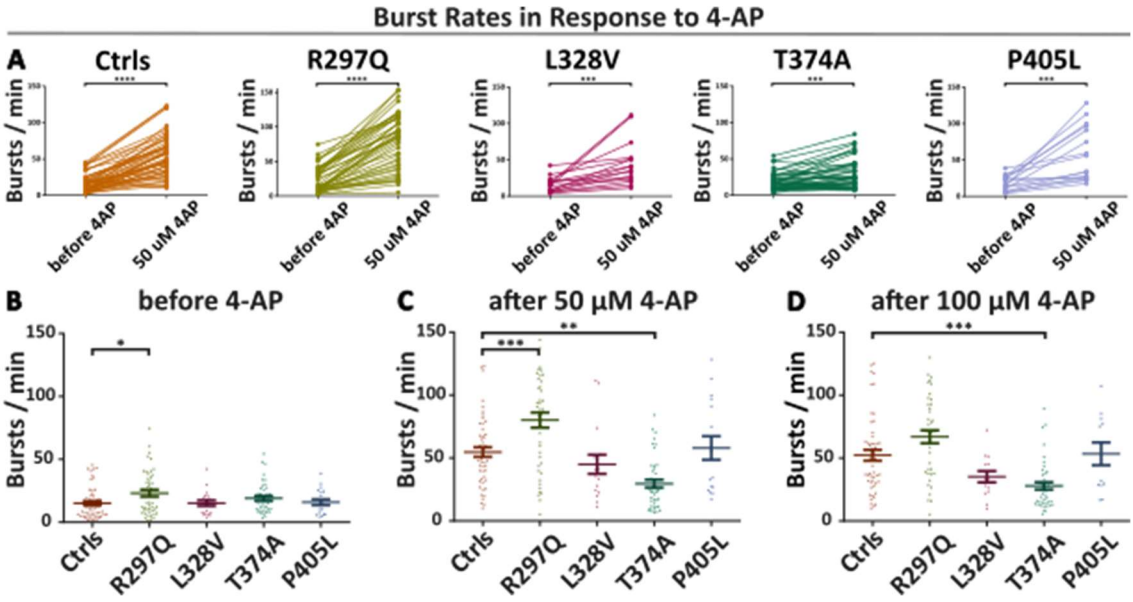

Figure 22| The effect of 4-aminopyridine on the burst rates of the iPSC-derived neuronal networks (A) The changes in the number of bursts detected per minute in (left to right) the control, *KCNA2*-R297Q, -L328V, T374A and -P405L patient-derived networks are depicted. The comparisons between the control and all patient-derived networks' burst rates are shown before 4-AP (C), after 50 µM 4-AP (D) and after 100 µM 4-AP (E). n-numbers before, after 50 µM and 100 µM 4-AP are 62, 51 and 55 for the control-, 48, 44 and 44 for the *KCNA2*-R297Q, 23, 16 and 18 for the *KCNA2*-L328V, 46, 42 and 45 for the *KCNA2*-T374A, 23, 16 and 16 for the *KCNA2*-P405L patient-derived neurons. (paired t-test and one-way ANOVA, *p < 0.05, **p < 0.01, ***p < 0.001 and ****p < 0.0001).

As the mean burst duration of the *KCNA2*-T374A neuronal cultures was significantly longer than that of the controls before 4-AP application and 4-AP did not change either of these lines' mean burst durations, the *KCNA2*-T374A neuronal cultures had still significantly longer bursts compared to the controls under 4-AP treatment (p=<0.0001 for before and after both 50 and 100 µM 4-AP, Tukey's multiple comparisons test) (Fig. 23C-D).

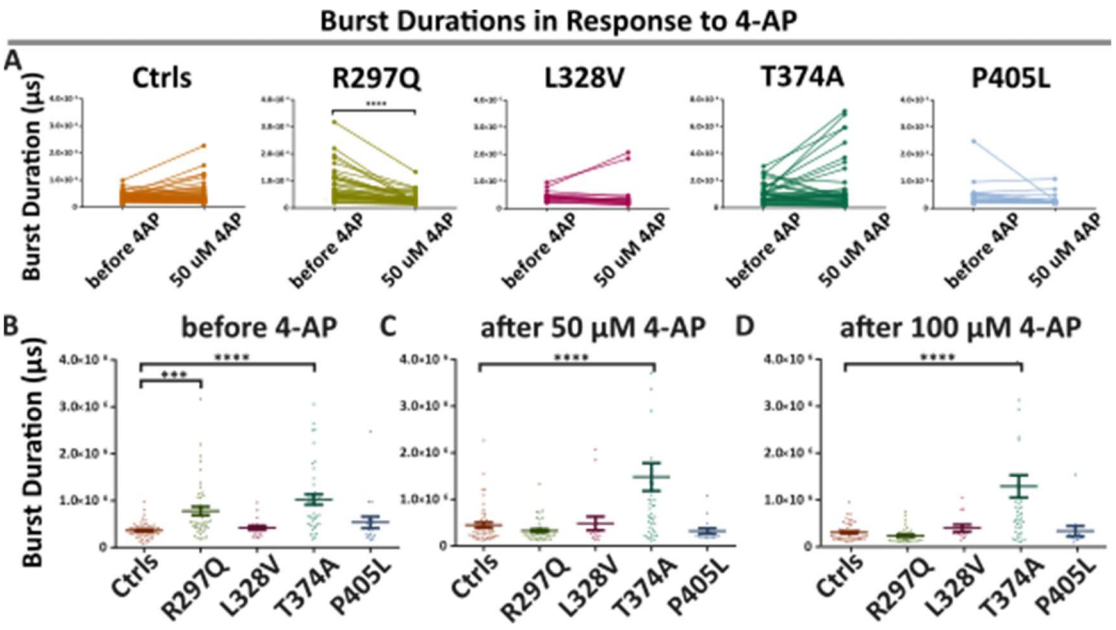

Figure 23| The effect of 4-aminopyridine on the mean burst durations of the iPSC-derived neuronal networks (A) The changes in the mean burst durations of (left to right) the control, *KCNA2*-R297Q, -L328V, T374A and -P405L patient-derived networks are depicted. The comparisons between the control and all patient-derived networks' burst durations are shown before 4-AP (C), after 50 µM 4-AP (D) and after 100 µM 4-AP (E). n-numbers before, after 50 µM and 100 µM 4-AP are 62, 51 and 55 for the control-, 48, 44 and 44 for the *KCNA2*-R297Q, 23, 16 and 18 for the *KCNA2*-L328V, 46, 42 and 45 for the *KCNA2*-T374A, 23, 16 and 16 for the *KCNA2*-P405L patient-derived neurons. (paired t-test and one-way ANOVA, *p < 0.05, **p < 0.01, ***p < 0.001 and ****p < 0.0001).

The spike frequency within the bursts was decreased in the control-derived cultures, when treated with 50 µM 4-AP, as well as in the *KCNA2*-R297Q and -P405L patient-derived cultures (p=0.0004, p<0.0001 and p=0.0034 respectively, paired t-test) (Fig. 23A). The *KCNA2*-R297Q cultures had a significantly higher burst spike frequency compared to the controls before 4-AP treatment (p=<0.0001, Tukey's multiple comparisons test) (Fig. 23B). After the application of 4-AP the difference between these two lines' burst spike frequencies was not significant anymore (p=0.2516 and p=0.9860 after 50 and 100 µM 4-AP, respectively, Tukey's multiple comparisons test) (Fig. 23C-D). Although the *KCNA2*-T374A cultures' mean burst firing frequency was not significantly different than that of the controls before 4-AP application, as the controls' frequency decreased whereas the *KCNA2*-T374A patient cultures' frequency was not affected by the 4-AP application, the *KCNA2*-T374A cultures were found to have a significantly higher burst firing frequency under 4-AP treatment (p=0.0070 and p< 0.0001 after 50 and 100 µM 4-AP, respectively, Tukey's multiple comparisons test) (Fig. 23C-D).

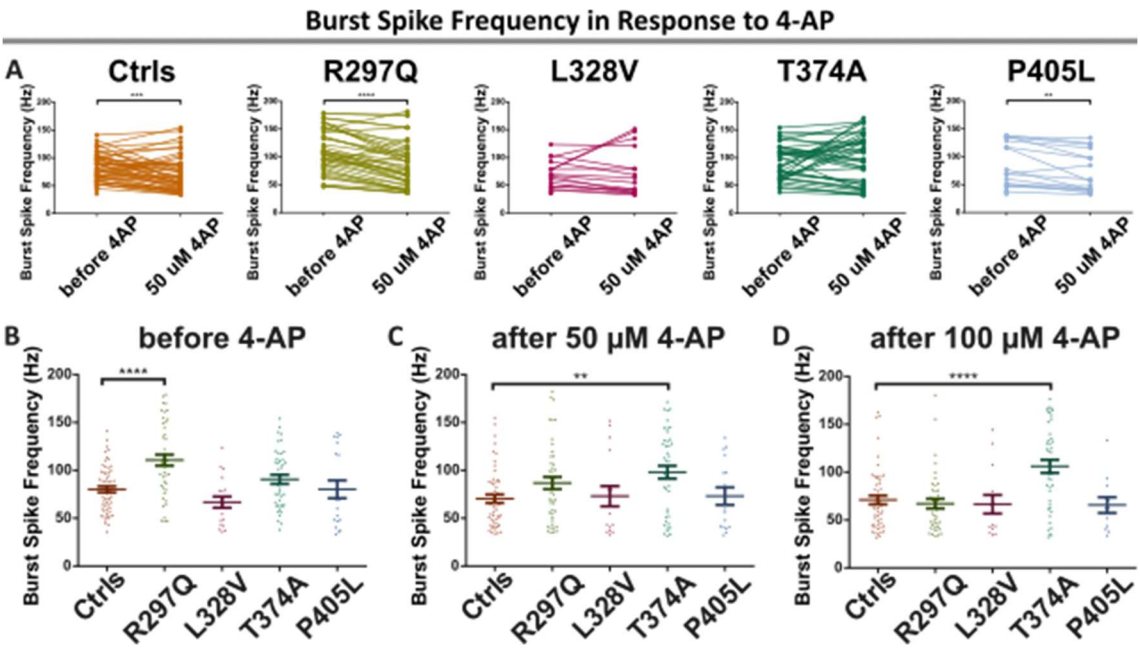

Figure 24| The effect of 4-aminopyridine on the mean burst spike frequency in the iPSC-derived neuronal networks (A) The changes in the mean burst spike frequencies in (left to right) the control, *KCNA2*-R297Q, -L328V, T374A and -P405L patient-derived networks are depicted. The comparisons between the control and all patient-derived networks' burst durations are shown before 4-AP (C), after 50 µM 4-AP (D) and after 100 µM 4-AP (E). n-numbers before, after 50 µM and 100 µM 4-AP are 62, 51 and 55 for the control-, 48, 44 and 44 for the *KCNA2*-R297Q, 23, 16 and 18 for the *KCNA2*-L328V, 46, 42 and 45 for the *KCNA2*-T374A, 23, 16 and 16 for the *KCNA2*-P405L patient-derived neurons. (paired t-test and one-way ANOVA, *p < 0.05, **p < 0.01, ***p < 0.001 and ****p < 0.0001).

4.3.4.3 Effect of 4-AP on network bursts of the neuronal networks

The effect of 4-AP application on network burst parameters was consistent with its effect on single burst parameters, as described in the previous part. Application of 50 µM 4-AP caused a significant increase in the mean network burst rates of the control-derived neuronal cultures as well as of *KCNA2*-R297Q, -L328V, -T374A, and -P405L patient-derived cultures (p< 0.0001, p< 0.0001, p=0.0014, p=0.0008, and p=0.0038 respectively, paired t-test) (Fig. 25A). Before the 4-AP application, *KCNA2*-R297Q cultures had a significantly higher mean network burst rate compared to the controls (p= 0.0188, Tukey's multiple comparisons test) (Fig. 25B). After the application of 100 µM 4-AP these patient-derived cultures had comparable burst rates to the controls (p=0.3070, Tukey's multiple comparisons test) (Fig. 25D).

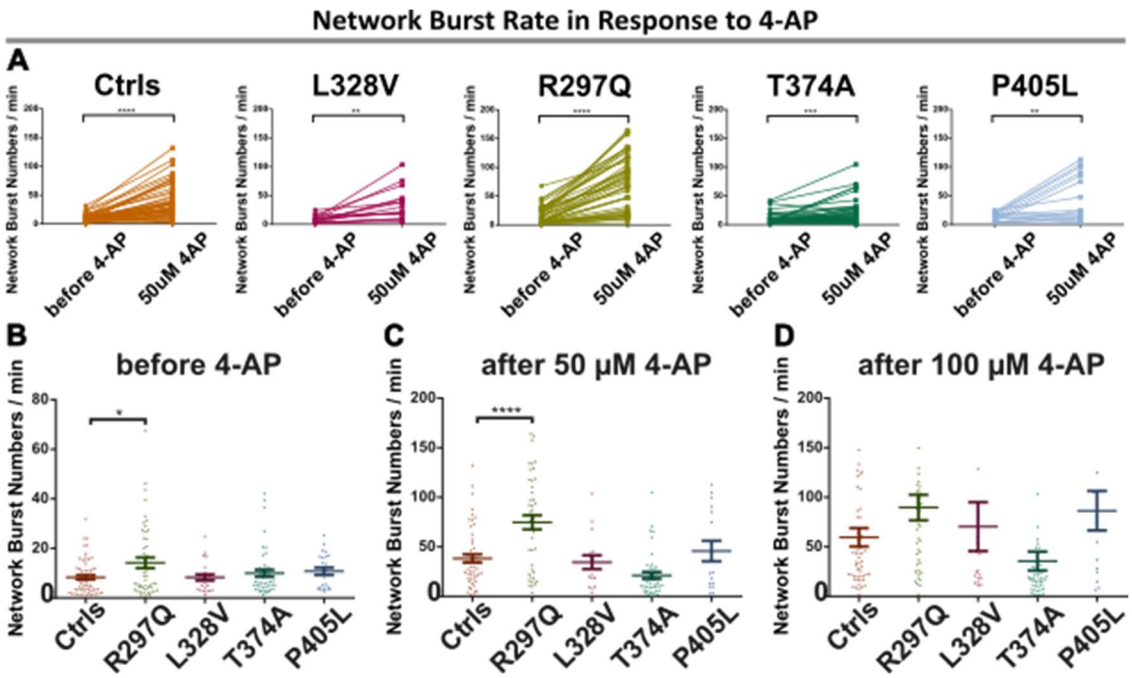

Figure 25| The effect of 4-aminopyridine on the network burst rates of the iPSC-derived neuronal networks (A) The changes in the mean number of network bursts per minute in (left to right) the control, *KCNA2*-R297Q, -L328V, T374A and -P405L patient-derived networks are depicted. The comparisons between the control and all patient-derived networks' network burst rates are shown before 4-AP (C), after 50 µM 4-AP (D) and after 100 µM 4-AP (E). n-numbers before, after 50 µM and 100 µM 4-AP are 62, 51 and 55 for the control-, 48, 44 and 44 for the *KCNA2*-R297Q, 23, 16 and 18 for the *KCNA2*-L328V, 46, 42 and 45 for the *KCNA2*-T374A, 23, 16 and 16 for the *KCNA2*-P405L patient-derived neurons. (paired t-test and one-way ANOVA, *p < 0.05, **p < 0.01, ***p < 0.001 and ****p < 0.0001).

Application of 50 µM 4-AP decreased the mean duration of the network bursts in the *KCNA2*-R297Q cultures whereas the network burst duration was not affected in the control- or the other patient-derived cultures (Fig. 26A). The *KCNA2*-R297Q neuronal cultures had significantly longer network burst durations before 4-AP application (p=0.0089) (Fig. 26B). Due to the shortening effect of the 4-AP on only their network burst durations, the *KCNA2*-R297Q cultures' mean network burst duration was comparable to the controls when treated with 4-AP (p=0.8635 and p=0.9983 for 50 and 100 µM 4-AP, Tukey's multiple comparisons test) (Fig. 26C-D).

The mean network burst duration of the *KCNA2*-T374A neuronal cultures was not affected by the application of 4-AP, that's why it was significantly longer than that of the controls before and after the 4-AP application (p=<0.0001, p=0.0267 and p=0.0002 before and after 50 and 100 µM 4-AP, respectively, Tukey's multiple comparisons test) (Fig. 26C-D).

The mean spike frequency within the network bursts was decreased in the control-derived cultures, when treated with 50 µM 4-AP, as well as in the *KCNA2*-R297Q and -P405L patient cultures (p=0.0083, p-value <0.0001 and p= 0.0104 respectively, paired t-test) (Fig. 27A). Although the *KCNA2*-R297Q cultures had a significantly higher mean network burst spike frequency compared to the controls before 4-AP, there was no significant difference anymore after the application of 4-AP (p=<0.0001, p=0.2516 and p=0.9860 before and after 50 and 100 µM 4-AP, respectively, Tukey's multiple comparisons test) (Fig. 27C-D).

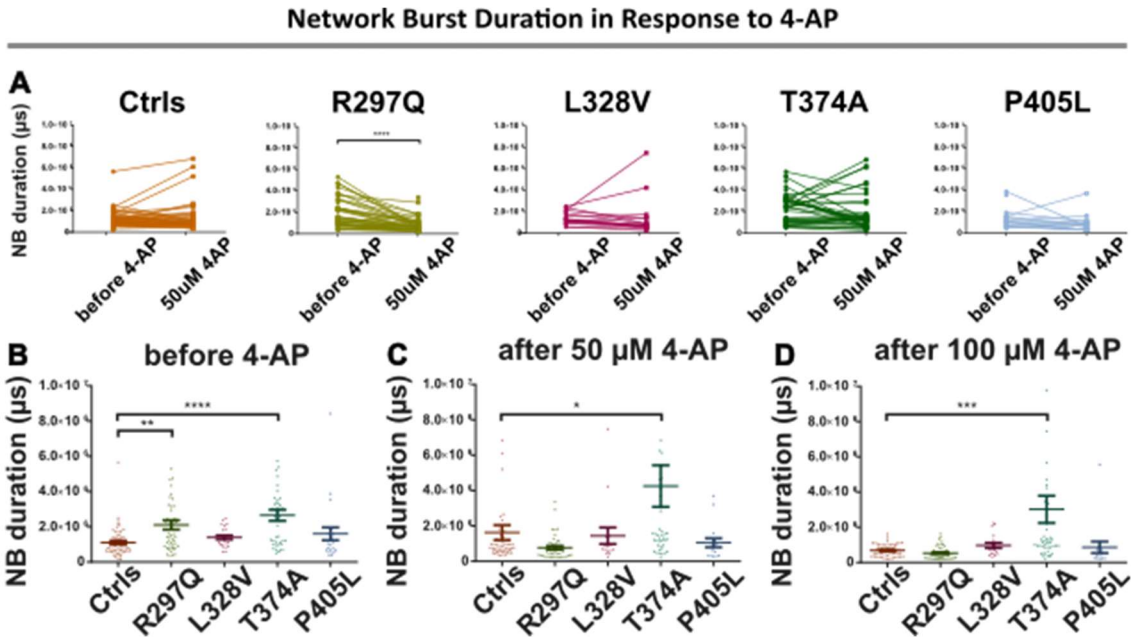

Figure 26| The effect of 4-aminopyridine on the mean network burst durations of the iPSC-derived neuronal networks (A) The changes in the mean network burst durations in (left to right) the control, *KCNA2*-R297Q, -L328V, T374A and -P405L patient-derived networks are depicted. The comparisons between the control and all patient-derived networks' network burst durations are shown before 4-AP (C), after 50 µM 4-AP (D) and after 100 µM 4-AP (E). n-numbers before, after 50 µM and 100 µM 4-AP are 62, 51 and 55 for the control-, 48, 44 and 44 for the *KCNA2*-R297Q, 23, 16 and 18 for the *KCNA2*-L328V, 46, 42 and 45 for the *KCNA2*-T374A, 23, 16 and 16 for the *KCNA2*-P405L patient-derived neurons. (paired t-test and one-way ANOVA, *p < 0.05, **p < 0.01, ***p < 0.001 and ****p < 0.0001).

The *KCNA2*-T374A cultures' network burst firing frequency was not affected by the application of 4-AP, therefore it was significantly higher than that of the controls before and after the 4-AP application (p=0.0038 before 4-AP, p<0.0001 after both 50 and 100 µM 4-AP, Tukey's multiple comparisons test) (Fig. 27B-D).

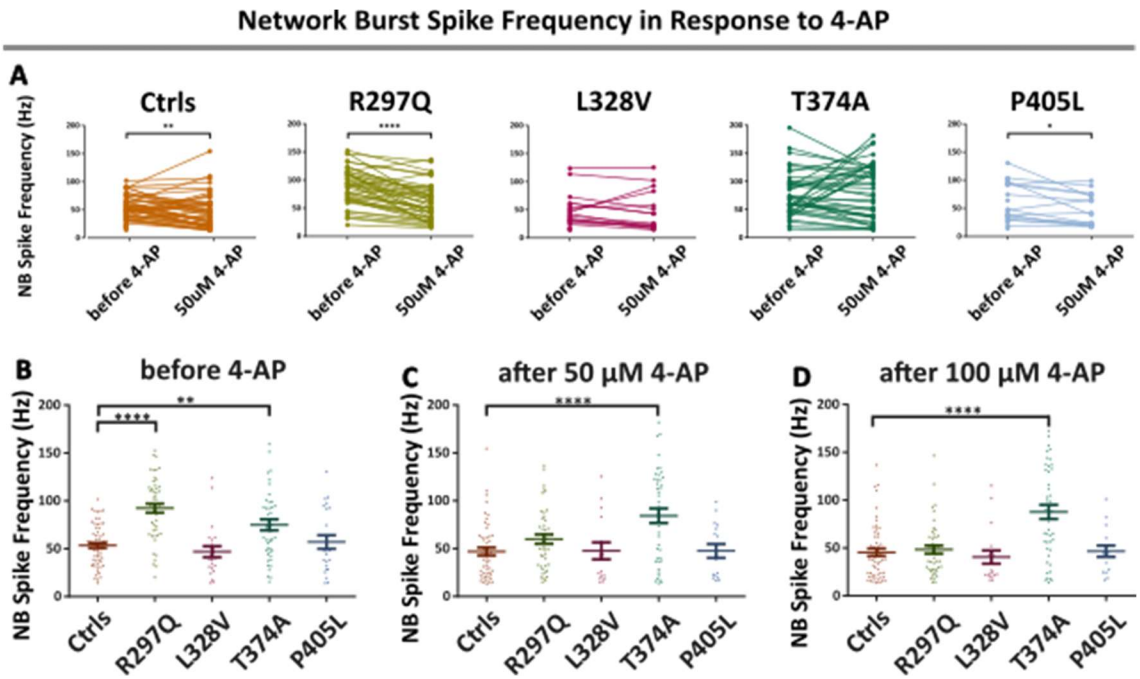

Figure 27| The effect of 4-aminopyridine on the mean network burst spike frequencies of the iPSC-derived neuronal networks (A) The changes in the spike frequencies during network bursts in (left to right) the control, *KCNA2*-R297Q, -L328V, T374A and -P405L patient networks are depicted. The comparisons between the control and all patient-derived networks' network burst spike frequencies are shown before 4-AP (C), after 50 µM 4-AP (D) and after 100 µM 4-AP (E). n-numbers before, after 50 µM and 100 µM 4-AP are 62, 51 and 55 for the control-, 48, 44 and 44 for the *KCNA2*-R297Q, 23, 16 and 18 for the *KCNA2*-L328V, 46, 42 and 45 for the *KCNA2*-T374A, 23, 16 and 16 for the *KCNA2*-P405L patient-derived neurons. (paired t-test and one-way ANOVA, *p < 0.05, **p < 0.01, ***p < 0.001 and ****p < 0.0001).

Table 9| Statistical summary of changes observed in the network activities of the neuronal populations carrying *KCNA2*-R297Q, -L328V, -T374A and -P405L mutations and healthy populations in response to 50 µM 4-AP treatment in comparison to before 4-AP. (*p < 0.05, **p < 0.01, ***p < 0.001 and ****p < 0.001, paired t-test)

50 µM 4-AP	Ctrls	R297Q	L328V	T374A	P405L
MFR	increased ****	increased ****	increased *	increased **	increased **
% random spikes	n.s.	increased ***	n.s.	n.s.	n.s.
burst rate	increased ****	increased ****	increased ***	increased ***	increased ***
burst duration	n.s.	shortened ****	n.s.	n.s.	n.s.
burst spike frequency	decreased ***	decreased ****	n.s.	n.s.	decreased *
NB rate	increased ****	increased **	increased ****	increased ***	increased **
NB duration	n.s.	shortened ****	n.s.	n.s.	n.s.
NB spike freq	decreased ***	decreased ****	n.s.	n.s.	decreased *

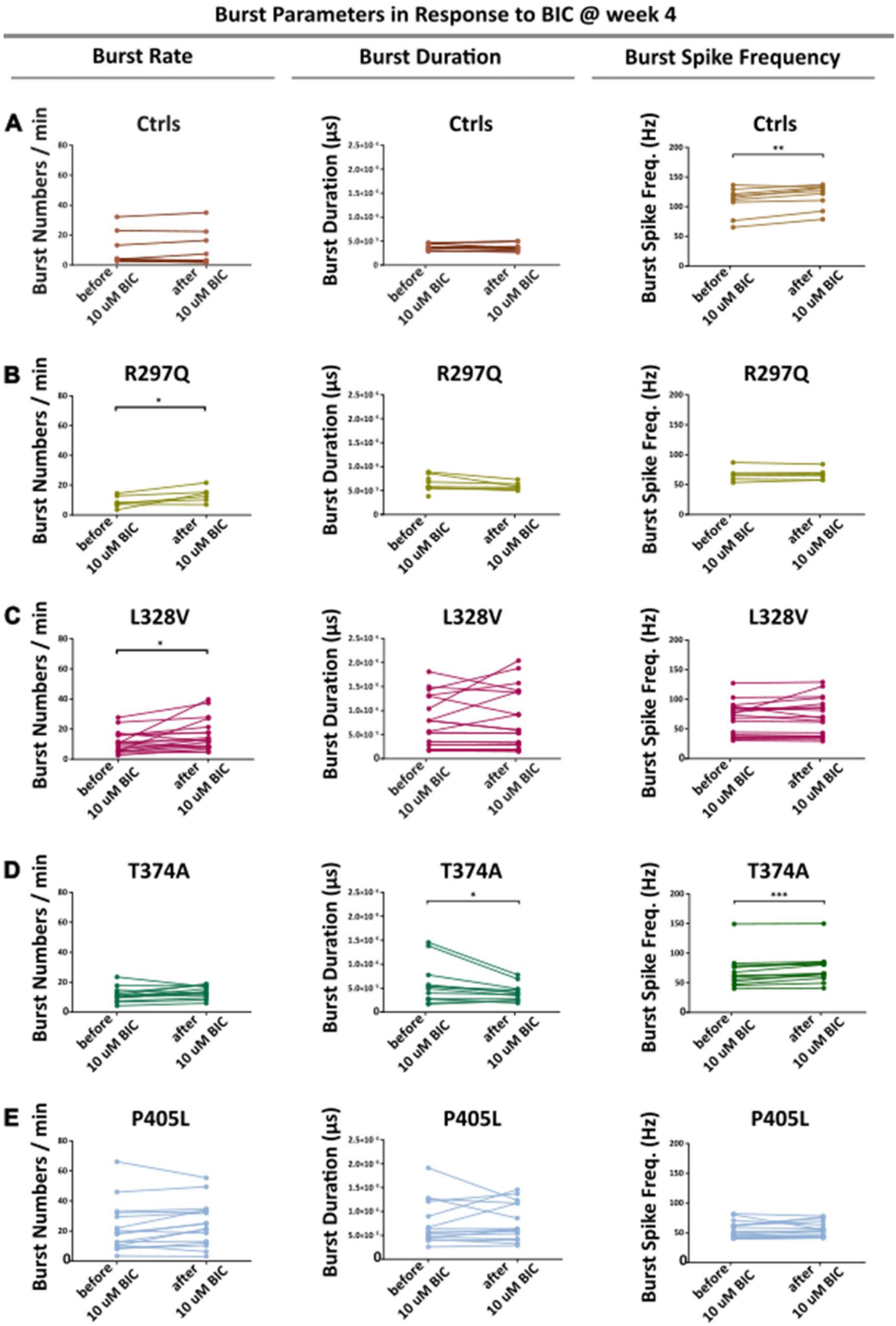

Figure 28| The effect of Bicuculline on bursting behavior of the patient and control iPSC-derived neurons. The changes in the burst rate (left), duration (middle) and spike frequency (right) of the control, *KCNA2*-R297Q, -L328V, T374A and -P405L patient-derived networks (A-E) are depicted.

4.3.5 Effect of BIC on the network activity of IPSC-derived neuronal cultures with GOF, LOF and GOF+LOF KCNA2 mutations

To assess the involvement of inhibitory neurons, that are generated as a by-product of the NGN2 protocol, in network activity and potential role in the comparison between the control- and patient-derived neuronal cultures, the cultures were treated with 10 µM BIC. The effect on the bursting behavior of the cultures was assessed comparing the MEA recordings performed before and after BIC applications.

4.3.5.1 Effect of BIC on four-weeks-old neuronal cultures' bursting behavior

In response to the 10 µM BIC treatment, the *KCNA2*-R297Q and -L328V patient-derived neuronal cultures' burst rates significantly increased compared to the burst rates measured before the BIC application (p=0.0430 and p=0.0222 respectively, paired t-test). The mean burst duration was affected only in the *KCNA2*-T374A cultures, which was significantly shortened upon the 10 µM BIC treatment (p=0.0335, paired t-test). Moreover, spike frequency within the bursts was significantly increased only in the control- and the *KCNA2*-T374A patient-derived cultures (p=0.0029 and p=0.0005 respectively, paired t-test) (Fig. 28A-E, right).

4.3.5.2 Effect of BIC on the four-weeks-old neuronal cultures' network bursts

When treated at week four, BIC increased the network burst rates in the *KCNA2*-R297Q, -L328V and -T374A cultures (p=0.0440, p=0.0339 and p= 0.0026 respectively, paired t-test). The control and the *KCNA2*-P405L patient cultures' network burst rates were not affected by the BIC treatment. The mean network burst duration was significantly shortened in the control- and the *KCNA2*-R297Q and -T374A patient-derived cultures in response to the 10 µM BIC treatment (p=0.0117, p=0.0160 and p=0.0006 respectively, paired t-test). (Fig. 29A-E).

Figure 29| The effect of Bicuculline on network burst features of the patient and control iPSC-derived neurons. The changes in the network burst rate (left), duration (middle) and spike frequency (right) of the control, *KCNA2*-R297Q, -L328V, T374A and -P405L patient-derived networks (A-E) are depicted.

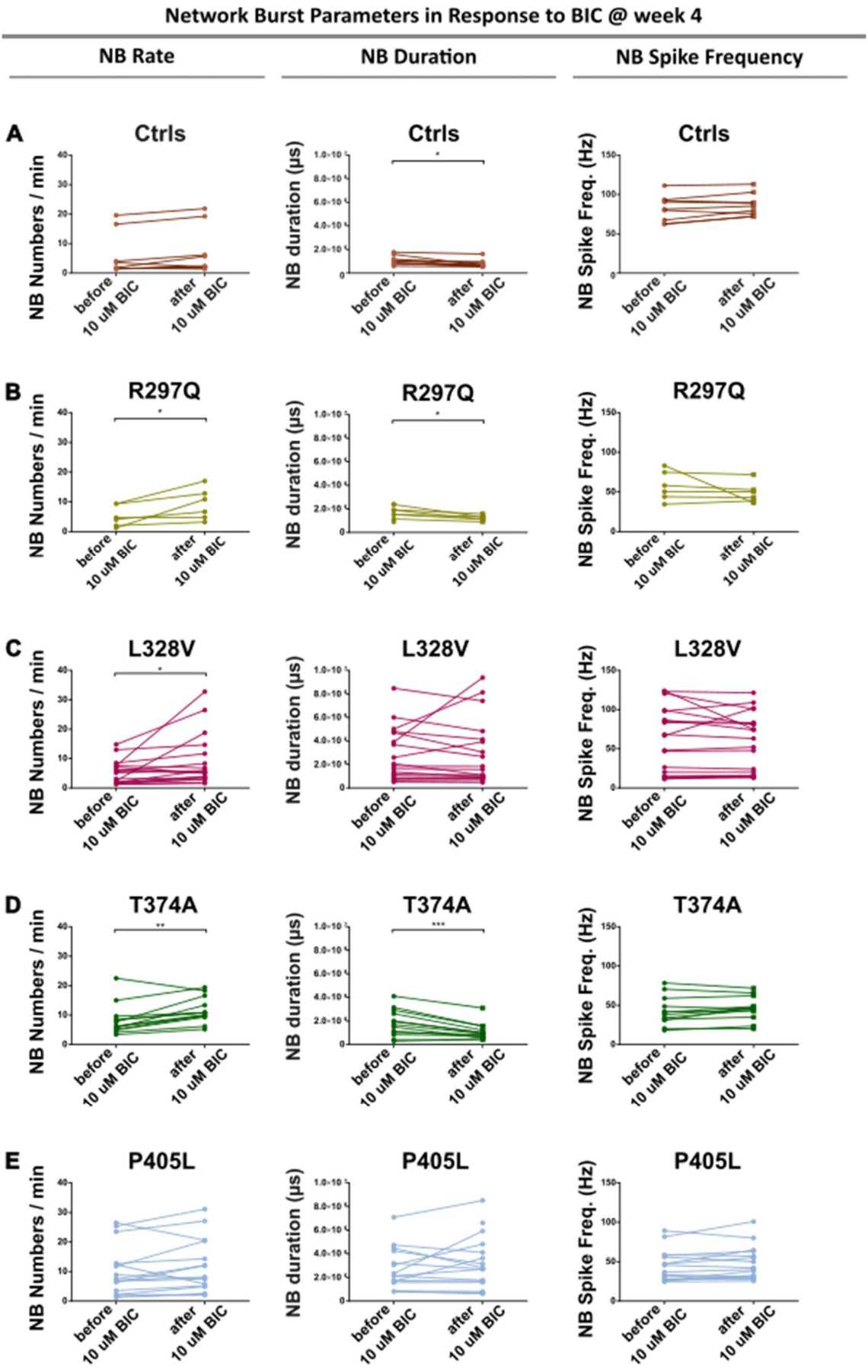
Network Burst Parameters in Response to BIC @ week 4
NB Rate
NB Duration
NB Spike Frequency
A
Ctrls
B
R297Q
C
L328V
D
T374A
E
P405L
NB Numbers / min
NB duration (µs)
NB Spike Freq. (Hz)
before 10 uM BIC
after 10 uM BIC
*
**
***

4.3.5.3 The effect of BIC on the six-weeks-old KCNA2-R297Q neuronal cultures' network activity

At week six, the number of bursts recorded per minute significantly decreased in both control- and *KCNA2*-R297Q patient-derived neuronal networks in response to 10 µM BIC treatment (p=0.0111 and p=0.0003 respectively, paired t-test). The patient cultures had significantly higher burst rates before and after the 10 µM BIC treatment (p= 0.0104 and p=0.0047, respectively, unpaired t test) (Fig. 30A). Although BIC did not affect the *KCNA2*-R297Q patient cultures' mean burst duration, it significantly decreased the mean burst duration in the control-derived neuronal cultures (p= 0.0072, paired t-test). After the BIC treatment, the *KCNA2*-R297Q cultures' burst duration was found to be significantly longer than that of the controls (p=0.0011, unpaired t test) (Fig. 30B)

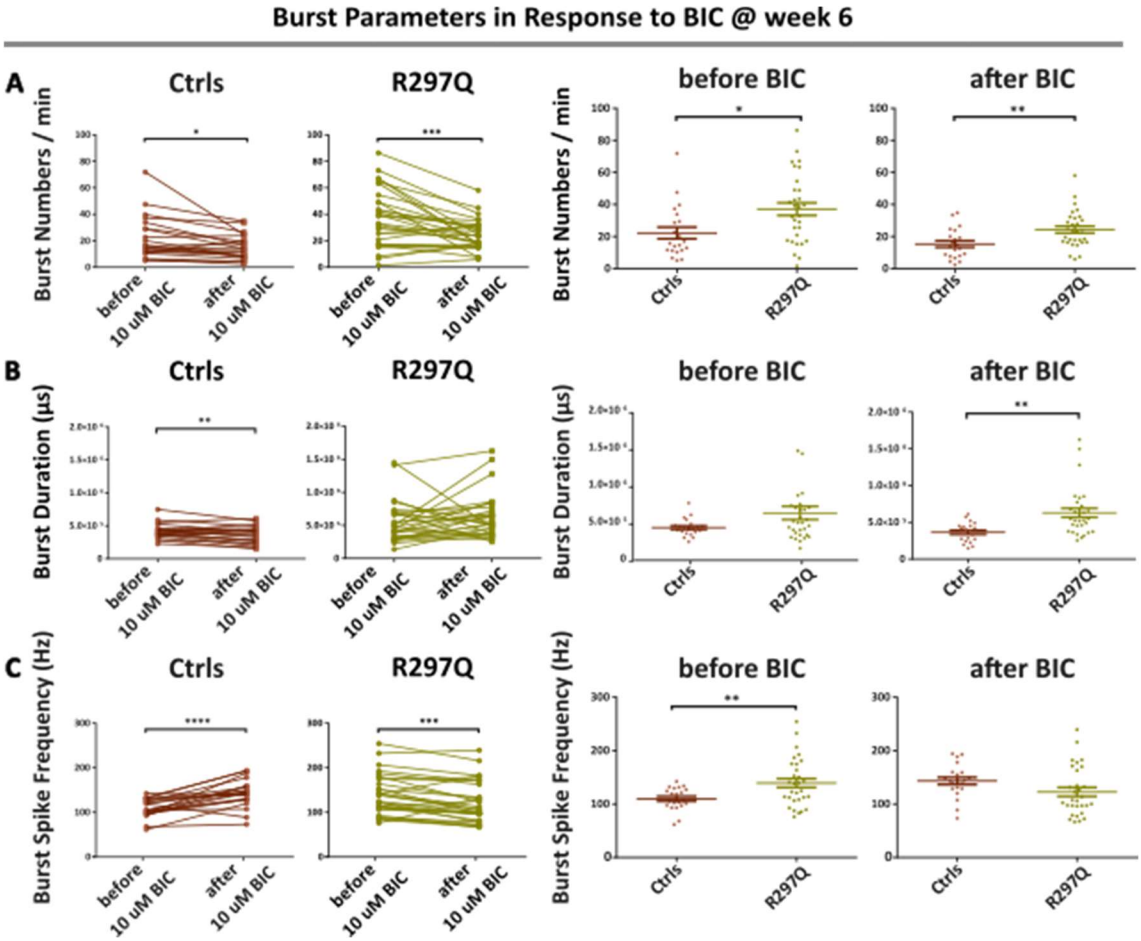

Figure 30| The effect of bicuculine on the bursting parameters of the *KCNA2*-R297Q patient-derived networks compared to the controls at week six. The change in the burst rate (A), duration (B) and spike frequency (C) in control and the *KCNA2*-R297Q patient-derived networks as well as the comparison between these two lines before and after BIC treatment is depicted (left to right). n-numbers before and after 10 µM BIC are 21 and 21 for the control-, 30 and 30 for the *KCNA2*-R297Q patient-derived cultures. (Paired and unpaired t-test, *p < 0.05, **p < 0.01, ***p < 0.001 and ****p < 0.0001).

BIC increased the spike frequency within bursts significantly in the control-derived cultures whereas the *KCNA2*-R297Q cultures' burst spike frequency was significantly decreased ($p<0.0001$ and $p=0.0006$ respectively, paired t-test). Before the BIC treatment, the *KCNA2*-R297Q cultures had significantly higher burst spike frequency compared to the controls and there was no significant difference anymore after the 10 µM BIC treatment ($p=0.0079$ and $p=0.0775$ before and after BIC, unpaired t-test) (Fig. 30C).

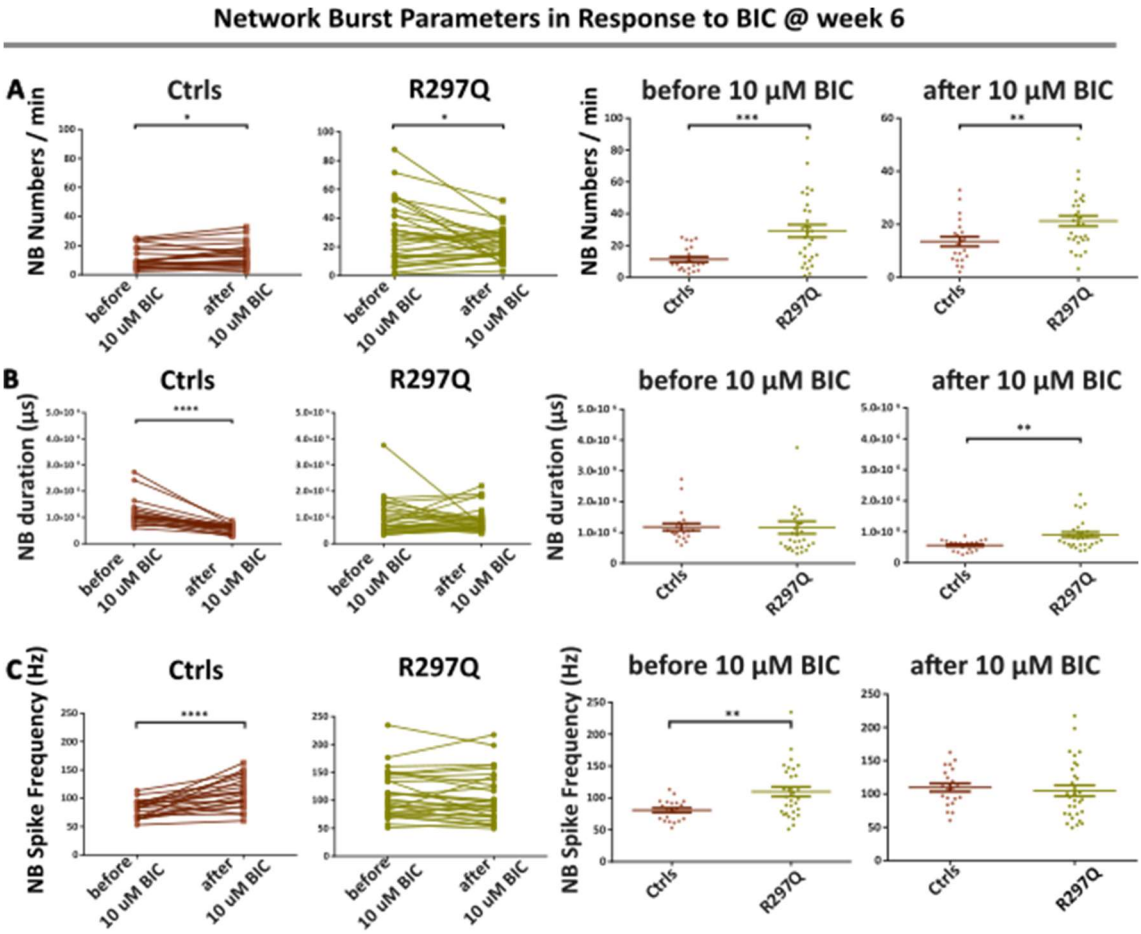

Figure 31| The effect of bicuculine on the network burst parameters of the *KCNA2*-R297Q patient-derived networks compared to the controls at week six. The change in the network burst rate (A), duration (B) and spike frequency (C) in control and the *KCNA2*-R297Q patient-derived networks as well as the comparison between these two lines before and after BIC treatment is depicted (left to right). n-numbers before and after 10 µM BIC are 21 and 21 for the control-, 30 and 30 for the *KCNA2*-R297Q patient-derived cultures. (Paired and unpaired t-test, *p < 0.05, **p < 0.01, ***p < 0.001 and ****p < 0.0001).

The network burst rates in both control- and the *KCNA2*-R297Q patient-derived cultures significantly increased in response to the 10 µM BIC treatment at week six ($p=0.0380$ and $p=0.0206$ respectively, paired t-test). The *KCNA2*-R297Q cultures had significantly higher network burst rates compared to the controls before the 10 µM BIC treatment

as well as after the 10 µM BIC treatment (p=0.0007 and p=0.0081 respectively, unpaired t-test) (Fig. 31A). While *KCNA2*-R297Q cultures' mean network burst duration was not affected, BIC shortened that of the control-derived cultures significantly (p<0.0001, unpaired t-test), leading to a significant difference between the mean network burst durations of the two lines after BIC application (p=0.0015, unpaired t-test) (Fig. 31B).

The *KCNA2*-R297Q patient cultures had a significantly higher mean network burst spike frequency compared to that of the controls before BIC application (p=0.0033, unpaired t-test). BIC did not affect the network burst spike frequency in the patient-derived cultures, while it elevated the frequency in control-derived cultures (p<0.000, paired t-test). Therefore, the difference between the two lines' network burst spike frequencies was not significant anymore after the 10 µM BIC treatment (Fig. 31C).

Table 10| The statistical summary of the changes observed in the network activities of the neuronal populations carrying *KCNA2*-R297Q, -L328V, -T374A and -P405L mutations and healthy populations in response to 10 µM Bicuculine treatment at week four. (*p < 0.05, **p < 0.01, ***p < 0.001 and ****p < 0.001)

10 µM BIC @ week 4	Ctrls	R297Q	L328V	T374A	P405L
burst rate	n.s.	increased *	increased *	n.s.	n.s.
burst duration	n.s.	n.s.	n.s.	shortened *	n.s.
burst spike frequency	increased **	n.s.	n.s.	increased **	n.s.
NB rate	n.s.	increased *	increased *	increased **	n.s.
NB duration	shortened *	shortened *	n.s.	shortened ***	n.s.
NB spike freq	n.s.	n.s.	n.s.	n.s.	n.s.

Table 11| The statistical summary of the changes observed in the network activities of the neuronal populations carrying *KCNA2*-R297Q and healthy populations in response to 10 µM Bicuculine treatment at week six. (*p < 0.05, **p < 0.01, ***p < 0.001 and ****p < 0.001)

10 µM BIC @week 6	Ctrls	R297Q
burst rate	decreased *	decreased ***
burst duration	decreased **	n.s.
burst spike frequency	increased ****	decreased ***
NB rate	increased *	increased *
NB duration	decreased ****	n.s.
NB spike freq	increased ****	n.s.

4.4 Electrophysiological investigation of the *KCNA2*-R297Q, -L328V and -P405L mutations in IPSC-derived neurons using the patch-clamp technique

The functional effects of three different *KCNA2* mutations that belonged to different functional groups, *KCNA2*-R297Q (GOF), -L328V (GOF+LOF) and -P405L (LOF), were investigated in IPSC-derived cortical excitatory neuronal cultures also on a single cell level. Active and passive electric properties of single neurons were assessed and compared to those of the controls, via the patch-clamp technique, four and six weeks later after the start of the differentiations. The results are shown as mean±sem.

4.4.1 Passive electrical properties

The mean cell capacitance increased from week four to week six significantly only for control- and *KCNA2*-P405L patient-derived neurons (p=0.0008 and p=<0.0001, respectively, Sidak's multiple comparison test). The mean cell capacitance of any of the patient lines was not significantly different than that of the control-derived neurons, at week four or six.

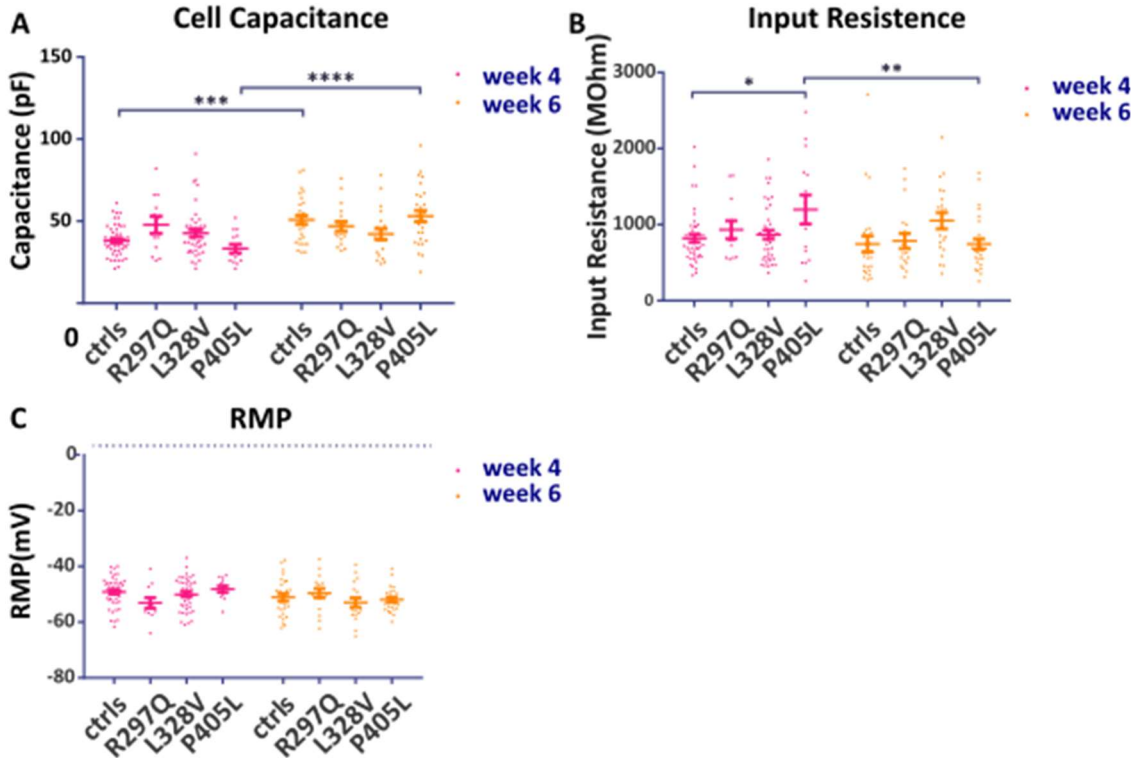

Figure 32| Passive electrical properties of the iPSC-derived four and six-weeks old neurons. Cell capacitances (A), input resistances (B) and resting membrane potentials (C) of the control and the *KCNA2*-R297Q, -L328V and -P405L patient-derived neurons were depicted both at week four and six and compared to each other. For weeks four and six, n-numbers are 46 and 28 for the control-, 12 and 18 for the *KCNA2*-R297Q, 43 and 20 for the *KCNA2*-L328V, 14 and 28 for the

KCNA2-P405L patient-derived neurons. (One-way ANOVA, Tukey's multiple comparisons test, *p < 0.05, **p < 0.01, ***p < 0.001 and ****p < 0.0001)

At week four, the mean input resistance of the *KCNA2*-P405L patient line was significantly higher than that of the controls (p=0.0296, Sidak's multiple comparison test). As it decreased significantly from week four to six, it was comparable to the controls at week six (p=0.0069, Sidak's multiple comparison test). The resting membrane potentials of the patient-derived neurons were also not significantly different than that of the controls at week four or at week six.

4.4.2 Evoked action potential trains

To assess intrinsic firing properties of the neurons, 800 ms long depolarizing current pulses of increasing amplitudes were given to the cells and the resulting action potential trains were examined when the neurons were four and six weeks old. The number evoked action potentials recorded from control- vs. patient-derived neurons are depicted separately for each patient line and at both time points in Figure 33.

At week four, the *KCNA2*-R297Q patient-derived neurons fired a smaller number of action potentials in response to injected current amplitudes up to 39 pA but in response to 44 pA and bigger amplitudes of current pulses they fired more action potentials compared to the control-derived neurons (Fig. 33A-left). At week six, the *KCNA2*-R297Q patient-derived neurons fired slightly higher number of action potentials up to 49 pA current injection level (Fig. 33A-right). Above 49 pA level, the number of evoked action potentials decreased with increasing current amplitudes for the patient-derived neurons, whereas the control-derived neurons' evoked action potential number kept increasing in response to increasing current amplitudes. Overall, the *KCNA2*-R297Q patient-derived neurons' action potential firing pattern in response a range of depolarizing current pulses was significantly different than that of the control-derived neurons both at week four and six (interaction p<0.0001 and interaction p=0.0298, respectively, two-way repeated measures ANOVA). The evoked firing pattern of the *KCNA2*-L328V patient-derived neurons was similar to that of the *KCNA2*-R297Q patient-derived neurons at both time points, significantly differing from that of the control-derived neurons at week four and six (interaction p<0.0001 at both time points, two-way repeated measures ANOVA).

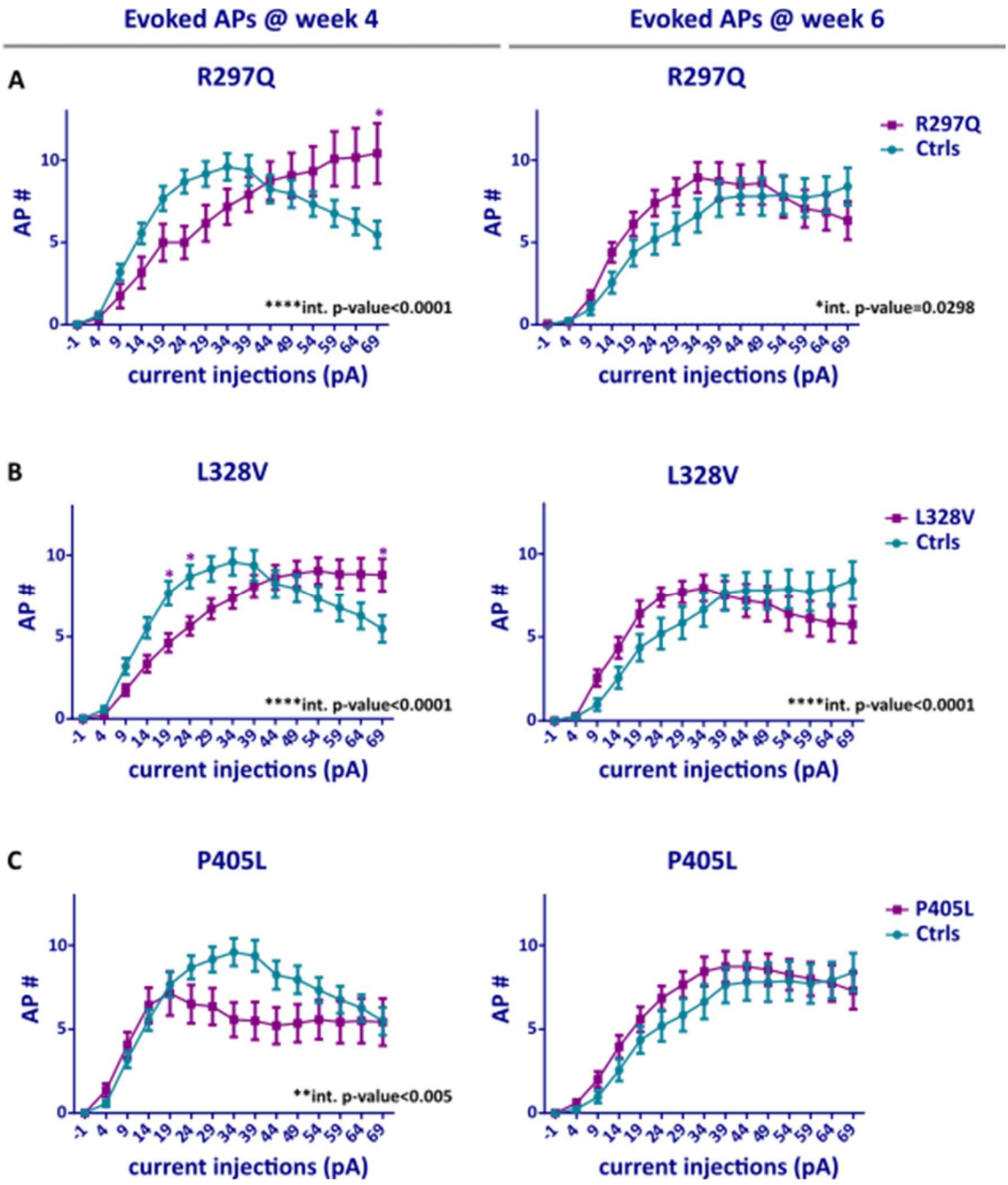

Figure 33| Input-output curves of the iPSC derived control versus *KCNA2*-R297Q (A), -L328V (B) and -P405L (C) patient-derived neurons. The number of evoked action potentials evoked in response to a range of depolarizing currents at week four (left) and week six (right) are compared between the control (blue) and patient (purple) neurons. For weeks four and six, n-numbers are 42 and 25 for the control-, 12 and 18 for the *KCNA2*-R297Q, 40 and 20 for the *KCNA2*-L328V, 14 and 27 for the *KCNA2*-P405L patient-derived neurons.(One-way ANOVA, Sidak's multiple comparisons test, *p < 0.05, **p < 0.01, ***p < 0.001 and ****p < 0.0001).

The *KCNA2*-P405L patient-derived neurons fired a smaller number of action potentials especially for the mid-amplitudes of current pulses given and the evoked firing pattern of these patient-derived neurons was significantly different than that of the controls at week four (interaction p<0.005, two-way repeated measures ANOVA). At week six, the patient-derived neurons fired comparable number of action potentials to the controls.

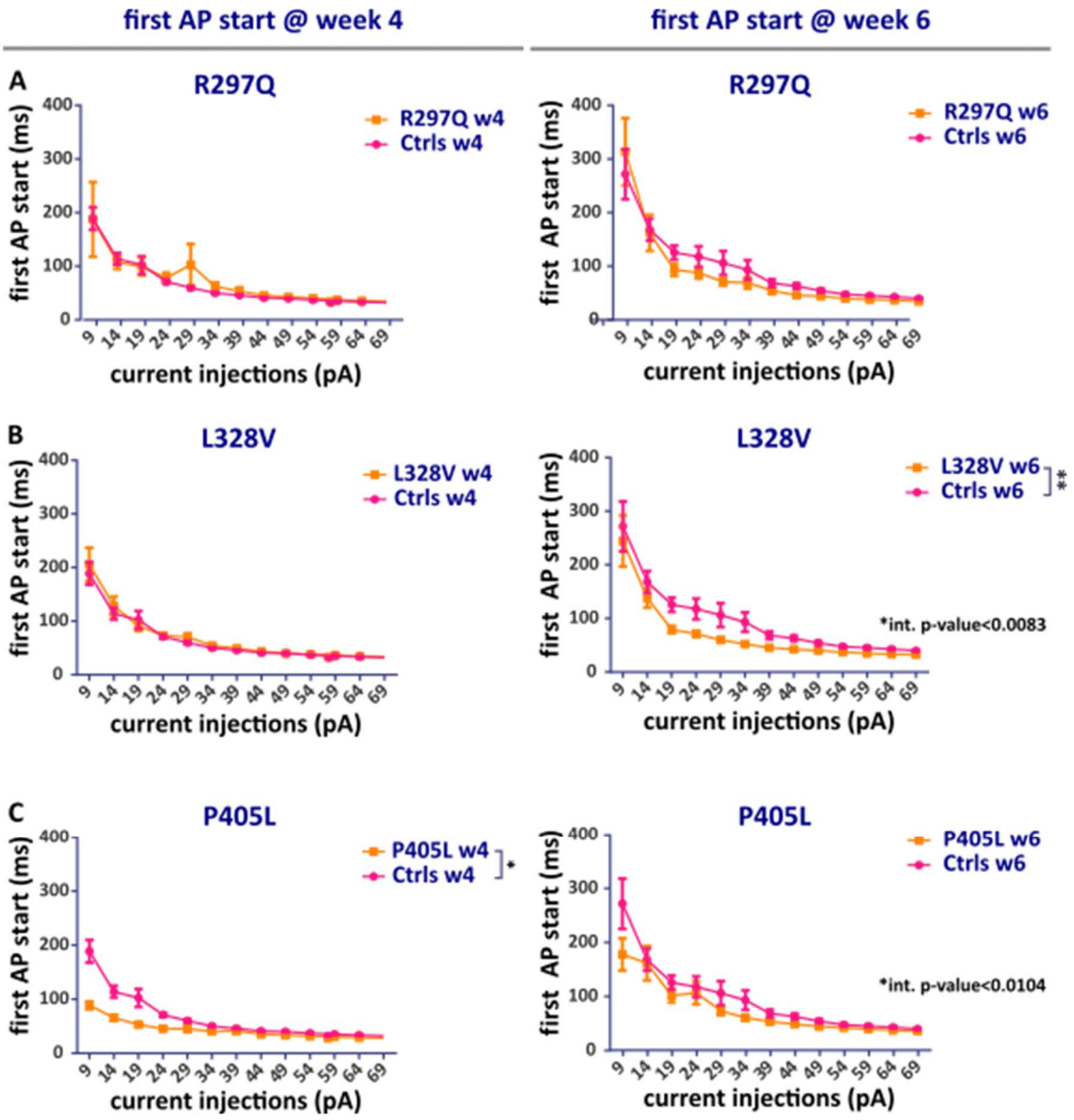

Figure 34|AP start times of the iPSC derived control versus *KCNA2*-R297Q (A), -L328V (B) and -P405L (C) patient-derived neurons. The start times of the first action potentials that were evoked in response to a range of depolarizing current injections were assessed and compared between the control and patient lines, at week four (left) and six (right). For weeks four and six, n-numbers are 42 and 25 for the control-, 12 and 18 for the *KCNA2*-R297Q, 40 and 20 for the *KCNA2*-L328V, 14 and 27 for the *KCNA2*-P405L patient-derived neurons.(One-way ANOVA, Sidak's multiple comparisons test, *p < 0.05, **p < 0.01, ***p < 0.001 and ****p < 0.0001).

Single AP parameters of the first action potentials fired in action potential trains, evoked in response to different amplitudes of depolarizing current pulses for each neuron recorded, were assessed. These parameters, being first AP half-width, area, time-to-peak, were compared between the control and patient lines at week four and six.

The mean first AP start times are depicted in Figure 34. All the cell lines needed longer time durations to start firing an action potential when they were stimulated with smaller amplitudes of current pulses compared to larger current pulses. The mean first AP start

time was not significantly different between the *KCNA2*-R297Q neurons and the controls at week four or six whereas the *KCNA2*-L328V neurons' mean AP start time was shorter than that of the controls at week six. The *KCNA2*-P405L neurons' first AP start time was shorter than the that of the controls at week four (Fig. 34C-left) (p=0.0431, two-way repeated measures ANOVA). It was shorter than that of the controls also at week six, especially for smaller current amplitudes (Fig. 34B-right).

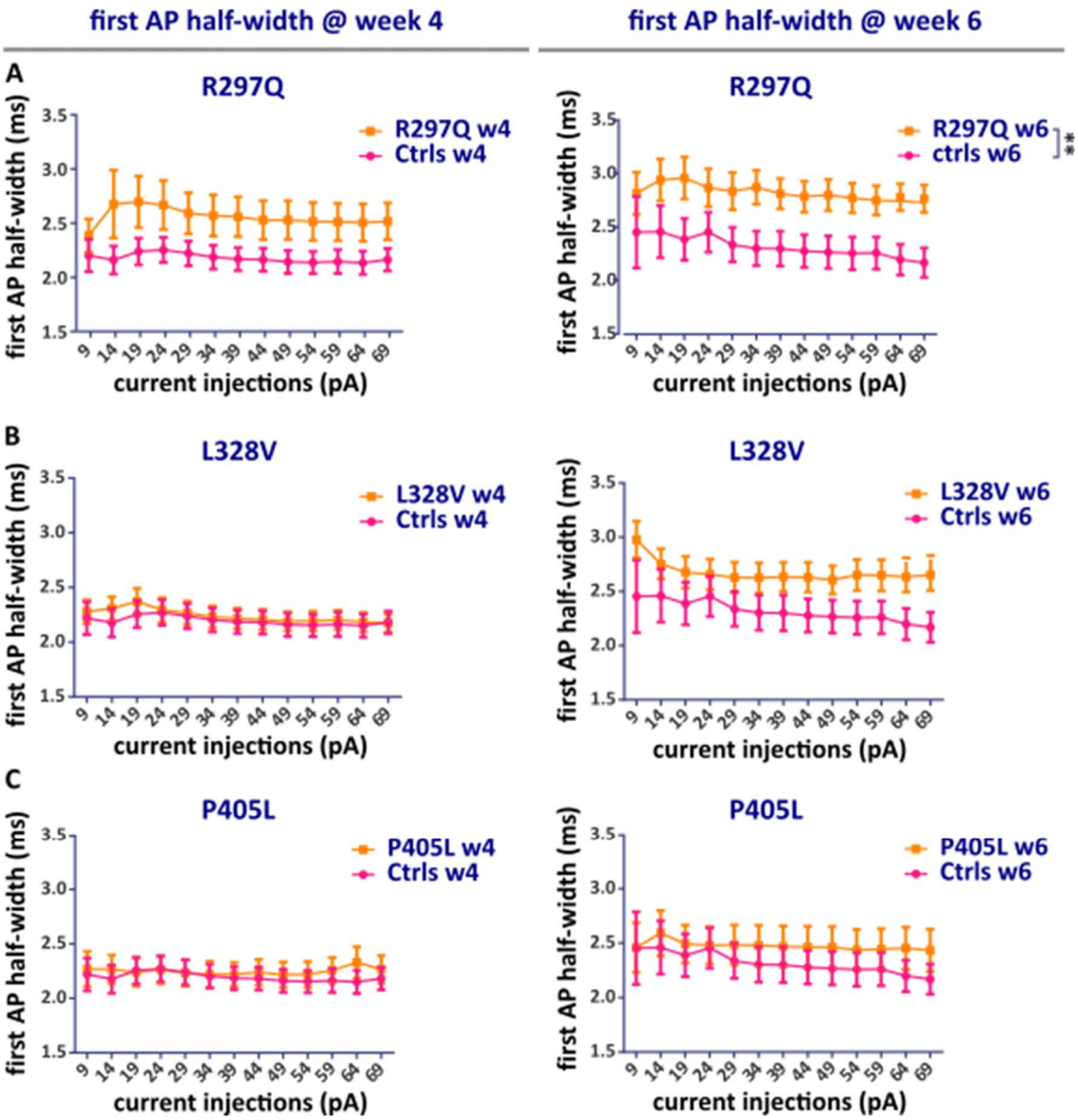

Figure 35 AP half-widths of the iPSC derived control versus *KCNA2*-R297Q (A), -L328V (B) and -P405L (C) patient-derived neurons. The half-width durations of the first action potentials that were evoked in response to a range of depolarizing current injections were assessed and compared between the control and patient lines, at week four (left) and six (right). For weeks four and six, n-numbers are 42 and 25 for the control-, 12 and 18 for the *KCNA2*-R297Q, 40 and 20 for the *KCNA2*-L328V, 14 and 27 for the *KCNA2*-P405L patient-derived neurons. (One-way ANOVA, Sidak's multiple comparisons test, *p < 0.05, **p < 0.01, ***p < 0.001 and ****p < 0.0001).

The *KCNA2*-R297Q patient-derived neurons' mean first AP half-width was significantly longer than the controls at week six (p=0.0085, two-way repeated measures ANOVA) (Fig. 35A-right). The mean first AP half-width of the *KCNA2*-L328V patient-derived neurons was only slightly longer than that of the controls at week six.

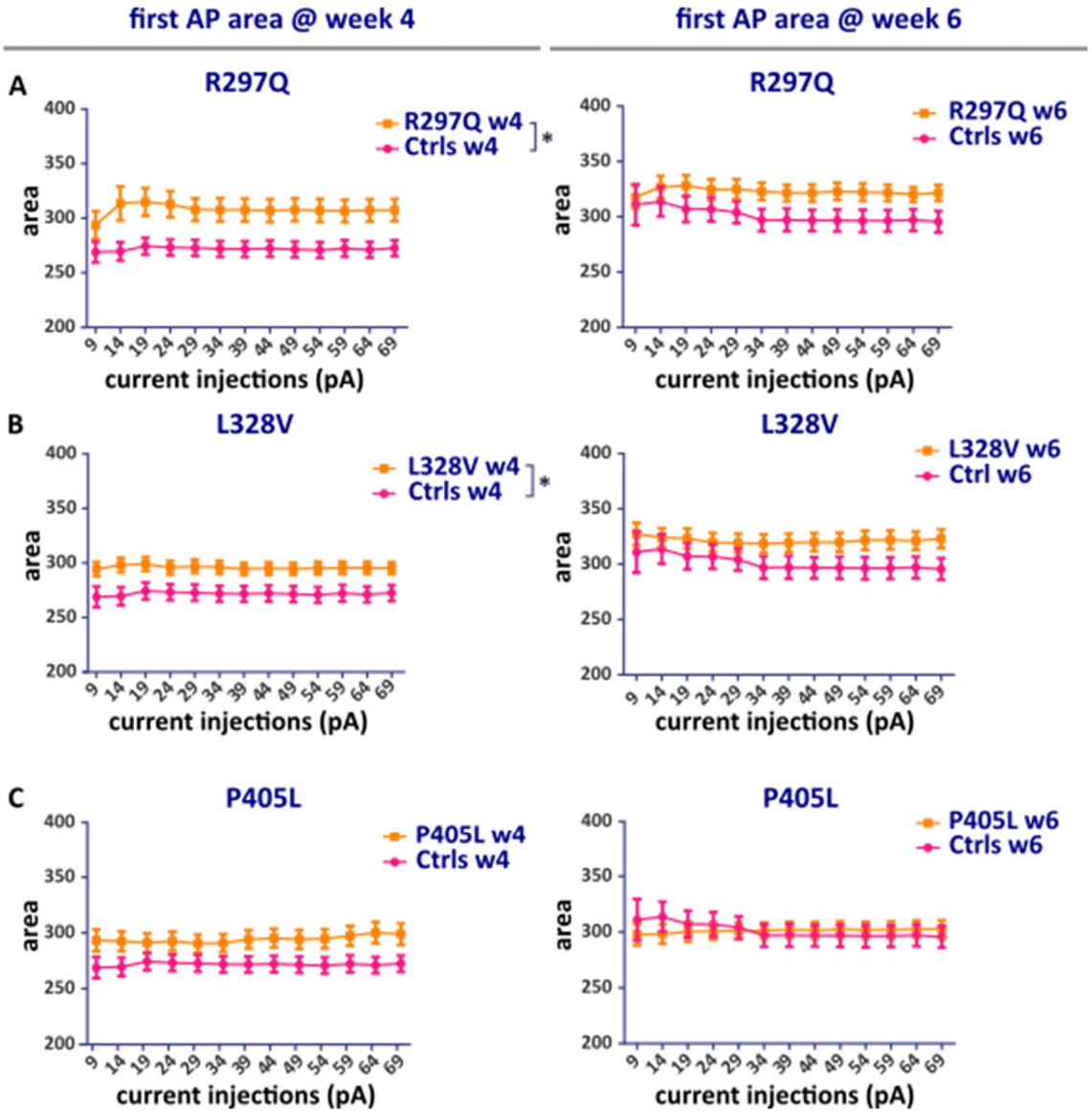

Figure 36| AP areas of the iPSC derived control versus *KCNA2*-R297Q (A), -L328V (B) and -P405L (C) patient-derived neurons. The total areas of the first action potentials that were evoked in response to a range of depolarizing current injections were assessed and compared between the control and patient lines, at week four (left) and six (right). For weeks four and six, n-numbers are 42 and 25 for the control-, 12 and 18 for the *KCNA2*-R297Q, 40 and 20 for the *KCNA2*-L328V, 14 and 27 for the *KCNA2*-P405L patient-derived neurons.(One-way ANOVA, Sidak's multiple comparisons test, *p < 0.05, **p < 0.01, ***p < 0.001 and ****p < 0.0001).

The mean areas of the first AP evoked by the *KCNA2*-R297Q and -L328V neurons were significantly bigger than that of the controls over the range of current amplitudes given

only at week four (p=0.0198 and p=0.012, respectively, two-way repeated measures ANOVA).

Both at week four and six, *KCNA2*-R297Q neurons' time-to-peak durations were significantly longer than that of controls (p=0.0107 and p=0.0007, respectively, two-way repeated measures ANOVA). The *KCNA2*-L328V neurons' first AP time-to-peak values were also significantly longer than that of controls at both week four and six (p=0.0177 and p=0.0008, respectively, two-way repeated measures ANOVA). The *KCNA2*-P405L neurons' mean time-to-peak duration was significantly longer than that of the controls only at week four (p=0.0297, two-way repeated measures ANOVA).

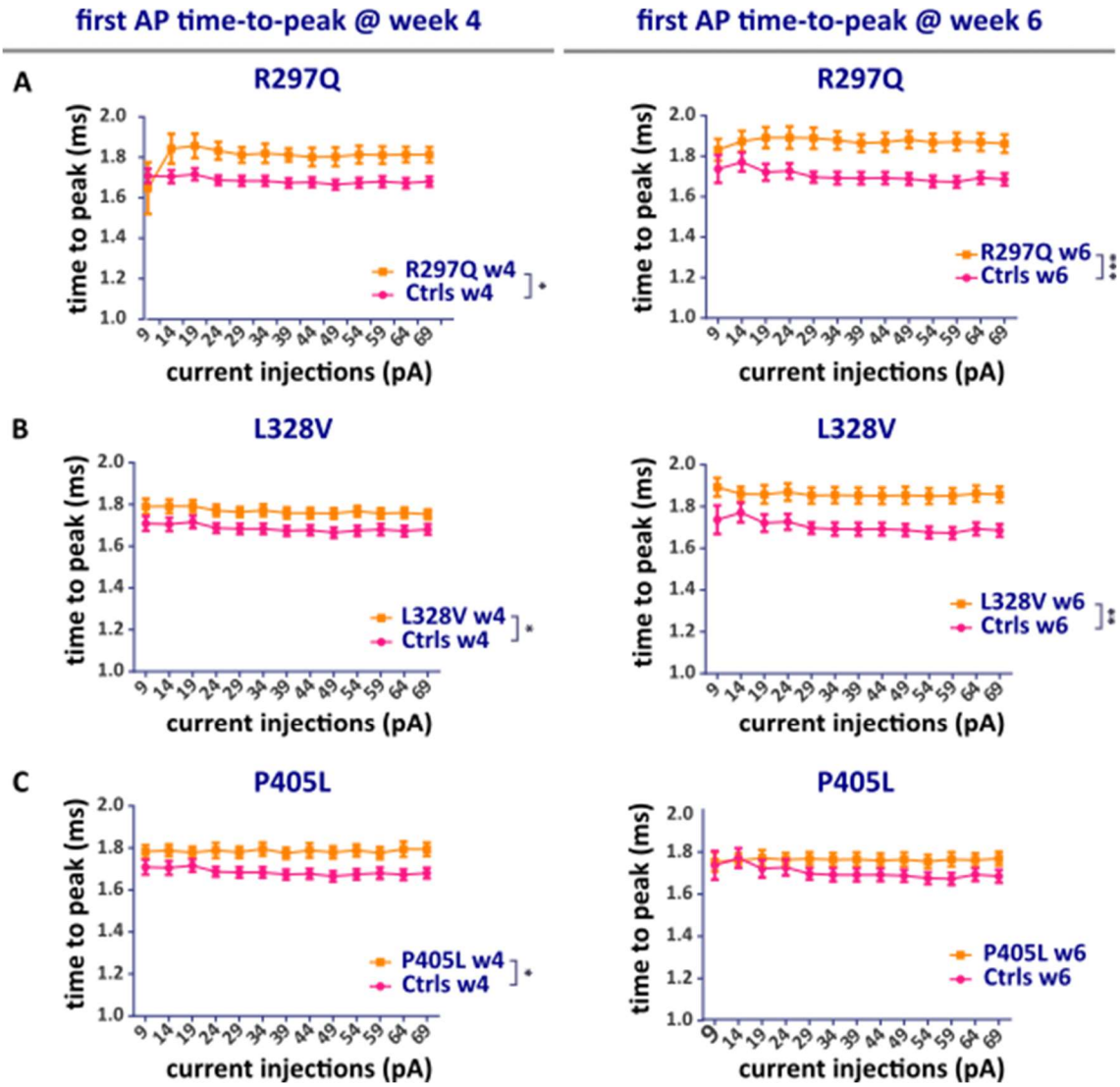

Figure 37| AP time-to-peak durations of the iPSC derived control versus *KCNA2*-R297Q (A), -L328V (B) and -P405L (C) patient-derived neurons. The time-to-peak durations of the first action potentials that were evoked in response to a range of depolarizing current injections were assessed and compared between the control and patient lines, at week four (left) and six (right). For weeks four and six, n-numbers are 42 and 25 for the control-, 12 and 18 for the *KCNA2*-

R297Q, 40 and 20 for the *KCNA2*-L328V, 14 and 27 for the *KCNA2*-P405L patient-derived neurons. (One-way ANOVA, Sidak's multiple comparisons test, *p < 0.05, **p < 0.01, ***p < 0.001 and ****p < 0.0001).

4.4.3 Single action potential properties

Single action potential parameters of the control- and *KCNA2*-mutation carrying patient-derived neurons were assessed also using the first action potential evoked in response to one ms long depolarizing pulses with increasing amplitudes, four and six weeks after the neuronal differentiation start. Rheobase, action potential threshold, time to peak and half-width values were compared between the lines at both time points, depicted in Figure 38.

The *KCNA2*-P405L patient-derived neurons had a lower rheobase compared to the controls at weeks four and six (p=0.0369 and p=0.0234 respectively, Sidak's multiple comparison test). Nevertheless, compared to the control-derived neurons, any of the patient-derived neurons did not significantly differ in their AP thresholds at either time points. At week four, none of the lines differed in their time-to-peak duration compared to the controls whereas at week six *KCNA2*-R297Q patient-derived neurons had significantly prolonged time-to-peak duration compared to the control-derived neurons (p= 0.0020, Sidak's multiple comparison test). Moreover, the mean single AP half-width of *KCNA2*-R297Q patient-derived neurons was significantly longer compared to that of the controls at week six (p= 0.0062, Sidak's multiple comparison test).

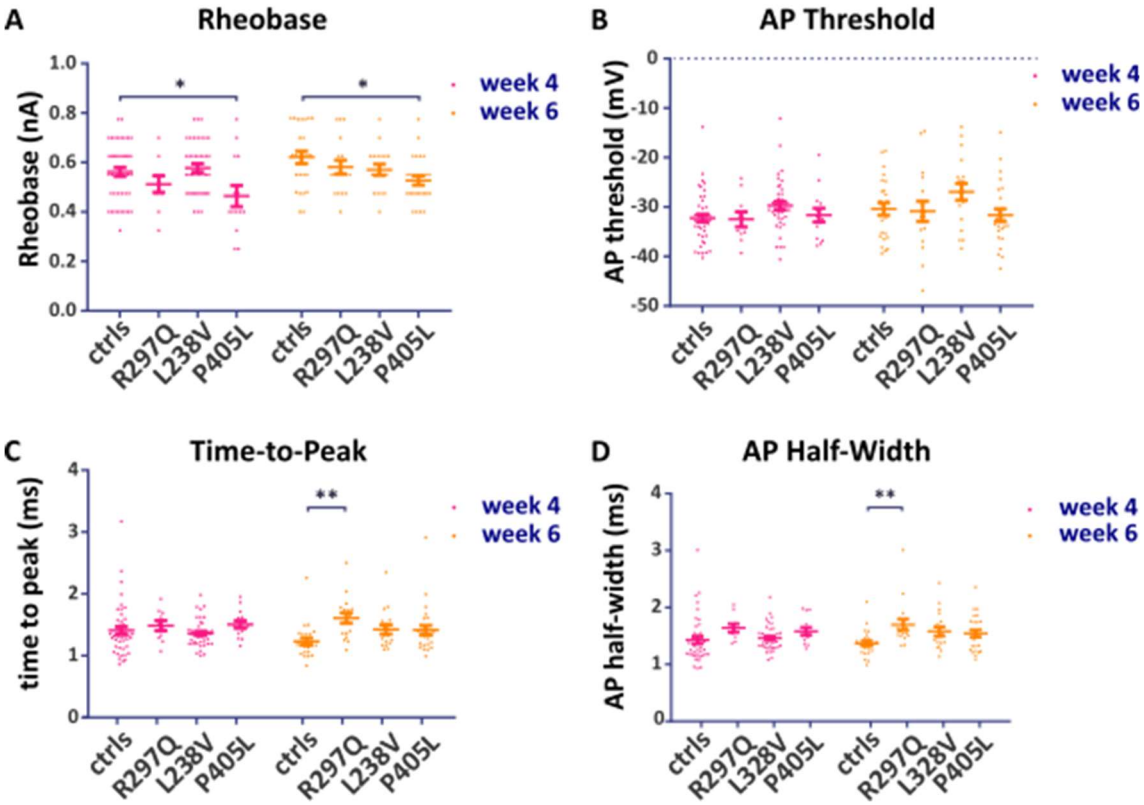

Figure 38| Single action potential parameters of the iPSC derived control versus *KCNA2*-R297Q, -L328V and -P405L patient-derived neurons. The action potential rheobase (A), threshold (B), time-to-peak (C) and half-width durations (D) were calculated using the action potentials evoked by a 1 ms long smallest depolarizing pulse that was enough to elicit an action potential, at week four and six and are compared between the control and patient-derived neurons. For weeks four and six, n-numbers are 43 and 25 for the control-, 10 and 17 for the *KCNA2*-R297Q, 40 and 18 for the *KCNA2*-L328V, 13 and 26 for the *KCNA2*-P405L patient-derived neurons.(One-way ANOVA, Sidak's multiple comparisons test, *p < 0.05, **p < 0.01, ***p < 0.001 and ****p < 0.0001).

5 DISCUSSION

In this thesis, the disease mechanism of the *KCNA2*-mediated developmental and epileptic encephalopathies has been investigated. The functional outcomes of four different *KCNA2* mutations were examined on both single cell and network levels in patient iPSC-derived cortical excitatory neuronal cultures, compared to healthy individual iPSC-derived cultures, using patch-clamp and multielectrode array techniques.

Following the identification of disease-causing genes and mutations, functional studies are needed to explain how these mutations alter physiology and cause pathological phenotypes in humans. Taking advantage of the Xenopus oocytes expression system, being a fast-screening method, the first insights regarding the disturbances on channel kinetics were promptly translated to clinics and the first therapeutic attempts have given successful results for the patients carrying *KCNA2* mutations with GOF effects (81). Nevertheless, the exact disease mechanisms of DEEs caused by mutations from different functional groups remained to be elusive. It is crucial to shed light on the disease mechanism beyond channel biophysics to better understand the disease and subsequently advance the clinical treatments.

To model *KCNA2*-related DEEs, the use of human iPSCs is very useful not only because of the translational advantage of human models but also due to the differential expression and localization pattern of $K_V1.2$-containing channels in human neurons. As the *KCNA2* gene encodes one $K_V1.2$ alpha-subunit which can form homo-tetramers as well as hetero-tetramers together with other K_V1 family subunits, it is difficult to replicate the same expression pattern as in complex systems in heterologous systems. Therefore, investigation of the *KCNA2* mutations in human iPSC-derived neurons, being an environment as close to the neurons in an actual human brain as possible, provides us with valuable insights regarding the altered $K_V1.2$ function and resulting pathophysiology of neuronal networks in humans.

As the most severe phenotypes were caused by the mutations with combined GOF and LOF effects, in the first part of this thesis the focus was on revealing the pathophysiological alterations mediated by one of those combined effect mutations; the *KCNA2*-T374A mutation. The patient carrying this mutation did not benefit from the 4-

AP treatment, and interestingly also did not experience any side effects or worsening effects due to the treatment in the clinical study (81). The disease mechanism as well as why the patient was not affected by the 4-AP treatment at all has remained to be solved. In this project, to investigate the effect of the *KCNA2*-T374A mutation on cortical excitatory neurons' behavior, patient-derived iPSCs were differentiated into cortical excitatory neurons, using the Neurogenin-2 overexpression method, and the electrophysiology of the single neurons were examined from week one to four via patch-clamp technique. In this longitudinal study, the aim was to detect the mutation-caused changes on passive or active properties of the neurons, during neuronal development.

Surprisingly, the investigation of the *KCNA2*-T374A mutation on single cell level did not reveal as drastic differences as expected when compared to the controls. Therefore, in the second phase of this thesis, network activity of the patient iPSC-derived cortical neuronal cultures, carrying mutations from all three functional groups, were investigated from the beginning of neuronal differentiation up to week six, using multi-electrode arrays to reveal the outcomes of these different mutations on the electrical activity of neuronal networks. Assessment of the neuronal network activity revealed that during the development electrophysiological features of the neuronal networks did not change only following the developmental stages, but these changes showed distinct patterns in networks carrying different mutations. Certain parameters that were observed to differ from the controls at earlier time points were sometimes not different at later time points anymore, or vice versa. To be able to explain time-dependent differences observed on a network level, active and passive electrical properties of the neurons carrying the *KCNA2*-R297Q, -L328V and -P405L mutations were examined also on a single cell level at two different time points, using patch-clamp technique.

The results, combining the electrophysiological findings on single cell and network levels, are discussed below separately for each mutation examined.

5.1 *KCNA2*-R297Q mutation

The iPSCs were derived from the patient carrying the *KCNA2*-R297Q (GOF) mutation, who manifested with febrile status epilepticus at the age of 5 months. Later, he presented with absence seizures, generalized tonic-clonic seizures as well as

psychomotor developmental delay, ataxia and moderate intellectual disability. The *KCNA2*-R297Q mutation was found to have a strong GOF effect on channel kinetics (12).

The cell capacitance of the *KCNA2*-R297Q patient-derived neurons did not change from week four to six while the control' neurons capacitance increased, suggesting that the patient-derived neurons did not get bigger in size, although the healthy neurons grew. Input resistance of neither the patient nor the control-derived neurons did change from week to four, suggesting that the ion channel composition on the neuronal membranes did not change between these two time points for either line. There was also no difference between the control and patient-derived neurons' input resistances, indicating that there was no big difference in the maturity level of the neuronal membranes when they were four or six-weeks old. The resting membrane potentials of the patient and control-derived neurons were not different when compared at week four or six, also did not change from week four to six for either line. Therefore, it can be inferred that the *KCNA2*-R297Q mutation does not affect the resting membrane potential of the cortical excitatory neurons at these maturity levels. Nevertheless, it was reported earlier that when the primary mouse hippocampal neurons were transduced to express either wild-type or the mutant $K_V1.2$ channels carrying the *KCNA2*-R297Q mutation, the neurons that expressed the mutant channels had hyperpolarized resting membrane potentials and needed higher current injections to elicit action potentials (81). Since it is not possible to control how many copies of transduced $K_V1.2$ channels are expressed and in what conformations they form functional channels in overexpression systems, it is difficult to compare these findings to the findings obtained from iPSC-derived neuronal cultures, where the neurons possessed the patient genome carrying the mutation only on one allele. However, the findings obtained from the over-enhanced expression of the mutant channels in hippocampal neurons provided a valuable hint that the *KCNA2*-R297Q mutation may cause a pathophysiology of the neuronal membranes on subthreshold levels.

The *KCNA2*-R297Q mutation carrying patient-derived neurons' evoked firing pattern significantly differed from the controls, not only in the number of action potentials evoked in response to a range of depolarizing currents but also in how this firing pattern changed from week four to six. At week four, the patient-derived neurons fired a smaller number of action potentials in response to smaller current pulses and a higher number

of action potentials in response to larger current pulses, compared to the controls. This pattern reversed at week six, with the patient-derived neurons firing slightly more action potential in response to smaller current pulses and less action potentials in response to larger current pulses. Although the patient-derived neurons' evoked AP number increased with increasing current amplitudes at week four, at week six the number of evoked APs dropped down after reaching the peak at mid-amplitudes of current injections. Developing neurons face depolarization blocks when they receive large inputs in the earlier phases of their development, whereas they can handle larger inputs better as they mature, responding with more action potentials without facing a depolarization block. Expectedly, in our control iPSC-derived neuronal cultures, the lower number of action potentials evoked in response to larger current injections versus smaller current injections, due to the depolarization block the neurons faced after firing a few action potentials at week four, fit to the known behavior of immature neurons. Changing response of the control-derived neurons to the same current amplitudes, firing increasing number of action potentials in response to increasing current stimulations, showed that the neurons matured from week four to six, as expected. Nevertheless, the patient-derived neurons' evoked firing behavior changed in the opposite manner. These observations suggested that the change in the patient-derived neurons' firing behavior do not follow the developmental trajectory of a healthy neuron.

Analysis of the parameters of first APs fired in AP trains revealed that the first AP widths, areas as well as time-to-peak durations were affected in the *KCNA2*-R297Q mutation carrying patient-derived neurons, resulting in wider action potentials when compared to controls. As their analysis suffered from some technical limitations, such as variable n-numbers of first APs fired in response different -smaller- current injections and resulting inconvenience for two-way ANOVA analysis, single action potentials were examined also separately. For this purpose, the neurons were stimulated with increasing amplitudes of 1-ms long depolarizing pulses, and the first action potential fired in response to the smallest current injection was used for the analysis of single action potential parameters. Consistently with the earlier findings, the action potential half-width and time-to-peak durations were found to be significantly longer in the patient-derived neurons compared to the controls at week six while the action potential threshold and rheobase were not different.

Having longer AP half-widths and time-to-peak durations, being even more prominent at week six, the patient-derived neurons were found to remain on depolarized potentials for an extended amount of time compared to the controls. As these differences were more prominent at week six, it could be that these neurons' larger AP half-widths and areas did not only decrease the number of action potentials that can be fired in a given time window, but also caused them to face depolarization blocks due to prolonged duration of depolarized states of the membrane, explaining the difference between the patient and control-derived neurons' evoked firing pattern at week six as well as the change in the patient-derived neurons' evoked firing behavior from week four to six, which was in the opposite manner of the controls. Although the prolonged depolarized states caused the patient-derived neurons fire less APs on a single cell level, neuronal activity was enhanced on a network level. During neuronal transmission, membrane depolarization reaching the synaptic terminals causes Ca^{+2} influx, which results in neurotransmitter release. Longer depolarized state of neuronal membrane would cause an increased Ca^{+2} influx and increased neurotransmitter release from the synaptic vesicles (82). One single excitatory neuron in the human cortex has hundreds of excitatory synapses, therefore increased neurotransmitter release from its synapses would influence the firing of many other neurons, enhancing the neuronal activity on a network level. This scenario may explain the increased burst durations robustly observed in the patient-derived networks, as well as increased burst frequency within bursts.

In a previously published study, a mouse model carrying a mutation in the $K_V1.1$ channels, which is co-expressed with the $K_V1.2$ channels, was used to study neuronal transmission alterations caused by the mutation. The authors showed that $K_V1.1$-mediated widening of action potentials at the axon terminals of basket cells significantly increased the Ca^{2+} influx and also confirmed the elevated amplitude and frequency of the postsynaptic inputs received by the Purkinje cells (83). In another study, the timing and magnitude of Ca^{2+} influx was investigated in hippocampal mossy fiber buttons, and it was also confirmed that broader APs results in larger Ca^{2+} influx in these excitatory synapses (84). In the same study, computational model was developed to understand AP waveform dependent kinetics of Ca^{2+} channel activation. Using this model, authors proved once more that AP broadening leads to a decrease in peak amplitude but an

increase in total charge of presynaptic Ca+2 influx, which was also experimentally proven earlier by the same group (54).

Whereas the same set of events, starting with action potential broadening and resulting in an increased neurotransmitter release, have been reported in different cell types of the brain, affecting both glutamatergic and GABAergic synapses, the reason for AP broadening was usually K_V1 loss-of-function caused by either a mutation or a blocker. It has been very intuitive that the loss of function or blockage of K_V1 channel causes AP broadening. Nevertheless, the *KCNA2*-R297Q mutation, which has been found to cause AP broadening in this project, had a gain-of-function effect on the channel kinetics. If the strongest impact of this mutation was on the repolarization phase of the action potential, APs should have been narrower. However, it is known that $K_V1.2$ channels play a role not only in AP repolarization but also in sub-threshold excitability of the neuronal membranes. In the subthreshold range, $K_V1.2$ currents accounted for as much as 50% of the depolarization-activated potassium current (85). As it has been previously reported that the *KCNA2*-R297Q mutation causes a strong hyperpolarizing shift of the activation curve and a significant increase in the current density of the $K_V1.2$ channels, the channels open and conduct significantly higher amount of potassium currents at much more hyperpolarized membrane potentials (8). Therefore, it can be suspected that in the subthreshold range, this mutation plays a major role to slow down the depolarization of the neuronal membranes, which is why the *KCNA2*-R297Q neurons had longer time-to-peak durations.

As the four patients carrying the *KCNA2*-R297Q mutation were involved in the recent clinical study and benefited from the 4-AP treatment, manifesting clinical improvements, K_V1 family blocker 4-AP has been suggested to antagonize the effect of this gain-of-function mutation on neuronal physiology in human brains (81). Nevertheless, the exact mechanism of 4-AP's therapeutic effect has remained to be elucidated. Therefore, in this study, the patient and healthy control iPSC-derived neuronal cultures were treated with 4-AP when they were six-weeks old and the resulting changes in their network activity were examined.

As expected, 4-AP increased the mean firing rates as well as bursting rates in both control- and the *KCNA2*-R297Q patient-derived networks. While the random spike

percentage was not affected by 4-AP in the control-derived networks, it was increased in the *KCNA2*-R297Q patient-derived networks, bringing the random spike ratio up to the comparable levels to the controls. Consistently with that, the mean burst duration was significantly shortened in the *KCNA2*-R297Q patient-derived networks although the 4-AP treatment did not affect the burst duration in the control-derived networks. The longer mean burst duration was one of the robust differences the patient-derived networks exhibited at all time points examined, and in response to the 4-AP treatment it shortened down to the heathy control levels, not revealing any difference anymore. This observation may be one of the key points to understand the disease mechanism. The network bursts parameters were affected by 4-AP treatment in the same way as the burst parameters. Importantly, the mean network burst duration of the patient-derived networks was also shortened to the control levels, while it did not change for the controls.

Altogether, the single cell and network recordings of the *KCNA2*-R297Q patient-derived neuronal cultures suggested that the root cause for the altered physiological activity of these patient-derived neurons is the increased $K_V1.2$ current conductance in the subthreshold range and depolarization phase of action potentials. K_V1 channel blocker 4-AP was already shown in a previously published study to affect the potassium conductance of the $K_V1.2$ channels on subthreshold potentials, reversing the pathophysiological effect of this mutation (81). Therefore, it can also be anticipated that the $K_V1.2$ channels expressed in *KCNA2*-R297Q patient-derived neurons were affected by 4-AP in a similar way. Based on the current findings and insights from literature, it can be hypothesized that due to antagonizing effect of the 4-AP on the $K_V1.2$-R297Q function in the subthreshold range as well as during the depolarization phase, action potential time-to-peak as well as half-width durations were not as prolonged anymore, which is why the neuronal membranes were not kept at depolarized potentials so long. As a result, neurotransmitter release was not elevated and did not cause longer bursts with higher spike frequencies compared to the controls. As the bursts did not last longer and not have higher spike frequencies, the random spike ratio was also reduced to the heathy network ratio after 4-AP treatment. Although the findings obtained in this thesis on the network level support this hypothesis, further experiments should be performed on a single cell level in presence and absence of 4-AP.

Due to the appearance of some inhibitory neurons in the neuronal cultures generated by the forced overexpression of Neurogenin-2, as a by-product, the impact of these inhibitory neurons on the overall network activity and on the relative comparison between the patient- and control-derived neuronal networks was examined. It was interesting that the BIC application increased the burst rate at week four but decreased it at week six in the control-derived networks. In a previously published study the authors also showed that the BIC treatment significantly increased the burst rate at an earlier age while did not affect the burst rate at a later age in commercially available iPSC-derived cortical neuronal cultures (86). This finding aligns with the observed effect of BIC on the bursting rate of networks in this project and may be attributed to a changing role of GABA receptors during development. Strikingly, the BIC application lowered the spike frequency during bursts in these patient cultures, while elevating it in the control cultures. If there were inhibitory inputs received by the networks, when it was blocked the spike frequency would have been expected to increase, as it was observed in the control-derived networks. Reduced spike frequency observed in the patient-derived networks was unexpected and raised the question of whether GABA plays a role as an inhibitory neurotransmitter in these networks or GABA switch did not occur and it is still excitatory at this time point. Further experiments should be performed, ideally with IPSC-derived inhibitory neuron models, to understand the effect of this *KCNA2* mutation on development and physiology of inhibitory neurons.

Although the effect of BIC application on network parameters was not as expected, characterization of the identity and maturity level of inhibitory neurons in these cultures was beyond the scope of this project. Nevertheless, taken together, when disinhibition was mediated via GABA-A receptor blockage, the patient-derived networks had still elevated burst rates and durations, indicating that the observed differences in these network features were caused by the inhibitory neurons that are generated by by-products in these cultures.

5.2 *KCNA2*-L328V mutation

The iPSCs were derived from the fibroblasts of the patient carrying the *KCNA2*-L328V mutation, who manifested febrile status epilepticus at the age of 6 months and later presented with psychomotor delay, moderate ataxia, severe intellectual disability as

well as delayed language acquisition. The *KCNA2*-L328V mutation was found to cause a combined gain- and loss-of-function effect on K_V1.2 channel kinetics (7).

Investigation of the passive properties of the *KCNA2*-L328V patient-derived neurons did not reveal any differences in the cell capacitance, input resistance or resting membrane potential of the patient versus control-derived neurons. Based on these results, it can be inferred that the patient-derived neurons did not have a bigger or smaller total membrane surface. The ion channel composition on the neuronal membranes was not different; the patient and control-derived neurons were on a comparable maturity level at week four and six. The *KCNA2*-L328V mutation did not affect the resting membrane potential of the neurons either. Nevertheless, in the previously published study, the oocytes expressing K_V1.2 channels with the *KCNA2*-L328V mutation had hyperpolarized membrane potentials (7). As the potassium currents recorded from the injected oocytes were conducted almost only by the K_V1.2 channels while in the human neurons recorded in this project K_V1.2 is only one of the potassium channels contributing to the resting membrane potential of the neurons, it is not surprising that the mutation did not cause such a significant change in the RMP of the neurons. However, the oocyte data gave us a valuable insight regarding the role of K_V1.2-mediated potassium currents at subthreshold membrane potentials.

In response to the increasing amplitudes of depolarizing current pulses, the evoked action potentials fired by the *KCNA2*-L328V patient-derived neurons showed a significant difference when compared to those of the controls at both weeks four and six. The change in the evoked firing pattern of the patient-derived neurons from week four to six did not fit to the developmental trajectory of healthy neurons and showed an opposite pattern of what was observed in case of the control-derived neurons. To understand the altered evoked firing behavior observed in the patient-derived neurons, the first action potentials of the evoked AP trains were further analyzed for single AP parameters.

Assessment of the first AP start time revealed that the patient-derived neurons started firing action potentials sooner than the controls especially when injected with smaller current amplitudes, at week six. It has already been reported that this mutation causes a hyperpolarizing shift in the voltage-dependent activation of the K_V1.2 channels,

however, when the channels are open, they can conduct only 50% of the current that is conducted by the wild-type channels (7). It has been also shown that in the subthreshold range, 50% of the depolarization-activated potassium current is conducted by the $K_V1.2$ channels (85). Between the opposing gain- and loss-of-function effects of the *KCNA2*-L328V mutation, if the LOF effect is more effective at the potentials where the neurons were stimulated, this would explain why they needed less time to fire the first action potential compared to the controls and fired a higher number of potentials in response to smaller amplitudes of current injections. Reduced potassium conductance would weaken the counteracting force of the potassium outflow, against the inward sodium current, and results in faster depolarization of the membranes to the AP threshold level. This scenario is likely to be the case because although the channels expressing the mutation open at more hyperpolarized potentials, the difference may not be big enough to compensate for the reduced conductance of the channels, resulting in smaller potassium currents than the controls. At the potentials where the neurons start to depolarize, the number of the open channels would need to be more than doubled to compensate for the reduction in the current density of these channels. Instead, shorter AP start times, in other words faster depolarization of the membranes, suggested that the LOF effect outweighs the GOF effect at the subthreshold potentials, reducing potassium outflow.

Moreover, increased AP half-width, time-to-peak and total area of the *KCNA2*-L328V patient-derived neurons points out the increased amount of time the neuronal membranes remained depolarized. These differences can be caused by the joint action of GOF and LOF effects. As the time-to-peak durations were longer, it can be inferred that above the AP threshold level the GOF effect, causing more channels to open earlier, plays an important role. On the other side, LOF effect may be slowing down the repolarization of the action potentials, contributing to the widening of action potentials. AP widening, resulting in increased neurotransmitter release, can increase the network activity, as discussed in the previous part. This would explain robustly increased burst durations, observed at all time points. However, as the repolarization phase of the action potentials should also be slowed down due to decreased current density of $K_V1.2$ channels, it is expected that between two action potentials the *KCNA2*-L328V neurons needed longer times. Consistently with this expectation, in highly active networks, these

neurons exhibited longer bursts, with lower burst spike frequencies. Nevertheless, the slowing down effect of the mutation on the repolarization of action potentials was not confirmed by the single cell dataset analyzed in this project.

Analysis of single AP parameters also showed that the action potential half-widths and time-to-peak durations were slightly longer compared to the controls, suggesting widening of action potentials, nevertheless this difference was not statistically significant.

In response to the application of 4-AP, the mean firing rate as well as the burst rate was expectedly increased in the *KCNA2*-L328V patient-derived networks, but the treatment did not change the relative comparison between the patient and control-derived networks' spiking or bursting behavior. 4-AP was applied only when the neuronal cultures were six weeks-old. At that time point, presumably due to the developmental and homeostatic plasticity of the neurons, some of the electrophysiological parameters which were earlier found to be different than the controls did not show significant differences anymore. Also, having a lower n-number for the 4-AP experiments may have affected the statistical power of the analysis of these dataset.

The spike frequency within bursts was significantly lower in earlier weeks and then as it increased, it did not reveal any significant difference anymore in the later weeks, although it was still slightly lower than the controls. The 4-AP treatment significantly reduced the spiking frequency within bursts in the control-derived networks whereas it did not affect the *KCNA2*-L328V patient-derived networks. It could be that the 4-AP treatment had an impact which was in the same direction as the LOF effect of mutation has on the channel kinetics, which is why affected the control cultures much more drastically and did not cause a big difference in the burst spike frequencies of the *KCNA2*-L328V patient-derived networks where the GOF effect of the mutation compensated for the 4-AP effect.

Unfortunately, the mechanism for the therapeutic effect of 4-AP, that was observed in one patient, could not be revealed in this study. However, as the data suggested that the GOF effect outweighs the LOF effect during the active firing of the neurons, resulting in increased AP durations, it can be suggested that 4-AP would antagonize the GOF effect and shorten the depolarization phase of the action potentials. Although LOF effect

would still be there, maybe even a bit stronger, overall AP durations would be shortened, reducing the neurotransmitter release which would in turn reducing the network activity.

5.3 *KCNA2*-T374A mutation

The iPSCs were derived from the patient carrying the *KCNA2*-T374A mutation, who presented with tonic seizures and was diagnosed at birth, later manifested with psychomotor developmental delay and spastic tetraplegia, as well as profound intellectual disability and no language acquisition. The *KCNA2*-T374A mutation was found to cause hyperpolarizing shift of the activation curve of the $K_V1.2$ channels, which is a gain-of-function effect, and a reduction in the conducted current amplitudes, which is a loss-of-function effect (7).

The cell capacitances of the *KCNA2*-T374A patient-derived neurons were continuously increasing from week one to four, reflecting the increase in cell membrane surface, and were comparable to those of the controls during the first three weeks of neuronal development whereas at week four the patient-derived neurons were found to have a significantly higher cell capacitance, which means that the four weeks-old patient-derived neurons were bigger in size than the four-weeks old control-derived neurons.

The resting membrane potentials of both the *KCNA2*-T374A patient and control-derived neurons became more hyperpolarized over weeks, getting closer to the resting membrane potential of a mature neuron by time. During the development, the RMP values of the patient-derived neurons were comparable to the RMPs of the control-derived neurons at every week although this mutation caused hyperpolarized resting membrane potentials when expressed in oocytes (7). The findings from oocytes, similarly to the other *KCNA2* mutations discussed in the previous parts, provided us with the valuable insight that the mutation's GOF effect was influential at the subthreshold levels, nevertheless the human iPSC-derived neuronal data showed that the altered $K_V1.2$-T374A currents did not hyperpolarize the resting membrane potential of the neurons significantly.

The input resistances of the of the *KCNA2*-T374A patient-derived neurons consistently decreased, from week one to four, reflecting an expected change in input resistance of

developing neurons. As neurons mature, due to expression and localization of more and more functional channels on the neuronal membrane, input resistance of the membrane becomes smaller, approaching to the mean input resistance of a mature human neuron that is considered to be around 100 mOhm (87). Therefore, the observed change in both control and patient-derived neurons' input resistances fit to what is known about input resistance of a developing neuron. Nevertheless, the four weeks long observation of the *KCNA2*-T374A patient-derived neurons revealed that the pattern of this change in the neurons' input resistances was significantly different compared to that of the controls. Especially at week two and three, the patient-derived neurons had a higher input resistance compared to control. This would mean that the patient-derived neurons did not have the same ion channel composition on their membrane as the controls, preventing the patient-derived neurons from handling received inputs in the same way as the control-derived neurons would do. This could have adverse consequences, affecting not only homeostasis but also the wiring of the neuronal networks. Taking the input resistance as a measure for maturity, it could be argued that the patient-derived neurons' development was behind the trajectory line of a healthy neuronal development.

Due to the forced expression of Neurogenin-2, the induced neurons were differentiated into neurons in less than a week and were able to fire action potentials when they were stimulated with depolarizing current pulses already at week one. Both the patient and control-derived neurons had a depolarization block after only a few action potentials at earlier weeks, but the firing capabilities of the neurons improved over weeks. Only at week four, the pattern of the evoked action potentials in response to different amplitudes of depolarizing current pulses was found significantly different between the patient- and control-derived neurons. This finding suggests that the developmental disturbances observed in this patient line were reflected in the evoked firing of the single neurons for the first time when they were four weeks old.

The patient-derived neurons were found to have significantly longer action potential half-widths as well as time-to-peak durations, especially at week two and three, both of which contributes to broader action potentials, leading to longer depolarized times of the membranes compared to the controls. Although the difference in the number of action potentials fired by the control- versus patient-derived neurons was not significant

at week two and three, the reason for the patient-derived neurons to fire less action potentials before getting caught in depolarization blocks may be the longer action potentials durations, causing the neurons to enter depolarization block earlier than the controls.

Bursting analysis suggested that the patient cultures were much more active at week three, exhibiting higher number of bursts that also last longer, explaining higher percentage of spikes localized in bursts. Stabilization of the bursting frequency on a level comparable to the controls suggested the re-adjustment of the network activity at later stages while the burst duration remains to be an indicator of the elevated activity in patient-derived networks. Longer burst durations can also explain the higher MFR and lower percentage of random spikes detected in the *KCNA2*-T374A patient-derived networks at week six.

Assessment of the frequency and duration of the network bursts gave similar results to those of all bursts; the patient-derived networks exhibited higher frequency of network bursts only at the earliest time point, whereas the mean duration of the network bursts was much longer than the controls consistently at all time points. Differently than the single bursts' assessment, the mean spike frequency within the network bursts was higher from week five on in the patient cultures. This finding is interesting because when the mean spike frequency within all bursts was examined, it was observed that the spike frequency was lower than the controls at the earliest observation point but gradually increased over the next weeks. In the case on network bursts, spike frequency did not reveal a significant difference at the earliest weeks but was significantly higher in the later weeks, confirming the fastening of the spike frequency. This observation indicates that the mean spike frequency within network bursts was faster than within local bursts. The fastening of spike frequencies could have multiple underlying factors. Since developmental delay was observed during the early development of these patient-derived neurons, immature neurons may have slower action potential kinetics, resulting in slower spiking frequencies at earlier time points. In addition to the developmental changes affecting the neuronal membranes, the influence of the GOF and LOF effect of the mutation may be different at distinct time points. As the $K_V1.2$ channels are involved in a big consortium of channels regulating action potential firing, contribution of the $K_V1.2$ conductance to the depolarization and repolarization phase of the action

potentials may change during the development, enabling the same mutation influence firing pattern in different ways during early versus late development. For example, the mutation with a pure LOF effect on the $K_V1.2$ channels has been found, as discussed in the next section, to cause reduced spike frequency in the patient-derived neurons during early development. It could be argued that, in addition to the developmental delay, LOF effect of the *KCNA2*-T374A mutation may be the cause of the reduced spike frequency in these patient-derived networks, impeding the repolarization of the membranes and latening the next AP firing. Upon development, and changing ionic composition of the neuronal membranes, the LOF effect of the mutation may have become less effective on the spiking frequency, as it has been also revealed by the analysis of the evoked AP firing in single neurons. On single cell level, the patient-derived neurons fired slightly reduced number of APs in response to smaller current pulses at earlier timepoints whereas at later timepoints they fired even slightly higher number of APs in response to larger current pulses. In addition to the changes of AP kinetics on a single neuron level, another reason for the increased spike frequency within bursts at later time points could be the involvement of higher number of neurons in the network activity. Due to the widening of APs, the neuronal networks were assumed to be highly stimulated from the earlier timepoints on, reflected by increased MFRs, burst frequencies as well as burst durations. As the networks grow and mature, the number and strength of the synapses between the neurons as well as the number of neurons in the networks increase, which would amplify the effect of enhanced neurotransmitter release, even from a small number of neurons, on a network activity.

As this mutation was found to cause a hyperpolarizing shift of the activation curve of the $K_V1.2$ channels, causing the channels to open at more hyperpolarized levels, although the mutation also causes more than 50% decrease in the current conductance, it can be argued that at the depolarization phase of the action potentials depolarization-activated potassium current was increased and created a resisting force against the sodium inflow, at least during early development, which corresponds to the time when time-to-peak durations as well as AP half-widths were longer. At these time points the patient-derived neurons fired slightly lower number of action potentials, which may have been resulted from the wider APs and subsequently faced depolarization blocks. The time point when the wider APs were observed is also the time point when the MFR

was higher in the patient-derived networks. It could be argued that due to the widening of APs and resulting increase in neurotransmitter release, the network activity was elevated. Even if one single neuron faces a depolarization block after a few action potentials, during those action potentials it could stimulate more neurons than the controls due to the increased neurotransmitter release. It should also be bored in mind that weeks two and three were the time points when the patient-derived neurons were significantly behind a normal development and this may have adverse consequences on the action potentials kinetics, resulting in earlier-faced depolarization blocks on a single cell level.

Expectedly, the MFR of the *KCNA2*-T374A patient-derived networks increased in response to the 4-AP treatment, so did the MFR of the control-derived networks. Overall, it was found that the effect of 4-AP on the firing properties of the *KCNA2*-T374A patient-derived network was not strong. Previously it was also reported the $K_V1.2$ channels expressing the *KCNA2*-T374A mutation was not affected in oocytes either (81). 4-AP is believed to block the channels at the binding side inside the pore (88). For 4-AP to enter K_V1 channels, they must be fully activated and open. Once inside the channel, it blocks the conductance via strongly promoting the closed-gate conformation (89). In case of $K_V1.2$-T374A mutant channels, as the channels open even earlier than the wild-types, 4-AP is expected be able to enter the cavity, nevertheless, due to the mutation being located at the binding site of 4-AP it may not be able to bind to block the further channel conductance. This could also explain why the patients who were treated with 4-AP did not show any side-effects either. Due to the failure of 4-AP to bind to the channels, it could alter the physiology neither in therapeutic nor in unforeseen way.

5.4 *KCNA2*-P405L mutation

The iPSCs were derived from the fibroblasts of the patient carrying the *KCNA2*-P405L mutation, who presented with febrile status epilepticus at the age of 8 months. He later was manifested with psychomotor developmental delay, impairment of fine skills and coordination as well as ataxia, and also presented with moderate intellectual disability and severe language delay. The *KCNA2*-P405L mutation was found to cause a strong loss of function of the $K_V1.2$ channels (75). When expressed in *Xenopus* oocytes, the mutant channels had a dramatic reduction in the current density.

The cell capacitance of the *KCNA2*-P405L patient-derived neurons increased from week four to six, so did the cell capacitance of the controls, suggesting that the neurons were still growing during this period. The *KCNA2*-P405L mutation was not found to affect the resting membrane potentials of the neurons. Nevertheless, the mean input resistance of the patient-derived neurons was higher than the controls at week four, after which significantly decreased to the levels comparable to the controls' input resistance at week six. This finding suggest that the patient-derived neurons were behind the heathy developmental trajectory but closed the gap after six weeks in culture. It also fits to the observation that the patient-derived neurons' bursting behavior developed with a delay.

In these iPSC-derived neuronal cultures, the neurons were able to fire spontaneous action potentials one week after the differentiation start and exhibit bursting activity by the third week, which is why the bursting behavior of the neuronal networks were examined from week three on. In the case of the *KCNA2*-P405L networks, having comparable MFRs but higher random spike ratios, the transition from spontaneously spiking to bursting behavior was found to occur later than in the controls. At week three, higher percentage of spikes was still randomly fired in the patient-derived networks whereas smaller percentage of the spikes were localized in bursts. Taking the appearance of robust bursting behavior in neuronal networks as a measure for neuronal development, it can be argued that the patient-derived neurons were developmentally behind the controls. Nevertheless, in the following weeks there was no difference observed in the patient versus control-derived networks' spontaneously spiking to bursting ratio, suggesting that the patient-derived networks later matured to the comparable levels of the controls.

When stimulated with the increasing amplitudes of depolarizing current pulses, the patient-derived neurons responded significantly differently than the control-derived neurons, firing less action potentials at week four but interestingly, they were later able to fire as many action potentials as the controls, even slightly higher numbers, at week six. Analysis of the first action potentials fired in response to each current amplitudes revealed that the patient-derived neurons' first AP start time was shorter than the controls, implying that they were able to fire an action potential sooner than the controls when injected with the same current amplitude, especially for the smaller current amplitudes. The short AP start time may result from the LOF effect of the

mutation at the subthreshold membrane potentials. As discussed earlier, a big proportion of the depolarization-activated potassium currents comes from the $K_V1.2$ channels. Therefore, the significant reduction of $K_V1.2$ conductance would result in faster depolarization of the neuronal membranes and earlier AP firing, as observed here. Although the patient-derived neurons fired their first action potentials earlier than the controls, at least in response to smaller current pulses, they were able to fire only significantly reduced number of APs compared to the controls at week four. In addition to bigger first AP areas, having longer time-to-peak durations could explain why these patient-derived neurons faced depolarization blocks in response to smaller current pulses compared to the controls and could fire less APs. The reason for wider APs may not be directly related to the altered conductance of the $K_V1.2$ channels, but due to the resulting developmental delay of these neurons, the ionic composition of the neuronal membranes may not be adequately mature to fire action potentials with the same kinetics as the controls.

The mean first AP half-widths of the patient-derived neurons were not longer than the controls at week four but found to be slightly longer at week six. This could indicate that the LOF effect on the $K_V1.2$ function started to influence repolarization phase of the action potentials by week six, but not earlier.

Examining the parameters of single action potentials, the mean rheobase of the patient-derived neurons was found to be lower than the controls' rheobase at both weeks four and six. The lower rheobase currents are likely to be caused by the LOF effect of the mutation on the $K_V1.2$ function at subthreshold potentials. The hypothesis would be the following; as the membrane could conduct much less potassium currents than normal, power of the potassium outflow to counteract the sodium inflow was weaker and this resulted in much faster depolarization of the membranes to the AP threshold potentials in response to smaller inputs.

Increased burst duration of the patient-derived networks can be explained by the following set of events. At the time points, when the patient-derived neurons had shorter AP start times but widened APs, firing of the *KCNA2*-P405L patient-derived neurons resulted in longer lasting depolarization of the neuronal membranes which may have in turn increased the neurotransmitter release and elevated network activity.

These alterations could be caused by the LOF effect of the mutation on the subthreshold potentials as well as slower kinetics of the action potentials due to the developmental delay of the neuronal membranes. As the mean AP half-width was not significantly longer at early time points, the effect of the mutation on the repolarization phase of the APs was not found to be drastic yet but became more prominent in the later weeks. Slower repolarization of the neuronal membrane was not hinted only by longer AP-widths but also by slower spike frequencies within bursts. Longer bursts with reduced spike frequencies were observed consistently as a result of the LOF function of the mutation on the network activity.

In response to the 4-AP treatment, burst spike frequency was decreased in this patient line, as well as in the controls. This finding is interesting because the 4-AP treatment did not affect the burst spike frequency of the networks with GOF+LOF mutations, but only the control, pure GOF- and pure LOF-mutation-carrying networks. It can be inferred that 4-AP widened the APs of the *KCNA2*-P405L patient-derived neurons even more, bringing the spike frequency down.

The application of 10 µM BIC did not affect the activity of the patient-derived networks carrying the *KCNA2*-P405L mutation. As the BIC application experiments were performed using relatively small n-number of cultures, the reason could be that the statistical power not strong enough to reveal the differences. Nevertheless, with comparable n-numbers certain changes were observable in the other lines. Another explanation could be that due to the developmental delay of these patient-derived neurons, inhibitory neurons did not emerge at the same time point as in the control cultures. During the brain development, the neurons gain inhibitory neuronal identity much later than the excitatory neurons. It is also the case in the Neurogenin-2 overexpressed neuronal cultures; the characterization of the resulting neurons did not hint existence of any inhibitory neurons within the first weeks. The longer the cultures are maintained, and supported by glial factors, the higher the chance for inhibitory neurons to emerge is. Hence, in these patient cultures carrying the *KCNA2*-P405L mutation, which was observed to have a developmental delay, inhibitory fate may be gained even later than in the control cultures.

5.5 Overall conclusions

As the *KCNA2* mutations were found to have different effects on the channel kinetics, initial hypotheses, based on the conventional interpretation of the potassium channels' role in action potential repolarization, suggested that GOF effect of the mutations would silence the firing whereas LOF effect would enhance neuronal network activity. This assumption would require different neuronal populations being affected by the GOF versus LOF mutations so that they all cause epileptic phenotypes. Nevertheless, the *KCNA2* gene is expressed widely in the central nervous system, both in excitatory and inhibitory neurons. In this study only iPSC-derived cortical excitatory neuronal populations were examined. Even though the Neurogenin-2 overexpression-based neuronal differentiation protocol has been observed to generate also inhibitory neurons as by-products, involvement of these inhibitory neurons in the network activity of control- vs. patient-derived neuronal populations was not clearly defined.

The attempts to investigate involvement of inhibitory neurons in the network activity of iPSC-derived neuronal populations, generated by NGN2 protocol, failed to provide reliable conclusions mainly due to the small sample size in this thesis. As the obtained results were difficult to interpret and rather speculative, no clear conclusions can be drawn regarding the effect of *KCNA2* mutations on inhibitory neurons or general involvement of these inhibitory neurons in NGN2 network activity. One important finding came from the six-weeks old *KCNA2*-GOF mutation carrying networks whose mean burst rate and duration comparisons to those of the controls did not change after the application of bicuculine, as these were the robust differences observed in the patient cultures.

Despite the different, and even opposing, effects of the *KCNA2* mutations on $K_V1.2$ channel kinetics, these mutations were found to have some similar outcomes on the network activity, enhancing excitability. Strikingly, all the mutations, with GOF, GOF+LOF and LOF effects, were found to cause longer burst durations, which is a key finding to shed light on how these different functional groups of mutations of the same gene cause epileptic phenotypes. However, the pathological mechanisms leading these patient-derived networks to have longer-lasting bursts were slightly different for different mutations.

One of the key facts to bear in mind while interpreting the findings of this project is that the $K_V1.2$ currents do play an important role not only in the action potential repolarization but also in sub-threshold excitability (85). In the iPSC-derived excitatory neurons examined in this study, gain-of-function of the $K_V1.2$ channels created clearly more drastic effects on the subthreshold potentials as well as depolarizing phase of the action potentials whereas loss-of-function effect was assumed to be affect the repolarization of the action potentials more prominently.

The GOF effect caused increased time-to-peak as well as AP half-width durations in both GOF and GOF+LOF groups, resulting in enhanced network activity. The gain-of-function of the $K_V1.2$ channels could slow down the depolarization phase while speeding up the repolarization phase, which could be expected to compensate each other for the overall spike time. Nevertheless, in the case of pure GOF mutations, the depolarization phase was affected more drastically, resulting in slower depolarizations. As loss-of-function of the $K_V1.2$ channels would have an opposite effect, alterations observed in the patient-derived neurons carrying GOF+LOF mutations were milder, statistically less significant, compared to the patient-derived neurons carrying pure GOF mutations. Different magnitudes of the mutations' impact on depolarization versus repolarization phases of the action potentials must be also related to overall contribution of $K_V1.2$ currents to these events. While the contribution of $K_V1.2$ currents to the depolarization activated potassium currents is known to be up to 50%, quantitative contribution to the repolarization of action potentials is not clear.

The mutations with pure GOF effects caused severe, and the mutations with GOF+LOF effects cause the most severe phenotypes in the patients. In this thesis, on the network level, these mutations were observed to cause strong disturbances as well. In addition to having longer bursts, they all had increased MFRs, diverging from the controls' MFR level at different time points but remaining elevated later consistently. On the other hand, the LOF mutation which has caused milder symptoms in the patients, was also observed to have milder alterations on the network level. This mutation did not affect spiking or bursting rate but was observed to cause a delay in the maturation of neuronal membranes, which caused slower action potential kinetics contributing to the longer burst durations. A clear discrepancy between the LOF and GOF mutations was revealed in the burst spike frequency assessment. During bursting, GOF effect cause higher spike

frequency whereas LOF slowed down the spike frequency, revealing the unique observation where GOF and LOF mutations caused opposite outcomes.

Patient iPSC-derived neuronal cultures have been observed to show age-dependent differences when compared to the controls. For example, the GOF+LOF mutation carrying patient-derived networks had elevated burst rates at earlier weeks, which were later lowered to the comparable levels of the controls. Such observations may have multiple explanations. In addition to the developing neurons' changing physiology and differential involvement of the $K_V1.2$ channels in distinct events of neuronal transmission, compensatory mechanisms may have a role in adaptation of altered electrical activity of patient-derived neurons back to the healthy physiology. This may be achieved by modifications in the expression and function of other ion channels, especially other K_V1 family subunits, to compensate for the altered currents conducted by the $K_V1.2$-containing channels. Hyperexcitability-induced homeostatic plasticity has been poorly understood in complex systems (90). Nevertheless, based on the current knowledge, in a consistently hyperexcitable network, homeostatic mechanisms are expected to bring the network activity back to a healthy physiological state. However, in case of epilepsies homeostatic plasticity fails to maintain healthy physiological boundaries, causing the brain to stay in abnormal state. The reason for this failure is not clear, however, it has been suggested that in genetic epilepsies homeostatic processes may be even the basis of the hyperexcitable networks due to the infeasibleness of a biological system to compensate for a chronically altered proteins that are vital to maintain a healthy brain state (91). It remains to be elucidated why the compensational changes occur on a micro level but not on a macro level to prevent abnormal brain activity.

Although distinct network activity parameters indicated hyperexcitable networks of the patient cultures, in an age-dependent manner, burst durations remained to be the robust indicator of enhanced electrical activity in all patient-derived networks. This finding may suggest that due to the distorted activity of the neuronal networks at earlier weeks, permanent changes may have happened on a structural level, giving rise to abnormal physiological activities at later time points. In a recent study, synaptic rewiring and increased synaptic connectivity have been suggested as a cause for hyperexcitable networks, due to a mutation in the *KCNT1* encoded K_{Na} channels (92). This study

provides valuable insights for the *KCNA2*-mediated DEE mechanism as well because the authors showed that the epilepsy-causing *KCNT1* mutation caused a gain-of-function of the potassium channels which also play an important role in subthreshold excitability and this mutation caused disturbances in single cell excitability while increasing network activity. As the effect of this *KCNT1*-encoded potassium channels' altered function on the firing properties of neurons aligned with the findings from the *KCNA2*-GOF mutation carrying patient-derived networks examined in this thesis, it is reasonable to suggest that similar mechanisms may be responsible for hyperexcitable networks. If the number and strength of synaptic connections increased during the highly excitable time periods in the *KCNA2* patient-derived networks, even if the single AP parameters were comparable to those in the healthy networks in later stages, due to the increased connectivity and synchronicity bursts may last longer, resulting in increased electrical activity of patient-derived networks.

KCNA2-mediated prolongation of bursts is the key finding in this study, not only because all patient-derived neuronal networks carrying mutations from different functional groups were found to have longer-lasting bursts, but also because the 4-AP experiments showed that the clinical benefit of 4-AP must be related to the reversal effect of 4-AP on burst durations, shortening them to comparable levels of those of the healthy individual-derived networks. As the burst durations in the control cultures were not influenced by the 4-AP treatment but they were significantly shortened in patient cultures carrying the *KCNA2*-R297Q mutation, it can be argued that longer duration of bursts is the key contributor of the pathophysiological brain activity in patients, and the therapeutic effect of 4-AP is achieved by shortening the burst durations.

In this project, the underlying disease mechanism for *KCNA2*-mediated DEEs was investigated mainly using electrophysiological methods. Nevertheless, to have a complete understanding of the *KCNA2*-mediated epileptogenesis multiple dimensions of research must be brought together; synaptic and cellular features as well as transcriptome of the same networks should be studied to test arising new hypotheses, and ultimately to reveal underlying causes of epileptogenesis.

6 ACKNOWLEDGEMENTS

First of all, I would like to thank Prof. Dr. Holger Lerche for having me in his research group first as a master student, and then as a PhD candidate, supporting me to improve myself as a scientist throughout these years as well as letting me work independently on my thesis.

I would like to thank also to Dr. Ulrike Hedrich-Klimosch, who was my first supervisor in the lab, for all her support and suggestions during the last years.

Special thanks go to Dr. Niklas Schwarz, who in the beginning had to answer my endless questions and later had to bear my non-stop talking. Thank you for letting me be Ms. Green of the team, thank you for making the work in the lab enjoyable, making not-the-best times bearable and good times even better over the last years in the lab / office. Thank you for all the cakes you shared with me. Thank you for peeling potatoes with me! It is so “okay” (in Swabian), my dear friend, that you are there.

Thank you, Carolin Fischer, for joining the iPS team, contributing to the fun and home-like office environment we had. Thank you for random hugs! I may not continue the teamwork in the lab anymore but I’ll happily continue to team up to discuss how beautiful the neurons fire - or some other things - always!

I would also like to thank all AG Lerche members for just being there, cheering for good news, complaining about annoying things, complaining more about not-changing annoying things, funny lunch discussions, for all the big French press coffees prepared, and of course for making sure that there is always a reason for someone to bring a cake!

Last but not least, many thanks to my entire family who have always supported me, for being there for me and for making me always feel loved and cared. My beloved nephews, you are the reason for going back to Turkey every second month, which was always worth the tiredness as soon as I got my hugs and kisses. Thank you for your pure love.

7 REFERENCES

1. Fiest KM, Sauro KM, Wiebe S, Patten SB, Kwon CS, Dykeman J, et al. Prevalence and incidence of epilepsy: A systematic review and meta-analysis of international studies. Neurology. 2017 Jan 17;88(3):296–303.

2. Scheffer IE, Berkovic S, Capovilla G, Connolly MB, French J, Guilhoto L, et al. ILAE classification of the epilepsies: Position paper of the ILAE Commission for Classification and Terminology. Epilepsia. 2017;58(4):512–21.

3. Lerche H, Shah M, Beck H, Noebels J, Johnston D, Vincent A. Ion channels in genetic and acquired forms of epilepsy. J Physiol. 2013;591(4):753–64.

4. Hedrich U, Maljevic S, Lerche H. Mechanisms of genetic epilepsies. E-Neuroforum. 2013 Jun 1;19(2):23–30.

5. Liao Y, Anttonen AK, Liukkonen E, Gaily E, Maljevic S, Schubert S, et al. SCN2A mutation associated with neonatal epilepsy, late-onset episodic ataxia, myoclonus, and pain. Neurology. 2010 Oct 19;75(16):1454–8.

6. Maljevic S, Naros G, Yalçin Ö, Blazevic D, Loeffler H, Cağlayan H, et al. Temperature and pharmacological rescue of a folding-defective, dominant-negative KV 7.2 mutation associated with neonatal seizures. Hum Mutat. 2011 Oct;32(10):E2283-2293.

7. Masnada S, Hedrich UBS, Klee EW, Lanpher BC, Gavrilova RH, Synofzik M, et al. Clinical spectrum and genotype-phenotype associations of KCNA2-related encephalopathies. Brain J Neurol. 2017 Sep 1;140(9):2337–54.

8. Syrbe S, Hedrich UBS, Riesch E, Djémié T, Müller S, Møller RS, et al. De novo loss- or gain-of-function mutations in KCNA2 cause epileptic encephalopathy. Nat Genet. 2015 Apr;47(4):393–9.

9. Hedrich UBS, Lauxmann S, Wolff M, Synofzik M, Bast T, Binelli A, et al. 4-Aminopyridine is a promising treatment option for patients with gain-of-function KCNA2-encephalopathy. Sci Transl Med. 2021 Sep;13(609):eaaz4957.

10. Pena SDJ, Coimbra RLM. Ataxia and myoclonic epilepsy due to a heterozygous new mutation in *KCNA2* : proposal for a new channelopathy: Ataxia and myoclonic epilepsy due to a heterozygous new mutation. Clin Genet. 2015 Feb;87(2):e1–3.

11. Masnada S, Hedrich UBS, Gardella E, Schubert J, Show C, Eric K, et al. Clinical spectrum and genotype–phenotype associations of KCNA2-related encephalopathies. Brain. 2017;140(9):2337–54.

12. Syrbe S, Hedrich UBS, Riesch E, Djémié T, Müller S, Møller RS, et al. De novo loss- or gain-of-function mutations in KCNA2 cause epileptic encephalopathy. Nat Genet. 2015 Apr;47(4):393–9.

13. Allen NM, Conroy J, Shahwan A, Lynch B, Correa RG, Pena SDJ, et al. Unexplained early onset epileptic encephalopathy: Exome screening and phenotype expansion. Epilepsia. 2016 Jan;57(1):e12–7.

14. Corbett MA, Bellows ST, Li M, Carroll R, Micallef S, Carvill GL, et al. Dominant *KCNA2* mutation causes episodic ataxia and pharmacoresponsive epilepsy. Neurology. 2016 Nov 8;87(19):1975–84.

15. Sachdev M, Gaínza-Lein M, Tchapyjnikov D, Jiang YH, Loddenkemper T, Mikati MA. Novel clinical manifestations in patients with KCNA2 mutations. Seizure. 2017 Oct;51:74–6.

16. Hundallah K, Alenizi A, AlHashem A, Tabarki B. Severe early-onset epileptic encephalopathy due to mutations in the KCNA2 gene: Expansion of the genotypic and phenotypic spectrum. Eur J Paediatr Neurol. 2016 Jul;20(4):657–60.

17. Döring JH, Schröter J, Jüngling J, Biskup S, Klotz KA, Bast T, et al. Refining Genotypes and Phenotypes in KCNA2-Related Neurological Disorders. Int J Mol Sci. 2021 Jan;22(6):2824.

18. Allou L, Julia S, Amsallem D, El Chehadeh S, Lambert L, Thevenon J, et al. Rett-like phenotypes: expanding the genetic heterogeneity to the *KCNA2* gene and first familial case of *CDKL5* -related disease: Genetic heterogeneity in Rett syndrome. Clin Genet. 2017 Mar;91(3):431–40.

19. Roux B. Ion channels and ion selectivity. Essays Biochem. 2017 May 9;61(2):201–9.

20. Purves D, editor. Neuroscience. 3rd ed. Sunderland, Mass: Sinauer Associates, Publishers; 2004. 1 p.

21. Hodgkin AL, Huxley AF. Currents carried by sodium and potassium ions through the membrane of the giant axon of Loligo. J Physiol. 1952 Apr 28;116(4):449–72.

22. Lai HC, Jan LY. The distribution and targeting of neuronal voltage-gated ion channels. Nat Rev Neurosci. 2006 Jul;7(7):548–62.

23. Tempel BL, Papazian DM, Schwarz TL, Jan YN, Jan LY. Sequence of a probable potassium channel component encoded at Shaker locus of Drosophila. Science. 1987 Aug 14;237(4816):770–5.

24. Ishida IG, Rangel-Yescas GE, Carrasco-Zanini J, Islas LD. Voltage-dependent gating and gating charge measurements in the Kv1.2 potassium channel. J Gen Physiol. 2015 Apr 1;145(4):345–58.

25. Trimmer JS, Rhodes KJ. Localization of Voltage-Gated Ion Channels IN Mammalian Brain. Annu Rev Physiol. 2004 Mar;66(1):477–519.

26. Rasband MN, Trimmer JS, Schwarz TL, Levinson SR, Ellisman MH, Schachner M, et al. Potassium Channel Distribution, Clustering, and Function in Remyelinating Rat Axons. J Neurosci. 1998 Jan 1;18(1):36–47.

27. Wang H, Ternpep L. Localization of Kvl .I and Kvl.2, Two K Channel Proteins, to Synaptic Terminals, Somata, and Dendrites in the Mouse Brain. :12.

28. Rivera JF, Chu PJ, Arnold DB. The T1 domain of Kv1.3 mediates intracellular targeting to axons. Eur J Neurosci. 2005;22(8):1853–62.

29. Gulbis JM, Zhou M, Mann S, MacKinnon R. Structure of the Cytoplasmic β Subunit--T1 Assembly of Voltage-Dependent K+ Channels. Science [Internet]. 2000 Jul 7 [cited 2022 Jan 20]; Available from: https://www.science.org/doi/abs/10.1126/science.289.5476.123

30. Rhodes KJ, Strassle BW, Monaghan MM, Bekele-Arcuri Z, Matos MF, Trimmer JS. Association and Colocalization of the Kvβ1 and Kvβ2 β-Subunits with Kv1 α-Subunits in Mammalian Brain K+Channel Complexes. J Neurosci. 1997 Nov 1;17(21):8246–58.

31. Campomanes CR, Carroll KI, Manganas LN, Hershberger ME, Gong B, Antonucci DE, et al. Kv beta subunit oxidoreductase activity and Kv1 potassium channel trafficking. J Biol Chem. 2002 Mar 8;277(10):8298–305.

32. Shi G, Nakahira K, Hammond S, Rhodes KJ, Schechter LE, Trimmer JS. Beta subunits promote K+ channel surface expression through effects early in biosynthesis. Neuron. 1996 Apr;16(4):843–52.

33. Manganas LN, Trimmer JS. Subunit Composition Determines Kv1 Potassium Channel Surface Expression *. J Biol Chem. 2000 Sep 22;275(38):29685–93.

34. Li D, Takimoto K, Levitan ES. Surface Expression of Kv1 Channels Is Governed by a C-terminal Motif *. J Biol Chem. 2000 Apr 21;275(16):11597–602.

35. Gu C, Jan YN, Jan LY. A Conserved Domain in Axonal Targeting of Kv1 (Shaker) Voltage-Gated Potassium Channels. Science [Internet]. 2003 Aug 1 [cited 2022 Jan 21]; Available from: https://www.science.org/doi/abs/10.1126/science.1086998

36. Tiffany AM, Manganas LN, Kim E, Hsueh YP, Sheng M, Trimmer JS. Psd-95 and Sap97 Exhibit Distinct Mechanisms for Regulating K+ Channel Surface Expression and Clustering. J Cell Biol. 2000 Jan 10;148(1):147–58.

37. Li M, Jan YN, Jan LY. Specification of Subunit Assembly by the Hydrophilic Amino-Terminal Domain of the Shaker Potassium Channel. Science [Internet]. 1992 Aug 28 [cited 2022 Jan 22]; Available from: https://www.science.org/doi/abs/10.1126/science.1519059

38. Shen NV, Chen X, Boyer MM, Pfaffinger PJ. Deletion analysis of K+ channel assembly. Neuron. 1993 Jul 1;11(1):67–76.

39. Bixby KA, Nanao MH, Shen NV, Kreusch A, Bellamy H, Pfaffinger PJ, et al. Zn2+-binding and molecular determinants of tetramerization in voltage-gated K+ channels. Nat Struct Biol. 1999 Jan;6(1):38–43.

40. Minor DL, Lin YF, Mobley BC, Avelar A, Jan YN, Jan LY, et al. The Polar T1 Interface Is Linked to Conformational Changes that Open the Voltage-Gated Potassium Channel. Cell. 2000 Sep 1;102(5):657–70.

41. MacKinnon R. Potassium Channels and the Atomic Basis of Selective Ion Conduction (Nobel Lecture). Angew Chem Int Ed. 2004;43(33):4265–77.

42. Doyle DA, Morais Cabral J, Pfuetzner RA, Kuo A, Gulbis JM, Cohen SL, et al. The structure of the potassium channel: molecular basis of K+ conduction and selectivity. Science. 1998 Apr 3;280(5360):69–77.

43. Long SB, Campbell EB, MacKinnon R. Crystal Structure of a Mammalian Voltage-Dependent Shaker Family K+ Channel. Science [Internet]. 2005 Aug 5 [cited 2022 Jan 21]; Available from: https://www.science.org/doi/abs/10.1126/science.1116269

44. Rudy B, Maffie J, Amarillo Y, Clark B, Goldberg EM, Jeong HY, et al. Voltage Gated Potassium Channels: Structure and Function of Kv1 to Kv9 Subfamilies. In: Squire LR,

editor. Encyclopedia of Neuroscience [Internet]. Oxford: Academic Press; 2009 [cited 2022 Jan 21]. p. 397–425. Available from: https://www.sciencedirect.com/science/article/pii/B9780080450469016302

45. Koopmann R, Scholle A, Ludwig J, Leicher T, Zimmer T, Pongs O, et al. Role of the S2 and S3 Segment in Determining the Activation Kinetics in Kv2.1 Channels. J Membr Biol. 2001 Jul;182(1):49–59.

46. Steidl JV, Yool AJ. Differential Sensitivity of Voltage-Gated Potassium Channels Kv1.5 and Kv1.2 to Acidic pH and Molecular Identification of pH Sensor. :9.

47. Scholle A, Dugarmaa S, Zimmer T, Leonhardt M, Koopmann R, Engeland B, et al. Rate-limiting Reactions Determining Different Activation Kinetics of Kv1.2and Kv2.1 Channels. J Membr Biol [Internet]. 2004 Mar [cited 2022 Jul 22];198(2). Available from: http://link.springer.com/10.1007/s00232-004-0664-0

48. Grissmer S, Nguyen AN, Aiyar J, Hanson DC, Mather RJ, Gutman GA, et al. Pharmacological characterization of five cloned voltage-gated K+ channels, types Kv1.1, 1.2, 1.3, 1.5, and 3.1, stably expressed in mammalian cell lines. Mol Pharmacol. 1994 Jun 1;45(6):1227–34.

49. Rezazadeh S, Kurata HT, Claydon TW, Kehl SJ, Fedida D. An Activation Gating Switch in Kv1.2 Is Localized to a Threonine Residue in the S2-S3 Linker. Biophys J. 2007 Dec 15;93(12):4173–86.

50. Waxman SG, Ritchie JM. Organization of ion channels in the myelinated nerve fiber. Science. 1985 Jun 28;228(4707):1502–7.

51. Black JA, Kocsis JD, Waxman SG. Ion channel organization of the myelinated fiber. Trends Neurosci. 1990 Feb;13(2):48–54.

52. Wang H, Kunkel DD, Martin TM, Schwartzkroin PA, Tempel BL. Heteromultimeric K+ channels in terminal and juxtaparanodal regions of neurons. Nature. 1993 Sep;365(6441):75–9.

53. Inda MC, DeFelipe J, Munoz A. Voltage-gated ion channels in the axon initial segment of human cortical pyramidal cells and their relationship with chandelier cells. Proc Natl Acad Sci. 2006 Feb 21;103(8):2920–5.

54. Geiger JRP, Jonas P. Dynamic Control of Presynaptic Ca2+ Inflow by Fast-Inactivating K+ Channels in Hippocampal Mossy Fiber Boutons. Neuron. 2000 Dec;28(3):927–39.

55. Southan AP, Robertson B. Electrophysiological Characterization of Voltage-Gated K+ Currents in Cerebellar Basket and Purkinje Cells: Kv1 and Kv3 Channel Subfamilies Are Present in Basket Cell Nerve Terminals. J Neurosci. 2000 Jan 1;20(1):114–22.

56. Robbins CA, Tempel BL. Kv1.1 and Kv1.2: Similar channels, different seizure models: Two Kv1s; Two Different Epilepsies. Epilepsia. 2012 Jun;53:134–41.

57. Llinás R, Mühlethaler M. An electrophysiological study of the in vitro, perfused brain stem-cerebellum of adult guinea-pig. J Physiol. 1988;404(1):215–40.

58. Schwindt PC, Spain WJ, Foehring RC, Stafstrom CE, Chubb MC, Crill WE. Multiple potassium conductances and their functions in neurons from cat sensorimotor cortex in

vitro. J Neurophysiol [Internet]. 1988 Feb 1 [cited 2022 Jan 22]; Available from: https://journals.physiology.org/doi/abs/10.1152/jn.1988.59.2.424

59. Hamilton KA, Kauer JS. Intracellular potentials of salamander mitral/tufted neurons in response to odor stimulation. Brain Res. 1985;338(1):181–5.

60. Sheng M, Tsaur ML, Nung Jan Y, Yeh Jan L. Subcellular segregation of two A-type K+ channel proteins in rat central neurons. Neuron. 1992 Aug;9(2):271–84.

61. Takahashi K, Yamanaka S. Induction of Pluripotent Stem Cells from Mouse Embryonic and Adult Fibroblast Cultures by Defined Factors. Cell. 2006 Aug 25;126(4):663–76.

62. Lowry WE, Richter L, Yachechko R, Pyle AD, Tchieu J, Sridharan R, et al. Generation of human induced pluripotent stem cells from dermal fibroblasts. Proc Natl Acad Sci. 2008 Feb 26;105(8):2883–8.

63. Mohan H, Verhoog MB, Doreswamy KK, Eyal G, Aardse R, Lodder BN, et al. Dendritic and Axonal Architecture of Individual Pyramidal Neurons across Layers of Adult Human Neocortex. Cereb Cortex. 2015 Dec 1;25(12):4839–53.

64. Herculano-Houzel S, Mota B, Wong P, Kaas JH. Connectivity-driven white matter scaling and folding in primate cerebral cortex. Proc Natl Acad Sci. 2010 Nov 2;107(44):19008–13.

65. DeFelipe J. The Evolution of the Brain, the Human Nature of Cortical Circuits, and Intellectual Creativity. Front Neuroanat [Internet]. 2011 [cited 2022 Jul 4];5. Available from: https://www.frontiersin.org/articles/10.3389/fnana.2011.00029

66. Shi Y, Kirwan P, Smith J, Robinson HPC, Livesey FJ. Human cerebral cortex development from pluripotent stem cells to functional excitatory synapses. Nat Neurosci. 2012 Mar;15(3):477–86.

67. Kirkeby A, Nelander J, Parmar M. Generating regionalized neuronal cells from pluripotency, a step-by-step protocol. Front Cell Neurosci. 2012;6:64.

68. Liu Y, Lopez-Santiago LF, Yuan Y, Jones JM, Zhang H, O'Malley HA, et al. DRAVET SYNDROME PATIENT-DERIVED NEURONS SUGGEST A NOVEL EPILEPSY MECHANISM. Ann Neurol. 2013 Jul;74(1):128–39.

69. Stanurova J, Neureiter A, Hiber M, de Oliveira Kessler H, Stolp K, Goetzke R, et al. Angelman syndrome-derived neurons display late onset of paternal UBE3A silencing. Sci Rep. 2016 Aug 3;6:30792.

70. Yamashita S, Chiyonobu T, Yoshida M, Maeda H, Zuiki M, Kidowaki S, et al. Mislocalization of syntaxin-1 and impaired neurite growth observed in a human iPSC model for STXBP1-related epileptic encephalopathy. Epilepsia. 2016 Apr;57(4):e81-86.

71. Shi Y, Kirwan P, Livesey FJ. Directed differentiation of human pluripotent stem cells to cerebral cortex neurons and neural networks. Nat Protoc. 2012 Oct;7(10):1836–46.

72. Zhang Y, Pak C, Han Y, Ahlenius H, Zhang Z, Chanda S, et al. Rapid Single-Step Induction of Functional Neurons from Human Pluripotent Stem Cells. Neuron. 2013 Jun 5;78(5):785–98.

73. Busskamp V, Lewis NE, Guye P, Ng AHM, Shipman SL, Byrne SM, et al. Rapid neurogenesis through transcriptional activation in human stem cells. Mol Syst Biol. 2014 Nov 17;10:760.

74. Lam RS, Töpfer FM, Wood PG, Busskamp V, Bamberg E. Functional Maturation of Human Stem Cell-Derived Neurons in Long-Term Cultures. Chen HCI, editor. PLOS ONE. 2017 Jan 4;12(1):e0169506.

75. Masnada S, Hedrich UBS, Gardella E, Schubert J, Kaiwar C, Klee EW, et al. Clinical spectrum and genotype–phenotype associations of KCNA2-related encephalopathies. Brain. 2017 Sep 1;140(9):2337–54.

76. Schildge S, Bohrer C, Beck K, Schachtrup C. Isolation and culture of mouse cortical astrocytes. J Vis Exp JoVE. 2013 Jan 19;(71):50079.

77. Frega M, van Gestel SHC, Linda K, van der Raadt J, Keller J, Van Rhijn JR, et al. Rapid Neuronal Differentiation of Induced Pluripotent Stem Cells for Measuring Network Activity on Micro-electrode Arrays. J Vis Exp. 2017 Jan 8;(119):54900.

78. Schwarz N, Uysal B, Rosa F, Löffler H, Mau-Holzmann U, Liebau S, et al. Establishment of a human induced pluripotent stem cell (iPSC) line (HIHDNEi002-A) from a patient with developmental and epileptic encephalopathy carrying a KCNA2 (p.Arg297Gln) mutation. Stem Cell Res. 2019 Apr 1;37:101445.

79. Uysal B, Löffler H, Rosa F, Lerche H, Schwarz N. Generation of an induced pluripotent stem cell (iPSC) line (HIHDNEi003-A) from a patient with developmental and epileptic encephalopathy carrying a KCNA2 (p.Thr374Ala) mutation. Stem Cell Res. 2019 Aug 1;40:101543.

80. Schwarz N, Uysal B, Rosa F, Löffler H, Mau-Holzmann UA, Liebau S, et al. Generation of an induced pluripotent stem cell (iPSC) line from a patient with developmental and epileptic encephalopathy carrying a KCNA2 (p.Leu328Val) mutation. Stem Cell Res. 2018 Dec;33:6–9.

81. Hedrich UBS, Lauxmann S, Wolff M, Synofzik M, Bast T, Binelli A, et al. 4-Aminopyridine is a promising treatment option for patients with gain-of-function KCNA2-encephalopathy. Sci Transl Med. 2021 Sep;13(609):eaaz4957.

82. Südhof TC. Calcium Control of Neurotransmitter Release. Cold Spring Harb Perspect Biol. 2012 Jan;4(1):a011353.

83. Begum R, Bakiri Y, Volynski KE, Kullmann DM. Action potential broadening in a presynaptic channelopathy. Nat Commun. 2016 Nov;7(1):12102.

84. Bischofberger J, Geiger JRP, Jonas P. Timing and Efficacy of Ca^{2+} Channel Activation in Hippocampal Mossy Fiber Boutons. J Neurosci. 2002 Dec 15;22(24):10593–602.

85. Shen W, Hernandez-Lopez S, Tkatch T, Held JE, Surmeier DJ. Kv1.2-Containing K^{+} Channels Regulate Subthreshold Excitability of Striatal Medium Spiny Neurons. J Neurophysiol. 2004 Mar;91(3):1337–49.

86. Odawara A, Katoh H, Matsuda N, Suzuki I. Physiological maturation and drug responses of human induced pluripotent stem cell-derived cortical neuronal networks in long-term culture. Sci Rep. 2016 May;6(1):26181.

87. Schwarz N, Uysal B, Welzer M, Bahr J, Layer N, Löffler H, et al. Long-term adult human brain slice cultures as a model system to study human CNS circuitry and disease. eLife. 2019 Sep 9;8.

88. Kirsch GE, Shieh CC, Drewe JA, Vener DF, Brownt AM. Segmental exchanges define 4-aminopyridine binding and the inner mouth of K+ pores. Neuron. 1993 Sep 1;11(3):503–12.

89. Armstrong CM, Loboda A. A model for 4-aminopyridine action on K channels: similarities to tetraethylammonium ion action. Biophys J. 2001 Aug;81(2):895–904.

90. Lee HK, Kirkwood A. Mechanisms of Homeostatic Synaptic Plasticity in vivo. Front Cell Neurosci [Internet]. 2019 [cited 2022 Jul 5];13. Available from: https://www.frontiersin.org/articles/10.3389/fncel.2019.00520

91. Lignani G, Baldelli P, Marra V. Homeostatic Plasticity in Epilepsy. Front Cell Neurosci [Internet]. 2020 [cited 2022 Jul 5];14. Available from: https://www.frontiersin.org/articles/10.3389/fncel.2020.00197

92. Shore AN, Colombo S, Tobin WF, Petri S, Cullen ER, Dominguez S, et al. Reduced GABAergic Neuron Excitability, Altered Synaptic Connectivity, and Seizures in a KCNT1 Gain-of-Function Mouse Model of Childhood Epilepsy. Cell Rep. 2020 Oct 27;33(4):108303.

To enable the experiments performed in this thesis, some previous work was performed previously for the reprogramming of the human fibroblasts obtained from different patients as well as from healthy individuals into induced pluripotent stem cells.

- Heidrun Löffler, the lab technician in Prof. Dr. Holger Lerche's research group, cultivated the skin biopsies that were sent to the lab by different collaboration partners, successfully obtained fibroblasts from them. She expanded and transduced the fibroblast cultures, as described in the Methods section of this thesis. Emerging iPSCs were then isolated, further expanded and backed up by her. She also contributed to some experiments on the characterization of the induced pluripotent stem cells, proving endogenous pluripotency.

- Dr. Niklas Schwarz also supported the reprogramming of the human fibroblasts into induced pluripotent stem cells, as well as characterization of some of the patient and control-derived lines.